Study and Test of a Beam Monitor Detector for the Bern Medical Cyclotron

Masterarbeit

der Philosophisch-naturwissenschaftlichen Fakultät
der Universität Bern

vorgelegt von

Elena Kirillova

2014

Leiter der Arbeit

Prof. Dr. Antonio Ereditato
PD Dr. Saverio Braccini

Albert Einstein Center for Fundamental Physics
Laboratory for High Energy Physics
Physics Institute
University of Bern, Switzerland

Abstract

Beam monitor detectors based on the emission of secondary electrons are an innovative instruments to improve beam monitoring in medical applications, radioisotope production and cancer hadrontherapy, in particular. This type of detector was studied, improved and tested in the framework of this Master thesis. BISE (Beam Imaging with Secondary Electrons) was developed in collaboration with the TERA Foundation at CERN and our group of the Albert Einstein Center for Fundamental Physics – Laboratory for High Energy Physics (AEC-LHEP) in Bern. A BISE device was installed at the Bern 18 MeV cyclotron laboratory and beam tests were performed with a dedicated beam transfer line. A precise on-line monitoring of the beam profile, position and intensity is a critical issue for the operation of all particle accelerators and, in particular, for medical ion cyclotrons. Being based on the detection of secondary electrons emitted by a thin aluminum foil traversed by the beam, the BISE detector is able to operate at large (micro-Ampere range) as well as at low (nano-Ampere range) beam intensities, providing non-destructive continuous monitoring during irradiation. Secondary electrons are directed and focused by an electrostatic focusing system to form an image, which is detected by a phosphor screen read-out by a CCD camera. All the results we obtained were compared to simulations. Beam profiles were measured in several conditions and the results of the beam tests performed with the BISE prototype demonstrated the effectiveness of this instrument and opened the way to future developments.

Contents

List of Figures

Introduction

Radioisotope production and hadrontherapy are two important medical applications of ion beams. The continuous control of target bombardment is crucial for a safe, efficient and reliable radioisotope production. In the case of cancer radiotherapy, it is very important to minimize damage to healthy tissues in proximity of the tumor and optimize the dose to the target. This requires precise control of the beam during acceleration, transport, extraction and patient irradiation.

Beam intensities are different in radioisotope production and hadrontherapy. In the former case, currents in the range of 10–500 µA are used. In the latter, the beam intensity is of the order of 1 nA. It would be highly beneficial to have a multipurpose instrument, which is able to monitor beams in both cases. Secondary emission by thin foils traversed by the beam represents a promising solution. Following the construction of a first prototype called SLIM (Secondary emission monitor for Low Interception Monitoring) [1], an innovative on-line beam-monitoring detector named BISE (Beam Imaging with Secondary Electrons) was developed in collaboration by the TERA Foundation at CERN and our group of the Albert Einstein Center for fundamental physics – Laboratory for High Energy Physics (AEC-LHEP). It is designed for currents in the nA and µA ranges, to be operated under vacuum and is based on the emission of secondary electrons. The BISE detector is designed to be installed in any beam line.

The aim of this thesis was to study, improve and test the BISE detector. Beam tests were performed at the new Bern 18 MeV cyclotron laboratory for radioisotope production and research [2]. In this framework, an independent vacuum system was designed with primary and turbo pumps to reach a high vacuum in BISE. Simulations in 2D and 3D were performed using the COMSOL Multiphysics software [3]. The dependence of image intensity on the beam current was studied. The demagnification of the electrostatic lens was estimated by means of simulations and experimentally measured. Preliminary results were presented at international conferences and published in conference proceedings [4, 5] reprinted in Appendix C.

An overview of the Bern cyclotron laboratory, its characteristic beam transfer line, and beam monitoring are presented in Chapter 1. The working principle of beam monitoring detectors based on secondary emission together with the design and construction of BISE are discussed in Chapter 2. Chapter 3 contains the development and the results of simulations. Finally, Chapter 4 describes the improvements implemented in BISE, the experimental set-up and the results of the beam tests.

Chapter 1

The Bern cyclotron laboratory and beam monitoring

This chapter describes the new cyclotron laboratory in Bern and different kinds of beam monitoring techniques. The laboratory was built for radioisotope production and multi-disciplinary research running in parallel. It is equipped with a 6.5 m long beam line ending in a separate bunker allowing experimental activities like the one presented in this thesis.

1.1 The Bern cyclotron laboratory

The Bern cyclotron laboratory is located at the Bern University Hospital (Inselspital). Besides the production of PET (Positron Emission Tomography) radio-tracers for the needs of several medical centers, the laboratory performs multidisciplinary scientific research activities [2].

The Bern cyclotron laboratory features an 18MeV cyclotron, a beam transport line (BTL), a physics laboratory and a workshop (Fig. 1.1). The main characteristics of the Bern cyclotron and its BTL are reported in Table 1.1. The cyclotron has two internal H^- ion sources (as an option D^- can also be accelerated) and provides beam currents up to 150 µA with a transmission rate of more than 95%. Low currents, down to a few pA, can also be obtained and used for research purposes. The apparatus can be used to produce different radioisotopes such as ^{18}F, ^{15}O and ^{11}C. Currently, ^{18}F is produced daily for FDG (fluorodeoxyglucose) radiotracer synthesis [6]. FDG is the most common PET radiotracer.

A schematic view of the BTL is presented in Figure 1.2. The X-Y steering magnet, which is placed near the cyclotron, can bend the beam to ±7 mrad vertically or horizontally. The BTL is equipped with two beam viewers, two quadrupole doublets and a neutron shutter. Two beam viewers are used for a visual control of the beam. By using the quadrupole doublets, the beam spot on the target can be adjusted according to specific needs. The neutron shutter is used to isolate the beam line bunker from neutrons during operation of the cyclotron. The four-finger collimator and a beam dump can be removed and replaced with an experimental apparatus, such as the detector developed in the framework of the present thesis. BISE was tested with the BTL at different beam conditions.
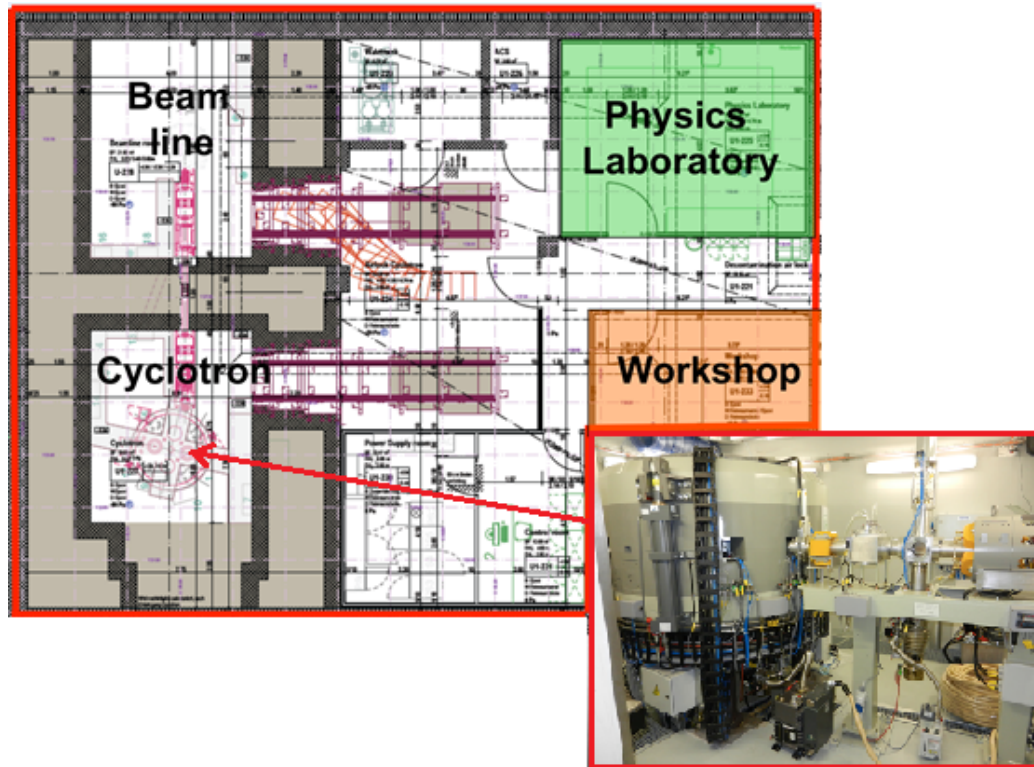
Figure 1.1: The Bern cyclotron laboratory with the 18MeV cyclotron, the beam transport line, the physics laboratory and the workshop.

Constructor	Ion Beam Applications (IBA), Belgium
Type	Cyclone 18/18 HC
Accelerated particles	H^- (D^- on option)
Energy	18 MeV (9 MeV for D^-)
Maximum current	150 μA (40 for μA D^-)
Number of sectors	4
Angle of the dees	30°
Magnetic field	1.9 T on the hills and 0.35 T on the valleys
Radio frequency	42 MHz
Weight	24000 kg
Dimensions	2 m diameter, 2.2 m height
Ion sources	2 internal PIG H^-
Extraction ports	8 (one of which connected with the BTL)
Extraction	Carbon foil stripping (for single or dual beam)
Strippers	Two per extraction port on a rotating carrousel
Isotope targets	4 $^{18}F^-$, ^{15}O (^{11}C and solid target are foreseen)
Beam Transport Line (BTL)	6.5 m long; two quadrupole doublets (one in each bunker); X-Y steering magnet; upstream collimator; 2 beam viewers; neutron shutter.

Table 1.1: Main characteristics of the Bern cyclotron and its beam transport line [6].
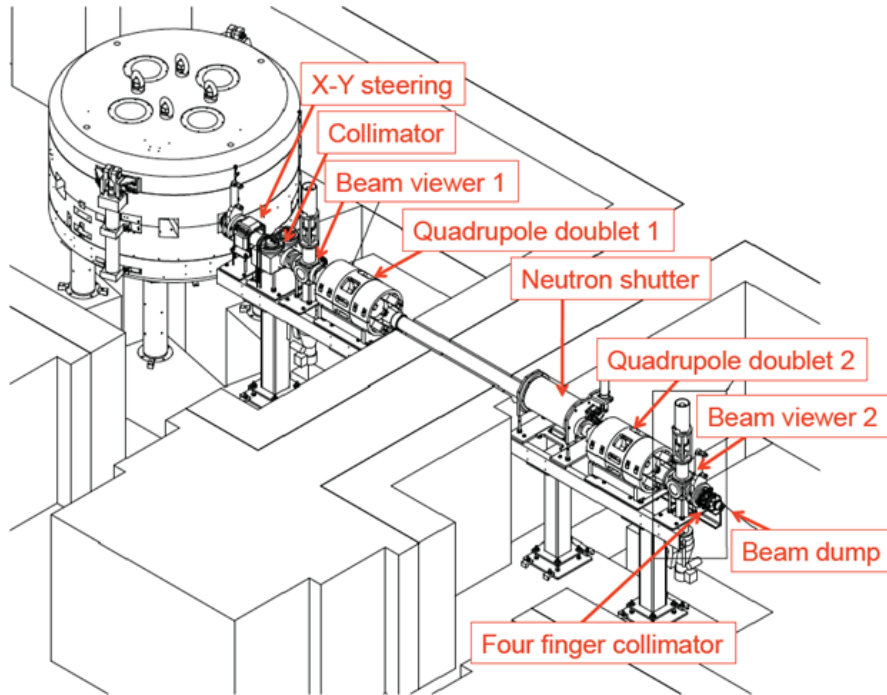
Figure 1.2: A schematic view of the BTL of the Bern cyclotron laboratory. The main components are highlighted [6].

1.2 Beam monitoring

Beam monitoring represents a crucial issue in any kind of particle accelerator. In medical applications, the control of the beam during irradiation is fundamental for hadrontherapy and radioisotope production. Beam monitors are usually installed along the beam transport line or in front of the target.

There are two general types of beam monitoring detectors: destructive and non-destructive [7]. The former are usually simple and more robust, but they have the disadvantage of stopping the beam. The latter, which are more sophisticated, allow controlling of the beam during irradiation. Examples of the two kinds of detectors are:

- Destructive:

  – Faraday Cup
  – Scintillator screens
  – Beam viewers

- Non-destructive:

  – Current transformers
  – Beam-position monitors (pick-ups)
  – Wire scanners
  – Residual gas monitors

As presented in Figure 1.2, the Bern cyclotron laboratory is equipped with two destructive beam viewers, one at the exit of the cyclotron and one at the end of the BTL. The manufacturer, IBA, provided only the possibility to read the intercepted current. Only currents larger than about 100 nA can be measured.

An intensive research program on beam monitoring detectors is underway in Bern. The two viewers were equipped with CCD cameras (Channel coupled devices) to obtain 2D destructive images of the beam (Fig. 1.3). A high sensitivity Faraday cup was installed (Fig. 1.4) allowing measurements of beam currents down to a few pA. A mono-dimensional non-destructive beam scanner (UniBeam) was developed [8, 9]. It is based on optical fibers moved across the beam. An on-line, continuous, non-destructive monitoring of intensity, position and shape, using secondary emission of electrons by thin foils traversed by the beam represents a very promising technique. This Master thesis was focused on the study, development and beam tests of a novel detector based on secondary emission, as described in the following Chapters.
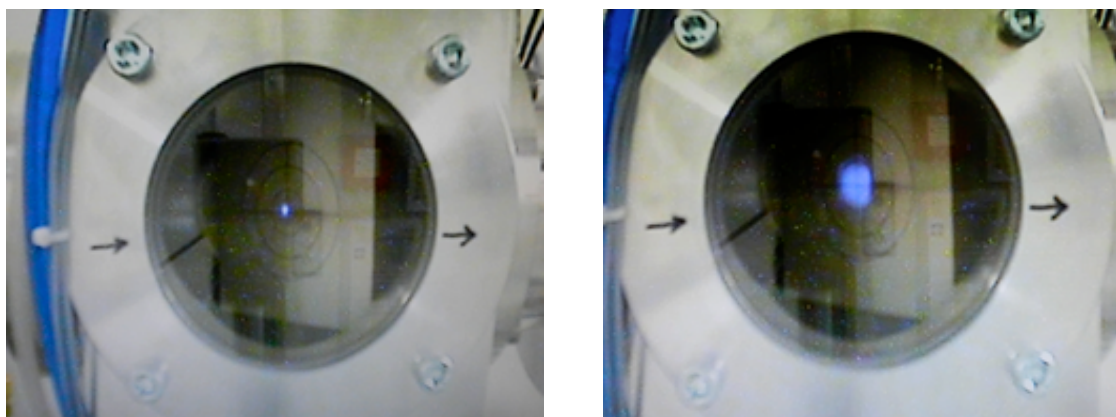
Figure 1.3: Images obtained with the beam viewer in Bern with focused (left) and defocused beam (right).

Figure 1.4: A high precision Faraday cup installed at the Bern cyclotron.

Chapter 2

A real-time on-line beam monitor detector based on secondary emission

Beam monitor detectors are fundamental instruments in medical applications of ions beams, such as radioisotope production and hadrontherapy. In particular, non-destructive detectors allow controlling the beam on-line during irradiation. In recent years, detectors based on secondary emission of electrons by thin metallic foils traversed by the beam were developed. After describing their working principle, the Beam Imaging with Secondary Electrons (BISE) detector is presented. This device is the main theme of the present thesis.

2.1 The working principle of the beam monitor detector

The working principle of beam monitor detectors based on secondary emission is shown in Figure 2.1. A thin metallic foil is located in vacuum and is traversed by the beam at a certain angle with respect to the foil. Ions extract electrons of different kinetic energies from the metallic surface with minimal perturbation of the beam. Most of these electrons have a kinetic energy below 50 eV and are denominated secondary electrons (SEs). An electric potential accelerates and focuses them on an electron detector, by which a 2D profile of the beam and the measurement of its current are obtained. The main features of such detectors are the minimal interaction with the beam and the large intensity range in which they can operate (from nA to μA). As an electron detector, a phosphor screen and a CCD camera can be used as well as silicon pixel detectors. For low currents, electron intensifiers (Microchannel plate detectors) can be added.
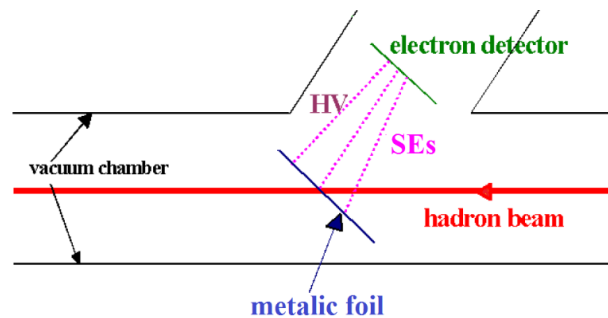
Figure 2.1: Working principle of beam monitor detectors based on secondary emission (HV = high voltage between the electron detector and the metallic foil).

Based on such working principles, the SLIM (Secondary emission monitor of Low Interception Monitoring) detector was developed by the TERA Foundation in the framework of the SUCIMA (Silicon Ultra fast Cameras for electrons and gamma sources In Medical Application) european project. Its primary goal was the development of an advanced imaging technique for beams in hadrontherapy beam lines [1, 10, 11]. For SLIM, an aluminum foil set at 45° with respect to the beam was used. SEs were accelerated to 20 keV by the field of an electrostatic lens and were focused on the electron detector. At the entrance of the beam in the focusing system (FS), 20 μm diameter wires with 2 mm spacing were used to assure a transparency to the proton beam of 99% together with the cylindrical symmetry of the accelerating electric field. The FS could rotate 45° around the vertical axis to have in and out positions of the system with respect to the proton beam. An actuator outside the vacuum chamber drove the FS via a rigid vertical axis connection to guarantee vacuum insulation. A CCD camera detected the light emitted in interactions of 20 keV accelerated SEs with a phosphor screen through a glass window. A schematic drawing of SLIM is shown in Figure 2.2.

The beam monitoring system SLIM was assembled in the TERA Foundation laboratory at CERN (Fig. 2.3). SLIM was successfully tested with proton beams at the cyclotron of the Joint Research Centre (JRC) of the European Commission in Ispra (Italy). These first tests highlighted some disadvantages such as the complexity, the high cost and the fact that delicate electronics located near the detector were damaged by the unavoidable neutron fluxes.

To overcome these disadvantages, the TERA Foundation proposed a new detector of this kind. This apparatus was further developed by our group in Bern and tested with the cyclotron at the Bern University Hospital (Inselspital), as described in the next Section.
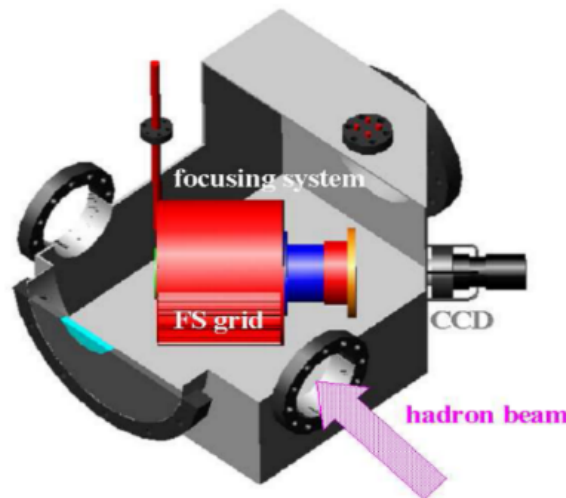
Figure 2.2: A schematic drawing of the SLIM detector [1].
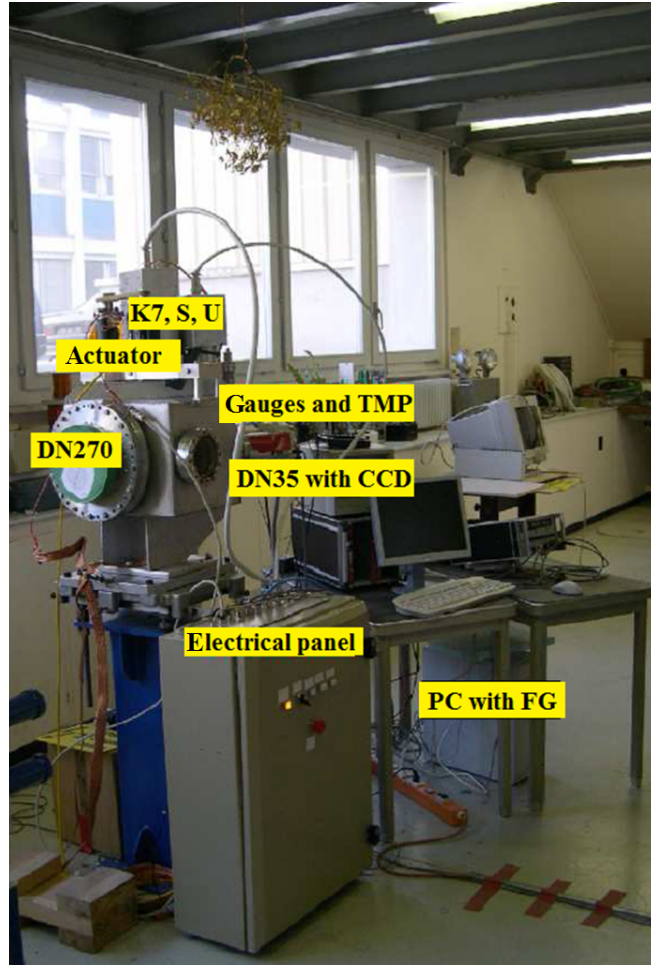
Figure 2.3: The SLIM beam monitor apparatus under test at the TERA laboratory at CERN [1].

2.2 The Beam Imaging with Secondary Electrons (BISE) detector

The BISE detector was constructed at the TERA laboratory at CERN and BISE was transferred at the Bern cyclotron laboratory in spring 2013. BISE is shown in Fig. 2.4 and consists of a vacuum chamber made of stainless steel with two CF-100 (Conflat Flange, 100 mm in diameter) flanges for the beam. KF-40 (Klein Flange, 40 mm in diameter) adaptors were constructed to match the standards adopted in Bern. At the bottom of the cylindrical chamber there is a window to observe the integrity of an aluminum foil. A copper focusing system is placed at an angle of 45 degrees with respect to the beam. A specific support was designed and constructed to install the detector in the beam line. In order to match the height of any beam line, a variable-height table support was chosen. A CCD camera is placed outside the vacuum on the top of the chamber. It allows detecting light from a P47 phosphor screen though a glass window. P47 was chosen for its conversion efficiency (150 photons/10 keV e) and fast decay time (~120 ns) [12].
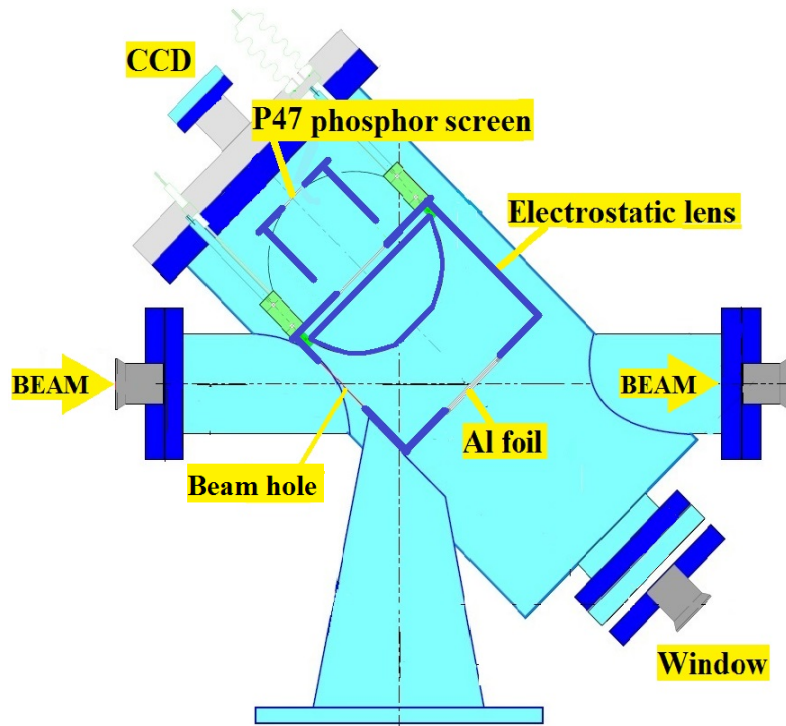
Figure 2.4: The schematic drawing of the BISE detector.
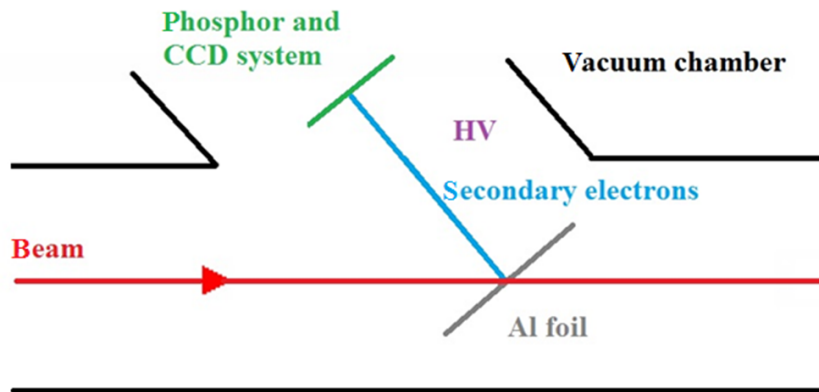
Figure 2.5: The working principle of the BISE detector.

The working principle of the BISE detector is shown in Figure 2.5. A thin aluminum foil (~800 Å) is set at 45° with respect to the beam, which extracts SEs from the foil surface. An electric potential (20 kV) accelerates SEs and focuses them on the phosphor screen, which is seen by the CCD camera. To avoid discharges, BISE operates at a vacuum better than 10^{-5} mbar. A specific interlock shuts the high-voltage down if the pressure inside the chamber goes above this value. Commercial equipment and technical details are reported in Appendix A.

To operate BISE in stand-alone mode in the laboratory and on the beam line, the required vacuum level has to be reached. For this purpose, a valve system was specifically developed (Fig. 2.6). This configuration allows achieving the desired

vacuum with the valves closed, independently of the beam line. This system is described in detail in Subsection 2.2.4.

BISE can operate in a large beam intensity range. The beam passes through the thin aluminum foil and is marginally modified. The image formed by the SEs on the P47 screen represents a 2D beam profile. The main components are described in the following subsections.
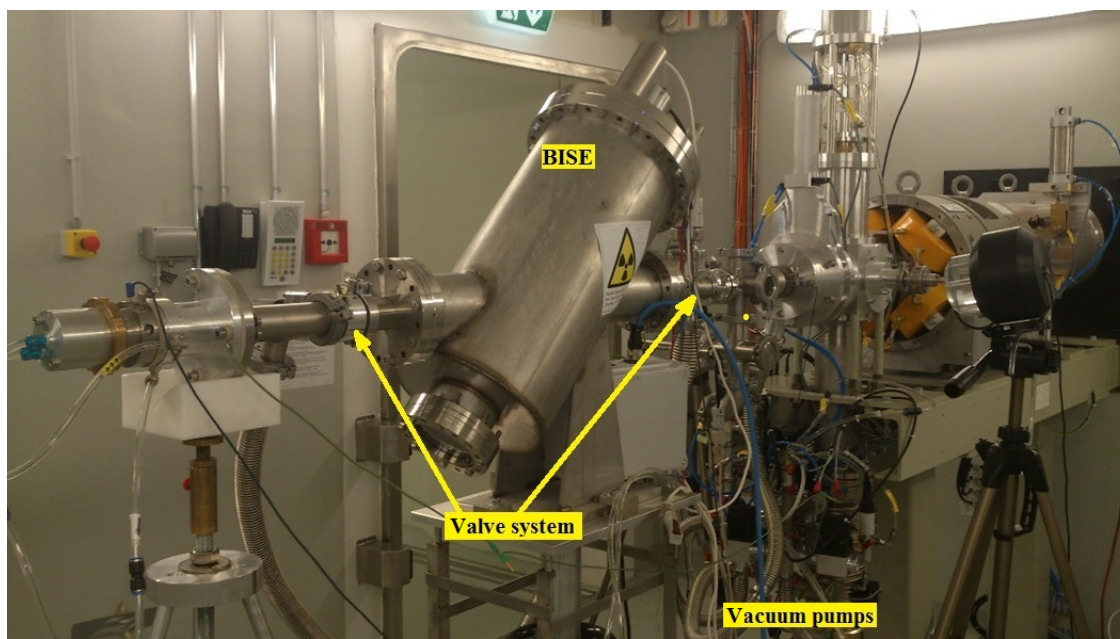
Figure 2.6: BISE with its independent vacuum system installed on the beam line. This configuration allows stand-alone and beam line operation.

2.2.1 Focusing system

The focusing system of BISE consists of an electrostatic lens which accelerates, transports and focuses SEs on the screen. This part of the system is crucial and I dedicated most of my work to its design, simulations and improvements.

The design of the lens provides focusing of the SEs on the phosphor screen, producing an image on the CCD camera (Fig. 2.7 and 2.8). At the beginning of the experiments performed in Bern, a simple hole was used for the entry of the incident beam. Due to the strong electric field distortions induced by the chamber and by the fact that the cylindrical symmetry was broken, it was decided to close this hole with a thin foil of the same kind as the sensing one. This issue will be described in detail later in Subsection 3.2.3 and Section 4.2.

To accelerate SEs, high voltage is provided by specific power supplies connected via a vacuum feedthrough. To shape the electric field, the required high voltage is supplied to the cylinder (-20000 V) and to the spherical segment electrode (-19142 V), as reported in Figure 2.9. The phosphor and its small cylinder are grounded as well as the stainless-steel vacuum chamber. The two values of the high voltage are obtained by means of a single power supply and a passive voltage divider (Fig. 2.8).
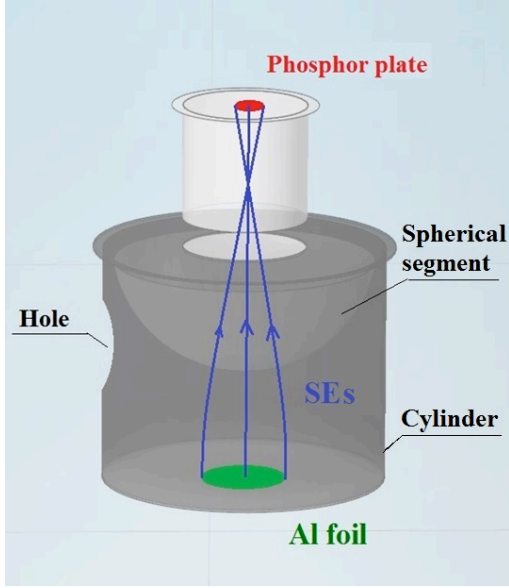
Figure 2.7: Schematic view of the electrostatic lens.
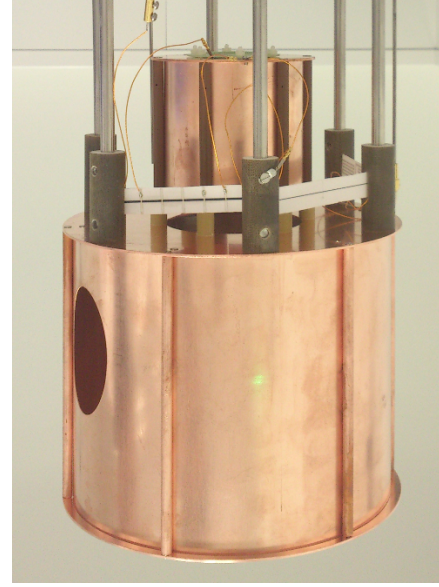
Figure 2.8: The electrostatic lens during maintenance. The voltage divider (white) is visible.
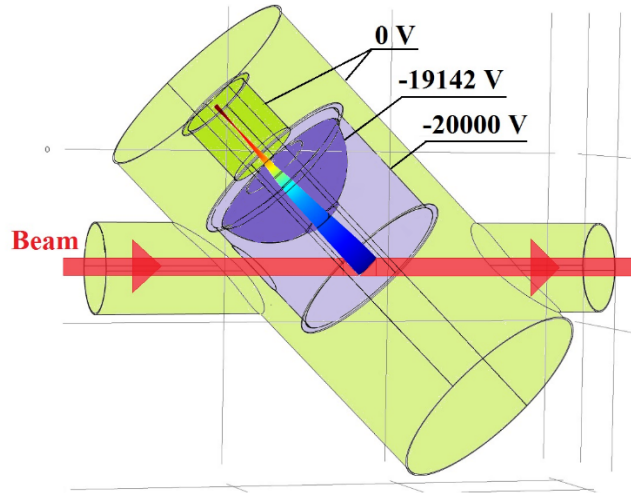
Figure 2.9: Applied voltage on the BISE electrostatic lens.

The electrostatic lens was first modeled in *Simion* software [13]. To improve the performance of this system, I performed simulations in COMSOL Multiphysics. This code is more sophisticated and complete and is commonly used in particle physics and electrostatics. The simulations I performed are described in Chapter 3.

The installation of the thin aluminum foil in its support requires particular care. For this reason, I spent a short period at CERN where I learned specific techniques and prepared several foils for the beam tests in Bern (Fig. 2.10 and 2.11). Foils of 800 Å thickness produced by GoodFellow were chosen to minimize the interaction with the beam. The support ring with the foil was then installed at the bottom of the electrostatic lens of BISE (Fig. 2.12). In April 2013, BISE was ready for beam tests and was transported to the cyclotron laboratory.
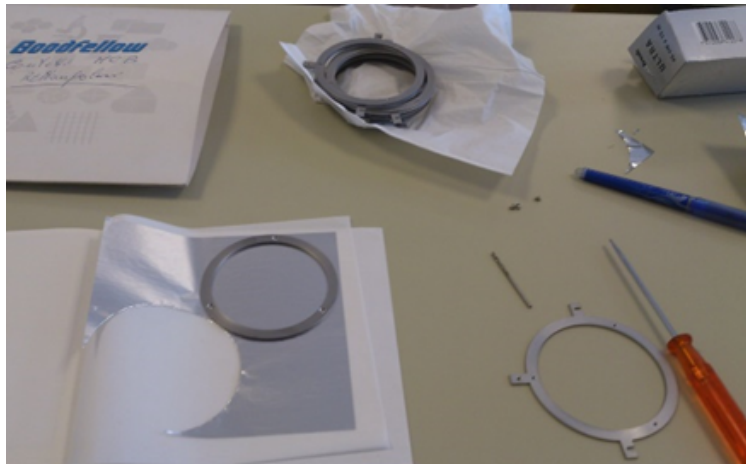
Figure 2.10: Installation of the 800 Å thin aluminum foils in the supports.

Figure 2.11: Aluminum foils stored in a container.

Figure 2.12: Installation of the support ring with the aluminum foil on the bottom of the electrostatic lens of BISE.

2.2.2 Demagnification

Demagnification is the process of reduction of the size an image. This reduction is quantified by a demagnification factor. This factor is given by the size of the *image x'* divided by the size of the *object x*.

For BISE, the *image* is given by the observation of the beam on the phosphor screen (Fig. 2.13). The following relation holds

$$D = \frac{x'}{x} \tag{1}$$

where D is the demagnification factor, x' the *image* the x the *object* (dimension of the beam).

In a beam monitor based on secondary electron emission (Fig. 2.1), the *object* is given by the real shape of the beam in the horizontal plane and by the real shape of the beam multiplied by a factor F in the vertical plane. F is due to the inclination of the foil with respect to the beam direction. For BISE, the inclination angle is 45 degrees.

As shown in Figure 2.14, F is the ratio of major and minor axes (*a* and *b*, respectively) of the elliptical shape on the aluminum foil produced by the beam (Fig. 2.15):

$$F = \frac{b}{a} = \sqrt{2}. \tag{2}$$
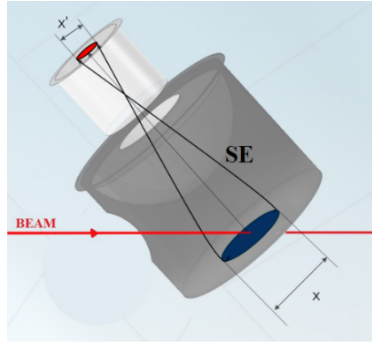
Figure 2.13: Scheme of demagnification for the electrostatic lens of BISE.
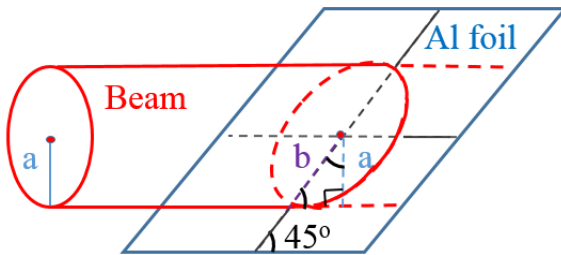
Figure 2.14: Circular beam passing through the aluminum foil set at 45° with respect to the beam.
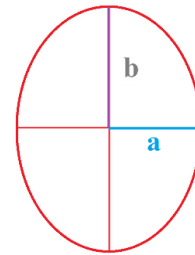
Figure 2.15: Major and minor axes of the beam elliptical shape on the aluminum foil.

2.2.3 Calculated yields for protons impinging on the Al and Al_2O_3 foils

The electron yield γ is a mean number of emitted electrons per incoming projectile. The total SE yield from a thin foil can be expressed as:

$$\gamma_t = \gamma_b + \gamma_f, \tag{3}$$

where γ_b is the backward yield and γ_f is the forward yield.

The material parameter for a particular proton energy impact is the ratio between the measured SE yield and the stopping power:

$$\Lambda_t = \frac{\gamma_t}{dE/dx}, \Lambda_b = \frac{\gamma_b}{dE/dx}, \Lambda_f = \frac{\gamma_f}{dE/dx}, \tag{4}$$

where dE/dx is an electronic energy loss per unit path length of protons in matter and $\Lambda_t, \Lambda_b, \Lambda_f$ are total, backward and forward material parameters, respectively.

The ratio R of forward to backward SE yields is given by [14]:

$$R = \frac{\gamma_f}{\gamma_b} = 1.2\frac{C_f}{C_b} = \frac{\Lambda_f}{\Lambda_b}, \tag{5}$$

where C_f and C_b are energy-loss reduction factors. For protons, $C_f = C_b = 1$.

In the case of BISE, the stopping power dE/dx was calculated using the SRIM software [15]. The aluminum (Al) superficial layer can be slightly oxidized (Al_2O_3), therefore Al_2O_3 is also included. According to [14], the mean value of Λ_t for thin foils was found to be 0.31 (Å/eV). Since $\Lambda_t = \Lambda_b + \Lambda_f$, the backward and forward yields are given by formulae:

$$\gamma_b = \frac{1}{R+1}\Lambda_t\frac{dE}{dx}, \tag{6}$$

$$\gamma_f = \frac{R}{R+1}\Lambda_t\frac{dE}{dx}. \tag{7}$$

For protons, γ_b and γ_f can be calculated in the following way:

$$\gamma_b = 0.14dE/dx, \tag{8}$$

$$\gamma_f = 0.17dE/dx, \tag{9}$$

where dE/dx is expressed in eV/ Å.

The electronic energy loss per unit path length, backward and forward yields on Al and Al_2O_3 targets for proton energy of 18 MeV are reported in Table 2.1.

Proton energy (MeV)	dE/dx (eV/Å)	γ_b (%)	γ_f (%)
Al foil			
18	0.5802	8.1	9.8
Al$_2$O$_3$ foil			
18	0.9119	12.8	15.5

Table 2.1: Backward and forward yields for protons on Al and Al$_2$O$_3$ targets for BISE.

2.2.4 Vacuum system

The cyclotron and its beam line require high vacuum for their operation. The Bern cyclotron and the BTL are equipped with oil diffusion vacuum pumps (ODP). The BISE detector can have its own independent vacuum system, or it can be installed directly in the BTL using beam line vacuum pumps.

To reach the high vacuum independently of the BTL, a specific vacuum system with three valves was developed (Fig. 2.6 and 2.16).
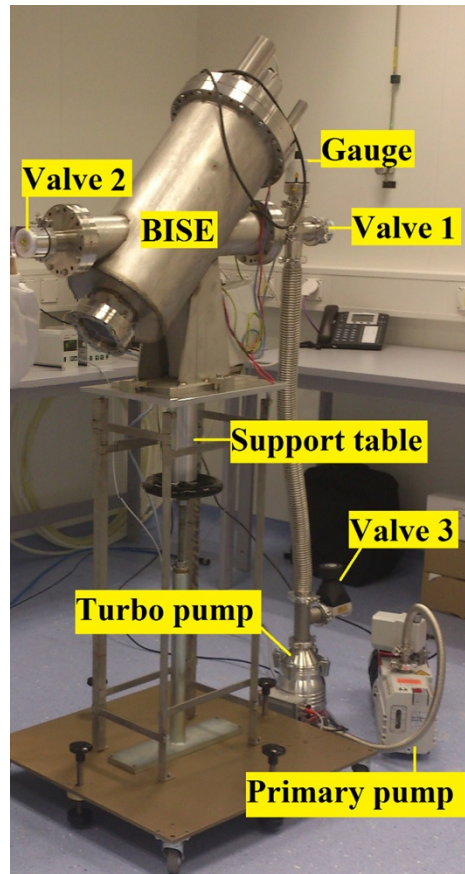
Figure 2.16: The BISE detector with the independent vacuum system consisting three valves, turbo and primary pumps.

Two valves are of the gate type and located along the beam path (Fig. 2.17). The third valve is of the diaphragm type and allowed for nitrogen venting of the vacuum chamber (Fig. 2.18). This method was used to prevent the humid air inside BISE. When breaking vacuum in detector, the tube with dry nitrogen was connected to the third valve and the gas filled the chamber and remained in it until the next test.

The independent vacuum system could be used in stand-alone mode or when the power of BTL vacuum pumps was not enough to reach high vacuum all along the beam line including the detector. The first gate valve provided the connection of the BTL to BISE. After this valve, a high vacuum gauge and a turbo pump are connected via a four-way cross joint. The vacuum gauge was placed as close to BISE as possible. The second gate valve connected BISE to a beam dump or a Faraday cup terminating the line. To assure vacuum to the beam dump or Faraday cup with both gate valves closed (stand-alone mode), a bypass tee was installed and connected with the BTL vacuum. The third diaphragm valve was installed directly after the turbo vacuum pump and was used to vent BISE for interventions such as inserting a collimator or changing the aluminum foil. The turbo and primary pumps for BISE were first tested at LHEP and then transported to the cyclotron laboratory at Inselspital. I took care of the installation and of the tests of the BISE vacuum system. A typical *pump down curve* is shown in Figure 2.19 and demonstrates that operating conditions ($< 5 \times 10^{-5}$ mbar) in independent vacuum system can be reached in about six hours. High voltage could be applied when the pressure reached 5×10^{-5} mbar and automatically shut down when the pressure fell above 8×10^{-5} (Fig. 2.20).

Figure 2.17: KF-40 manual blade gate valve.

Figure 2.18: KF-40 manual diaphragm valve.
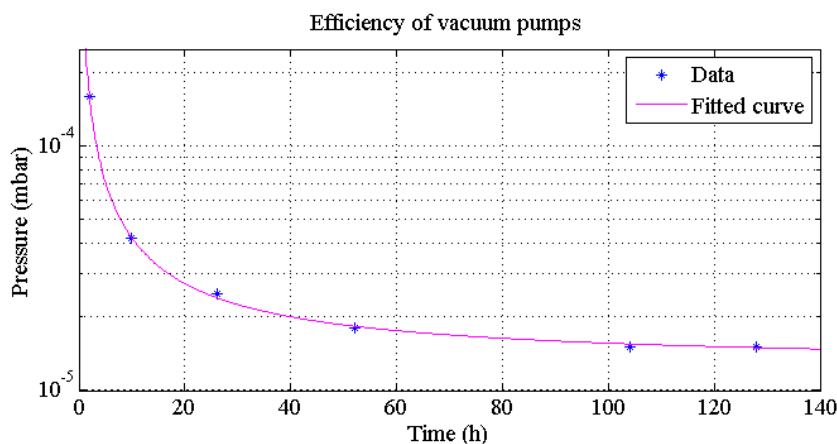
Figure 2.19: Pressure versus time chart for the BISE vacuum system.
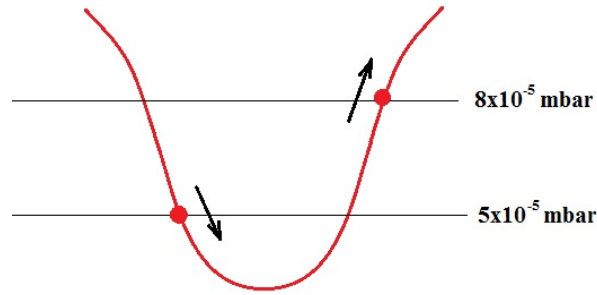
Figure 2.20: High voltage operating condition in BISE. The horizontal line corresponds to time. The first arrow determines the "HV-ON" condition while the second the "HV-OFF" condition.

For many of the tests, BISE was connected directly to the BTL vacuum and only the BTL pumps were used. The high pumping capacity of the ODP pumps of the BTL allowed reaching high vacuum in BISE in about 30 minutes (Fig. 4.1). Either the BISE vacuum system or the direct connection to the BTL vacuum were efficient and were used during experiments according to the specific needs.

Chapter 3

Detector optimization and simulations

The focusing system is one of the most important elements of the BISE detector. Since a large number of options are possible to determine the best configuration of the electric field, simulations are the best tool to study and optimize the path of the secondary electrons used to obtain an image of the beam. Following the first 2D simulations performed with the Simion software, I implemented a full 3D simulation using the COMSOL package. The simulations of BISE and the optimization of the focusing system are discussed in this chapter.

3.1 Two-dimensional simulations with Simion

Simion is an ion optics simulation software used in electrostatics and for the study of ion trajectories. This program was developed in 1985 by David A. Dahl [16]. Simion 8.0 (the version used in this work) was already used by the TERA Foundation for the first concept design of BISE. The software simulates the electric field and the particle trajectories inside the electrostatic lens.
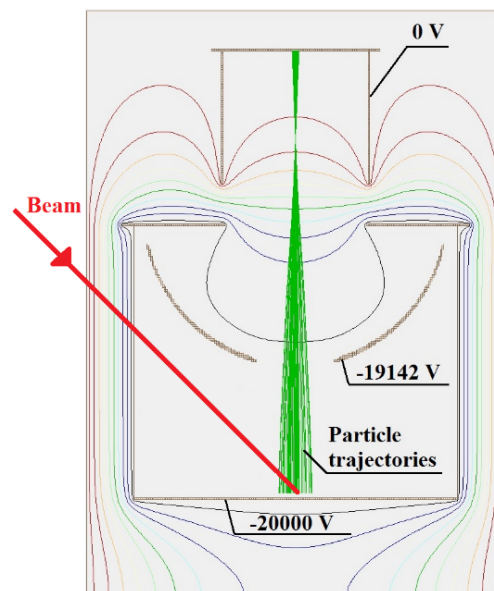
Figure 3.1: A 2D axially symmetric simulation of particle trajectories and electric potential in the BISE electrostatic lens performed with the Simion software (Voltage contours from blue – 19000 V to red – 1000 V with a step 2000 V).

A 2D axially symmetric model was used to simulate the focusing system. As shown in Fig. 3.1, the simulated structure includes the vacuum chamber and the electrostatic lens. In this first simulation, the hole needed for the beam to enter the focusing system is not considered. Since this hole necessarily breaks the cylindrical symmetry, a careful study is needed to assess its effects on the electric field and, consequently, on the electron trajectories.

3.2 Simulations with COMSOL

COMSOL is a flexible simulation platform, which is used in several fields of physics and engineering. It can be applied, among others, to electrostatics and to the study of particle trajectories inside an electromagnetic field. With COMSOL, very precise and close to reality models can be obtained. Different simulations are included and can be combined together, such as electrostatics and particle trajectories. COMSOL Multiphysics has a large number of advantages in solving physical problems with respect to simpler software programs.

The electric potential in electrostatics is described by the Poisson's equation:

$$\nabla^2 \varphi = - \frac{\rho_f}{\varepsilon},\tag{8}$$

where ∇ is the divergence operator, φ the scalar electric potential field, ρ_f the charge density and ε the permittivity of the medium.

The electric field E is obtained from the potential as:

$$E = - \nabla \varphi \tag{9}$$

To compute the electrostatic potential, COMSOL calculates the electric field on a grid inside a defined volume. The distance between the points in the grid - called "mesh" - can be defined. 2D and 3D simulations are possible. In the next subsections, the results obtained with COMSOL applied to BISE are presented.

3.2.1 Two-dimensional simulations

The first step in the simulations was to create a two-dimensional model. Potentials of -20000 V and -19142 V were applied on the cylinder and on the spherical segment of the focusing system respectively. For the 2D model, axial symmetry is assumed. Figure 3.2 shows that the 2D calculations of the model produce a nonphysical behaviour of the potential map. The -19000 V contour line is curved between two parts of the spherical segment. Such behaviour influenced particle trajectories and the localization of the focusing point. The hole, which allows the beam enter the focusing system, is not considered in these simulations.

Unfortunately, in the 2D model the program calculates the field of the spherical segment as two unrelated objects. This clearly is unphysical and does not correspond to

reality. With these conditions, the focusing point shifts downwards if compared to the simulation performed with Simion (Fig. 3.1). The spherical segment and the cylinders are continuous surfaces; consequently, improvements are needed. Axial symmetry can be introduced or a full three-dimensional simulation can be performed.
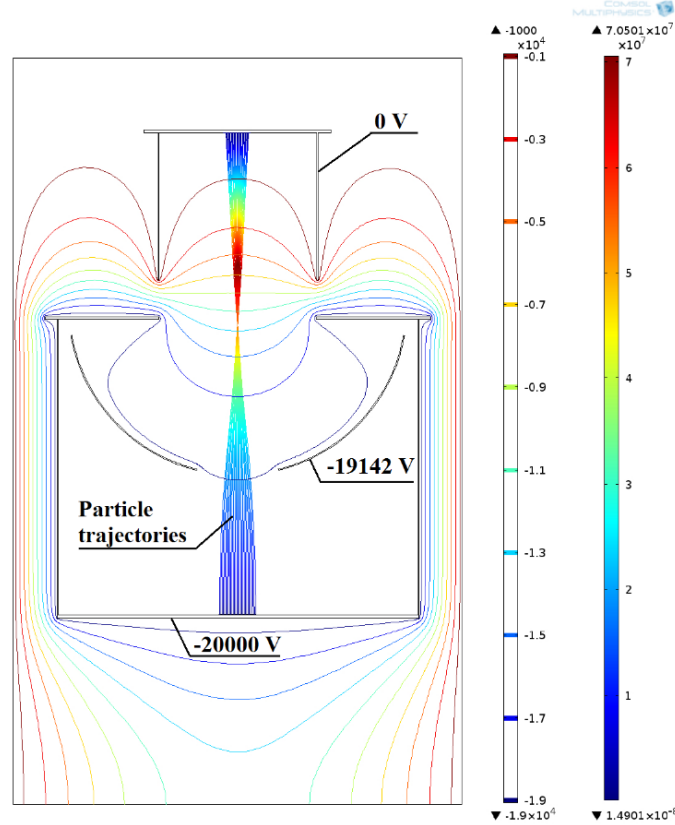
Figure 3.2: Particle trajectories and the electric potential obtained with COMSOL 2D.

3.2.2 Two-dimensional simulations with axial symmetry

Improved simulations using a 2D axially symmetric feature of COSOL were modelled. The goal was to cross check the results obtained with Simion (Section 3.1).

In axial symmetry, an object retains its shape and properties during rotation around an axis of symmetry. In these simulations it was chosen as the vertical axis in the middle of the electrostatic lens passing through the center of the large cylinder and the spherical segment. The downward boundary of the chamber was considered open in the simulation reported in Figure 3.2. Since this condition is unphysical and the chamber is actually closed, this simulation was improved by introducing a finite boundary. The result is shown in Figure 3.3.

The results of the inner voltage contour and particle trajectories were similar to the 2D axial symmetric simulations in Simion (Fig. 3.1). In particular, the focus point is located at the same position.

Unfortunately, 2D axial symmetry as well as 2D symmetry did not allow simulating the hole in the -20000 V cylinder. For this reason, a full 3D realistic model was developed. It included the vacuum chamber together with the electrostatic lens.
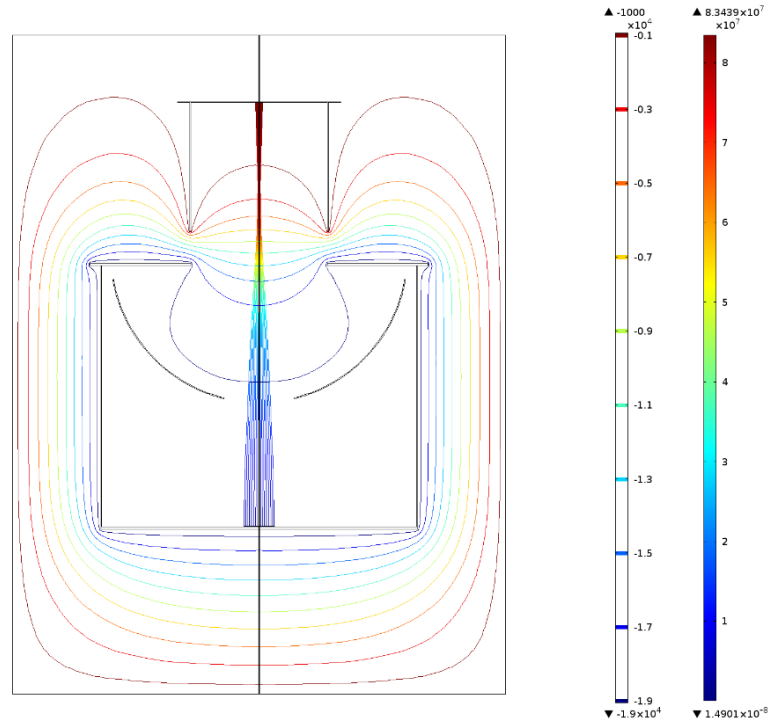
Figure 3.3: Particle trajectories and the electric potential obtained with COMSOL 2D axially symmetric simulations.

3.2.3 Three-dimensional simulations

There are several advantages to use the 3D COMSOL simulation tool, such as automation and the interactive analysis interface. With COMSOL, it is possible to create a realistic model including material and physical properties (temperature, geometry, pressure, etc.).

Using a 3D model, it was possible to include the beam tube hole in the electrostatic lens. It was also important to simplify the model during simulations. Initially the cylindrical form of the vacuum chamber had been recreated due to the dependence of the electric field (and consequently of the particle trajectories) on the size of the chamber (Figures 3.4 and 3.5). Seeing the results, it was decided to model the complete form of the vacuum chamber including the entry and exit flanges for the beam.

The COMSOL 3D full design of BISE was built on the basis of the engineering CAD (Computer-Aided Design) drawings (Appendix A). As can be seen in Figures 3.6 and 3.7, the full design of the vacuum chamber and electrostatic lens were considered. Particle trajectories were curved due to the presence of the hole. The field uniformity inside the chamber affects strongly the charged particle trajectories inside the electrostatic lens (Fig. 3.8). These simulations clearly put in evidence the need for an improvement of the focusing system.

To improve the symmetry of the electric field broken by the beam hole, adding a second oval hole at the opposite side of the electrostatic lens was considered. This second hole could compensate the perturbation induced by the first hole. The results are reported in Appendix B. Figure B.1 shows that the second hole has an influence on the

image of the beam. The original oval shape of the beam was distorted (Appendix B: Figure B.2).

It was then considered to add four oval holes disposed crosswise (Appendix B: Figure B.3). Also in this case, the original oval shape of the beam resulted in a distorted image (Appendix B: Figure B.4).

Following these attempts, it was eventually decided to close the beam hole with the thin 1000 Å aluminium foil to restore the cylindrical symmetry of the electric field still allowing the beam to pass through with minimal perturbation. This approach required studding additional particle trajectories of the secondary electrons emitted from this added foil. These electrons could reach the sensor and have negative implications on the observed image. Such simulations were performed and the results are shown in Figures 3.9 and 3.10. As one can see from the simulations, secondary electrons produced in the first aluminium foil do not influence the image of the beam in the sensor since they are fully stopped at the spherical segment. Furthermore, the original oval shape of the beam was not distorted after focusing, as shown in Figure 3.11. Following the results of these simulations, it was decided to close the beam hole with a thin foil as presented in Figures 2.8 and 4.6. This improvement was substantial, as described in the next chapter.

Discharges could happen while applying high voltage on the electrostatic lens. For this reason, possible areas of discharge in the electrostatic lens were studied. As can be seen in Figure 3.12 these areas are almost confined on the edges of cylinders, where the electric field if maximal. The effects of discharges are anyway minimal since no dark spots due to discharges were found in several visual inspections performed by BISE.
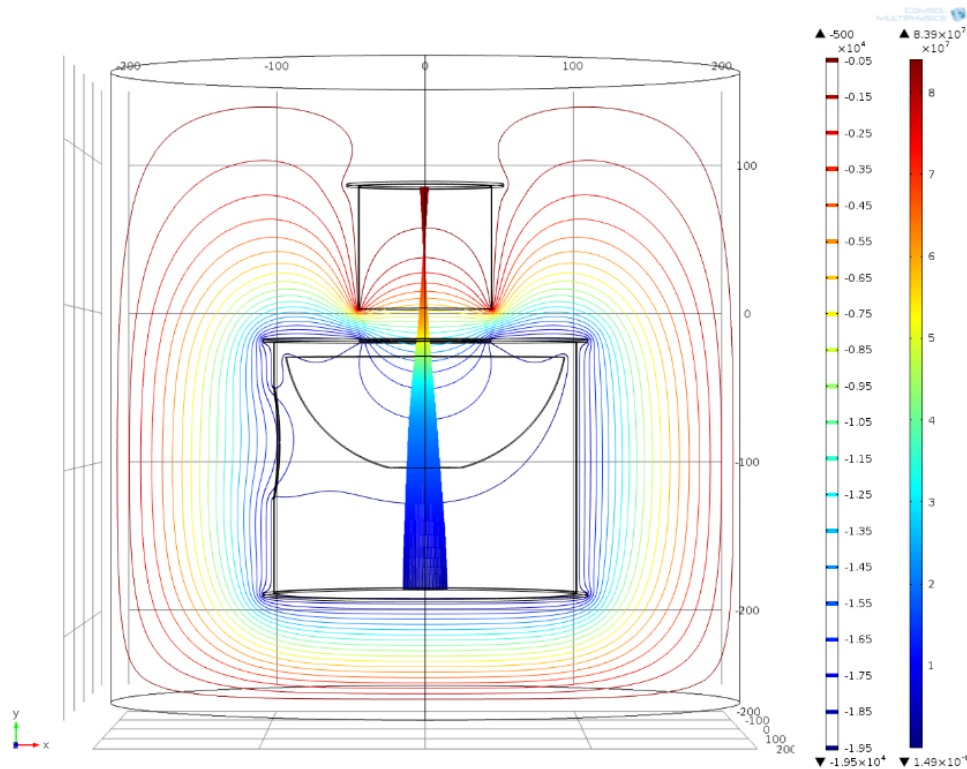
Figure 3.4: COMSOL 3D simulation of the particle trajectories and electric potential contours inside a large cylinder for the vacuum chamber. The electrostatic lens includes the beam hole.
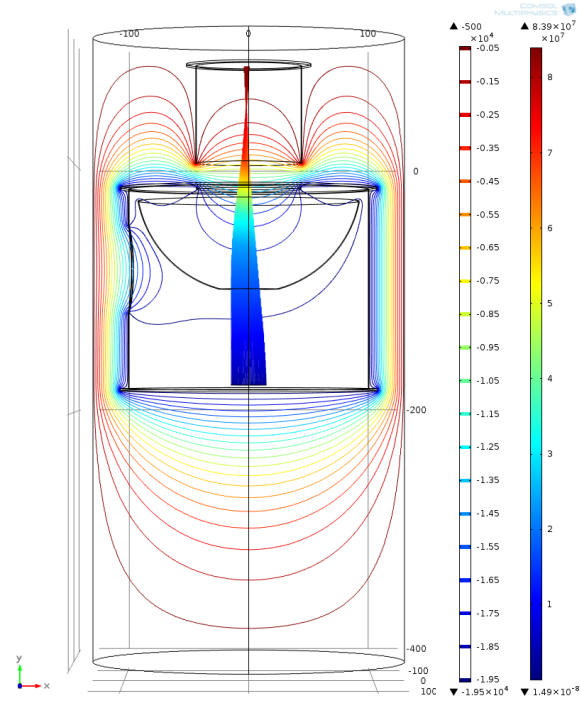
Figure 3.5: COMSOL 3D simulation of the particle trajectories and electric potential contours inside a realistic cylinder for the vacuum chamber. The electrostatic lens includes the beam hole.
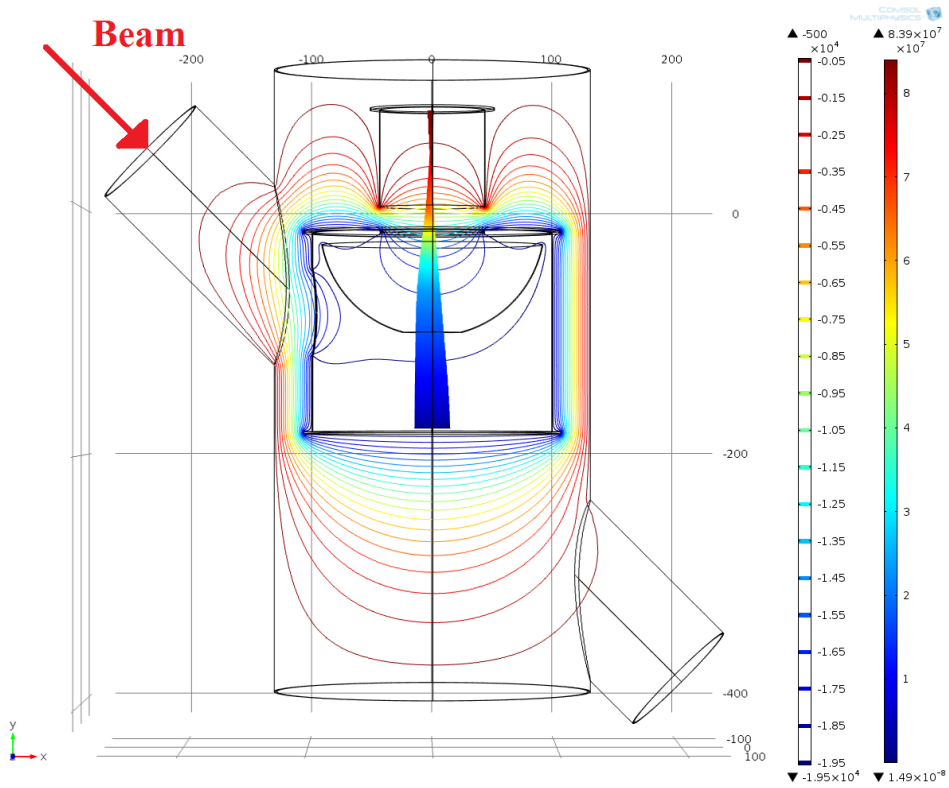
Figure 3.6: COMSOL 3D full simulation of the particle trajectories and electric potential contours inside the vacuum chamber and the electrostatic lens with the beam hole.
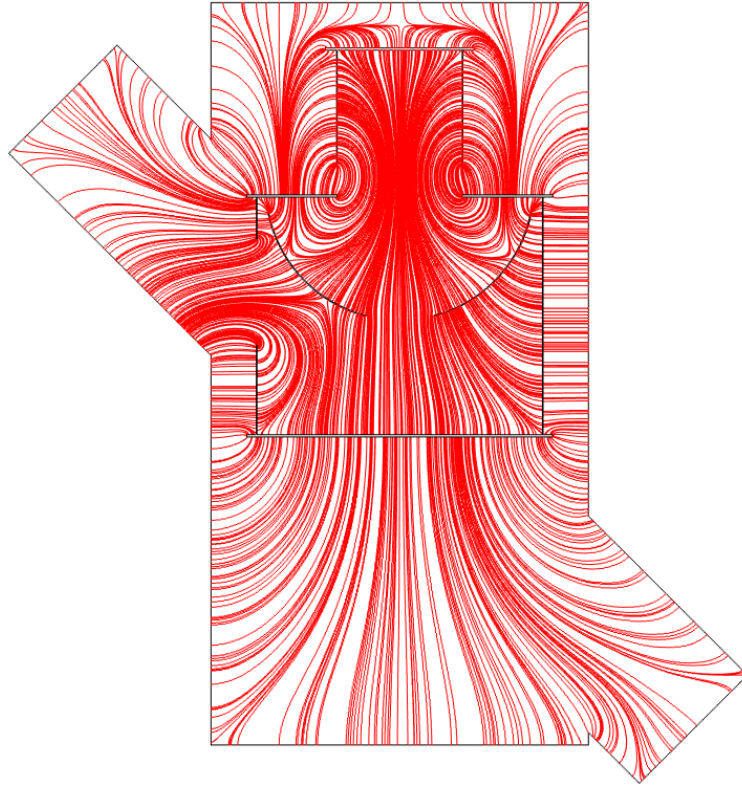
Figure 3.7: The electric field lines in the vacuum chamber with the beam hole.
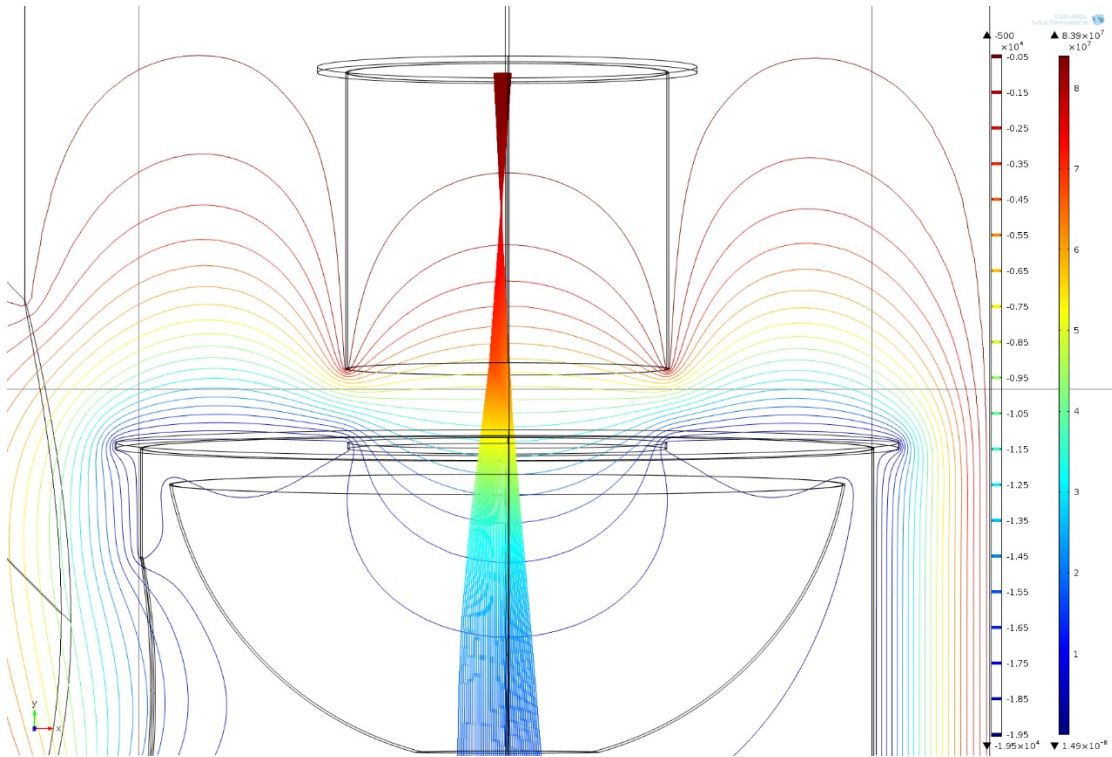
Figure 3.8: Zoomed COMSOL 3D full simulation of the electric potential contours and the curved particle trajectories inside the vacuum chamber and the electrostatic lens with the beam hole.
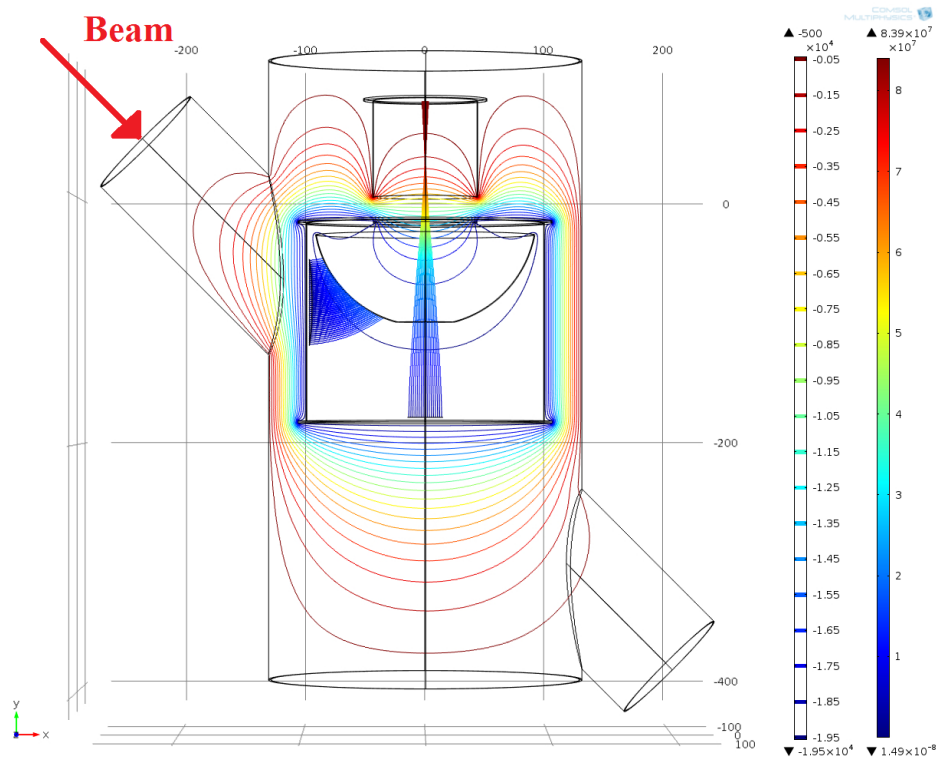
Figure 3.9: COMSOL 3D full simulation of the particle trajectories from the first and second aluminium foils. The beam hole is closed with a thin foil. The secondary electrons emitted by this second foil are fully stopped by the spherical electrode and do not spoil the image of the beam.
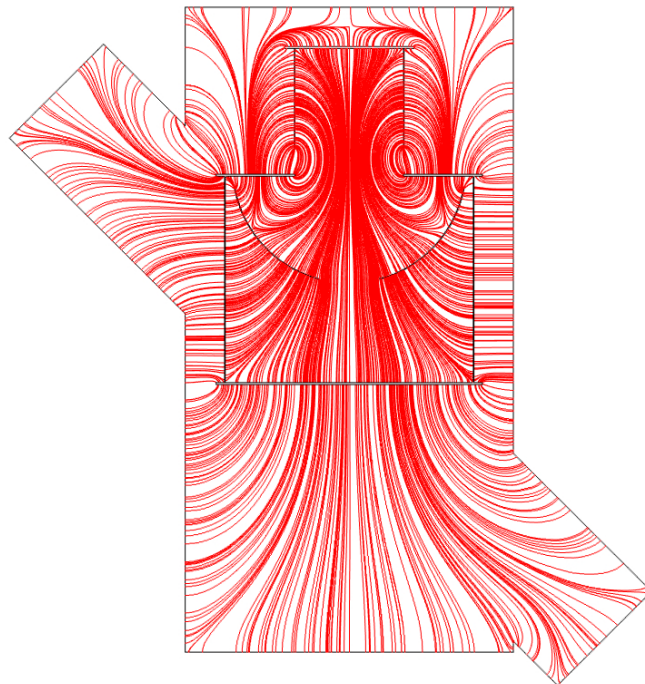
Figure 3.10: Electric lines in the vacuum chamber with the beam hole closed by a thin foil.
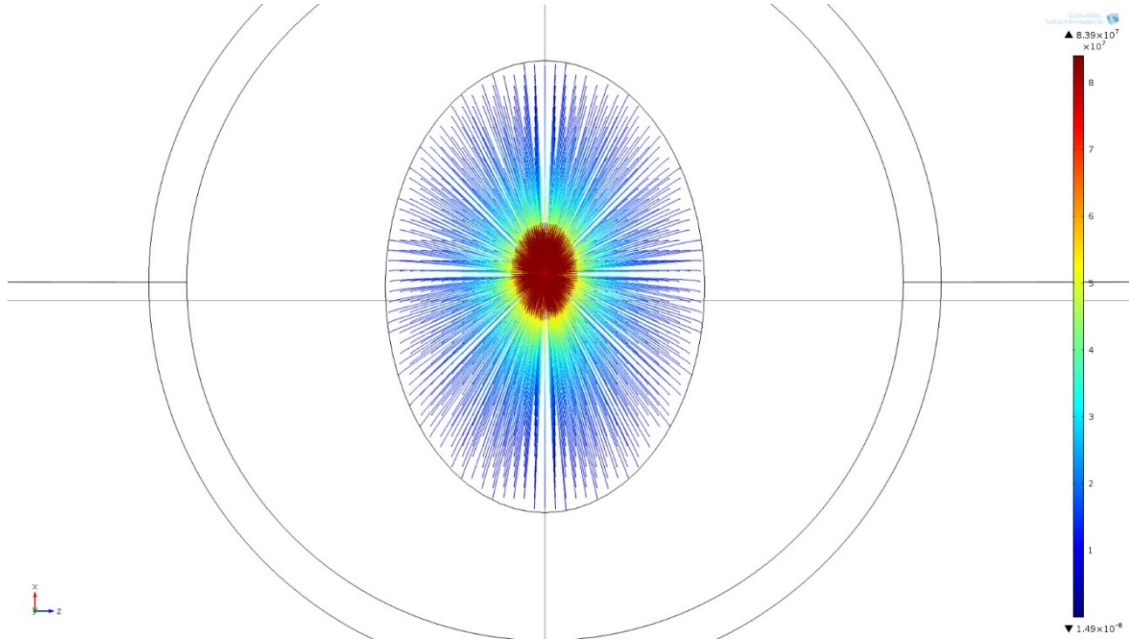
Figure 3.11: COMSOL 3D full simulation of the particle trajectories. Top view from the Figure 3.9. Particles start accelerating from the oval layer (dark blue) and stop on the phosphor screen (dark red). The closed beam hole is located at the bottom of the figure. The red spot corresponds to the image of the beam on the phosphor screen.
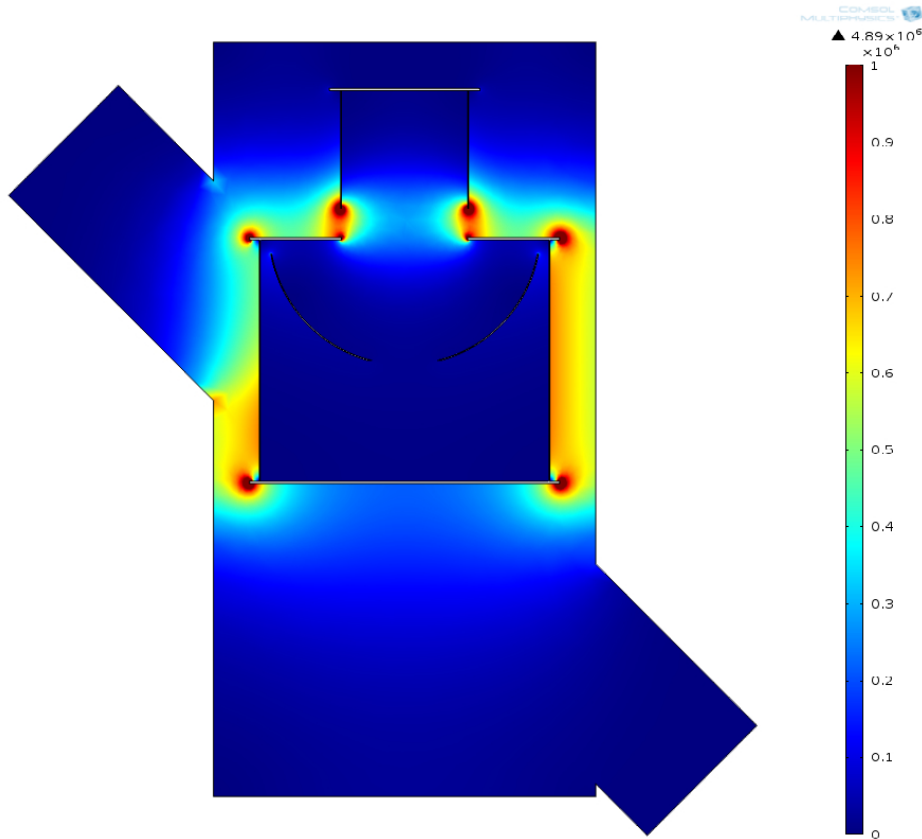
Figure 3.12: COMSOL 3D full simulation of the module of the electric field vector (in V/m) with the beam hole closed by the thin foil.

3.3 COMSOL and Simion: a comparison

Computer simulations are efficient tools for solving particle detector design problems. Unfortunately, primary simulations in Simion were performed only using the 2D axial symmetrical model. For this reason, only this configuration can be compared with COMSOL.

In both software programs, voltage contours can be set manually or automatically. To adjust results, I defined the lower boundary as infinity. As can be seen in Figures 3.13 and 3.14, good agreement between the two programs is found for the voltage contours. The voltage range is from -19000 V to -1000 V with steps of 2000 V. Particle trajectories are also similar (Figures 3.15 and 3.16) as well as the location of the docusing point.
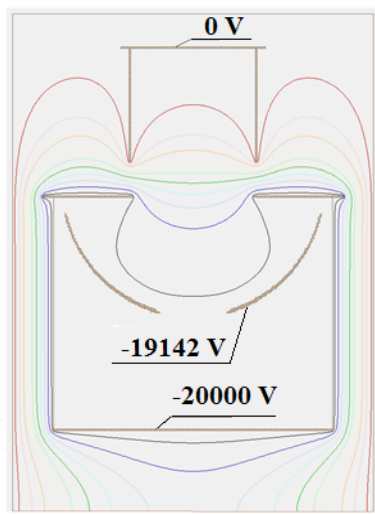
Figure 3.13: Voltage contours in Simion.
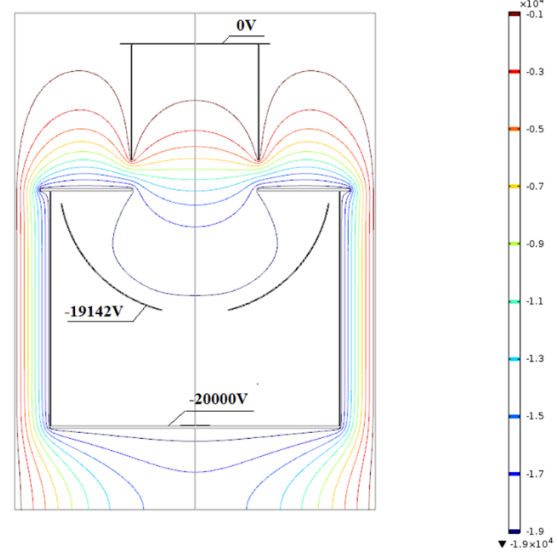
Figure 3.14: Voltage contours in COMSOL.
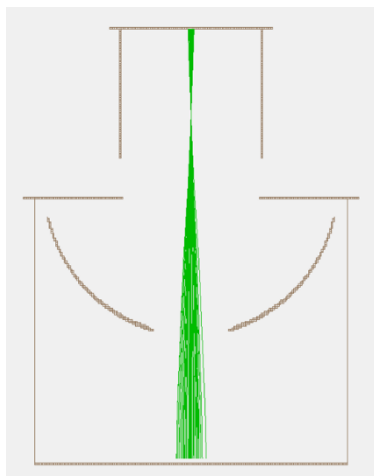
Figure 3.15: Particle trajectories in Simion.
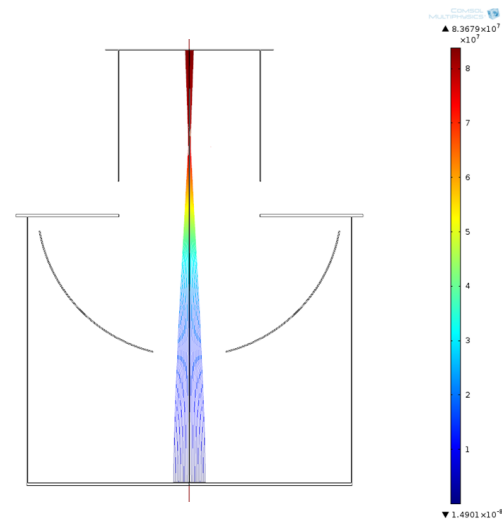
Figure 3.16: Particle trajectories in COMSOL.

Simion is a specific program for studying particle trajectories. In particular, there is the possibility to include a Gaussian distribution of the kinetic energy of the particles.

COMSOL is much more complete and flexible. It allows producing views of a surface or a contour plot, plotting the electrostatic potential, the electric field, the electric displacement field, the polarization field or the electric field distribution normalized to the incident field (Appendix B: Figures B.6 and B.7). Furthermore, it is possible to add arrow or streamline plots which describe more precisely the electric field (Fig. 3.10 and Appendix B: Fig. B.5). On the other hand, it does not allow for Gaussian distributions of the kinetic energy of the particles. Only flat distributions are possible. Anyway, this fact has no influence on the results presented in this chapter.

Chapter 4

Experimental results

The BISE detector was tested with the 18 MeV proton beam of the Bern cyclotron. The beam tests together with the simulations, allowed improving the performances of the apparatus. The beam profile was measured and the intensity of the image produced by the beam was determined as a function of the beam current. The demagnification was also measured and compared with the simulation. The beam tests and the obtained results are reported in this chapter.

4.1 Experimental setup

For the beam tests, three main devices were used:

- BISE
- Faraday cup (FC)
- Pumping system.

The vacuum system developed to BISE independently was not always used, as explained in Subsection 2.3.4. The power of the BTL vacuum system was usually enough to obtain the required vacuum level in relatively short time. When two vacuum systems were used at the same time, the vacuum level was reached faster, but the beam line was unnecessarily longer. The detector was installed on the BTL, as shown in Figure 4.1. Alignment is crucial in any beam line, especially when several devices are used as in the case reported here. For the alignment of BISE and the FC, two laser level devices, one on the ceiling and one the wall, were used (Fig. 4.2). In this way, a precise alignment at the level of a few millimeters was obtained in the two longitudinal directions. The high voltage was applied to the focusing system by means of a power supply (Subsection 2.2.1). The Faraday cup was placed after BISE and was used to measure the beam current. The image formed by the accelerated secondary electrons on the phosphor screen was observed through a glass window flange by means of a CCD camera located outside vacuum. The signal from the CCD camera was sent to a personal computer via a coaxial cable and processed by a frame grabber board and the *MultiCam Studio* program. The cable connection from BTL bunker to the physics laboratory was passed through underground pipes.
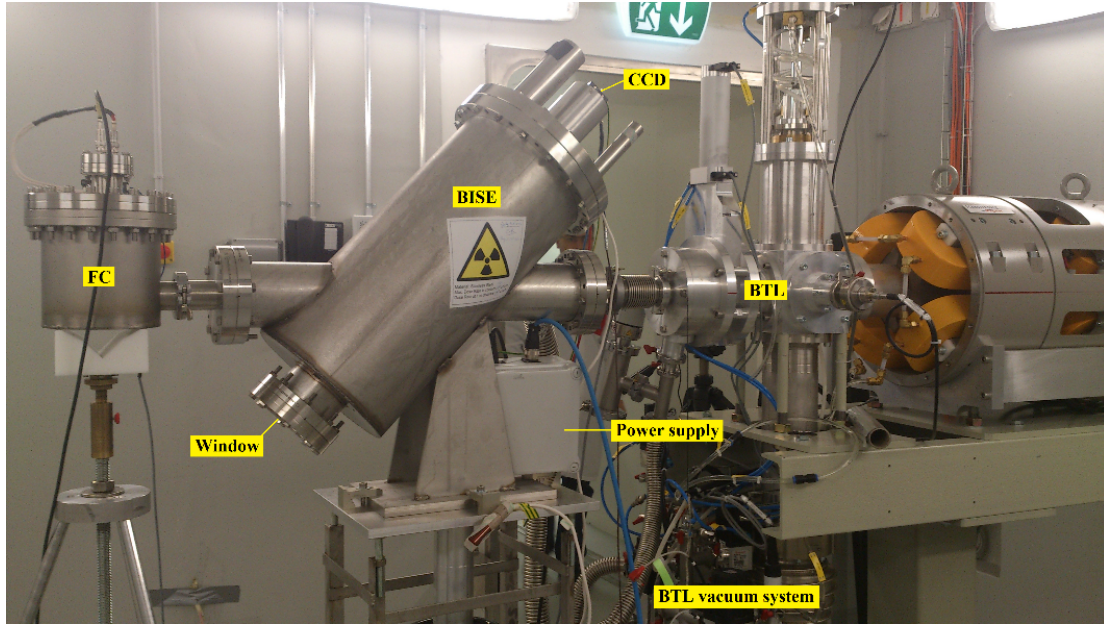
Figure 4.1: The BISE detector installed on the BTL with the Faraday cup (FC) at the end.
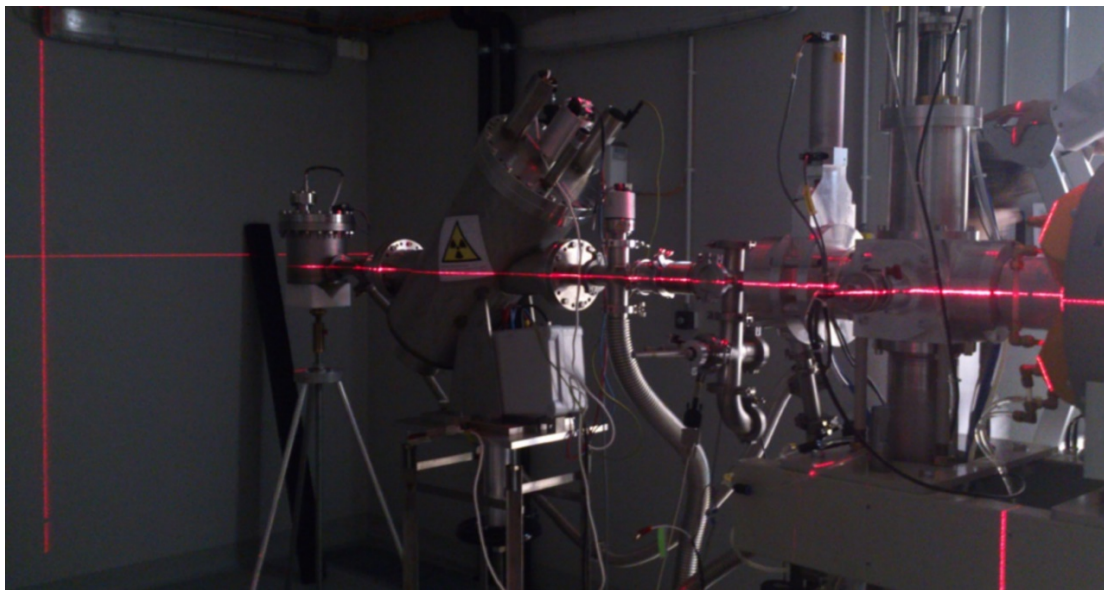
Figure 4.2: Alignment of BISE using two laser level devices installed on the wall and on the ceiling.

4.2 First tests and improvements of the detector

When the BISE detector was moved from CERN to Bern, its electrostatic lens was equipped with a microchannel plate (MCP) [17] detector and phosphor screen. The MCP detector is used to amplify the signal of the secondary electrons in case of low currents (nA or below). With this configuration, the first signals produced by the beam

were observed, as shown in Figures 4.3. During these tests saturated images were obtained. A saturated image could not be used for a quantitative measurement of the intensity. Since, the Bern cyclotron usually provides currents of 100 nA or larger, the MCP was removed after the first tests, as shown in Figure 4.4. After the removal of the MCP, it was verified that detection was possible only with the phosphor screen (Fig. 4.5). These measurements indicated that even currents in the nA range could be detected without the MCP.

As discussed in Chapter 3, simulations in COMSOL showed that the beam hole strongly influenced the trajectories of SEs (Fig. 3.6 and 3.8). Due to the results shown in Figure 3.9, the beam hole was closed with a thin aluminum foil which was fixed using conductive glue (Fig. 4.6). With such improvement of the detector, a uniform cylindrically symmetric electric field inside the electrostatic lens was achieved (Fig. 3.10).
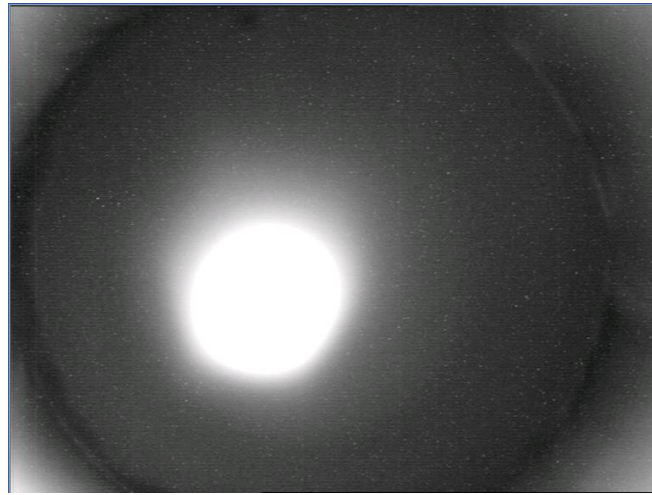
Figure 4.3: Saturated beam image using MCP.
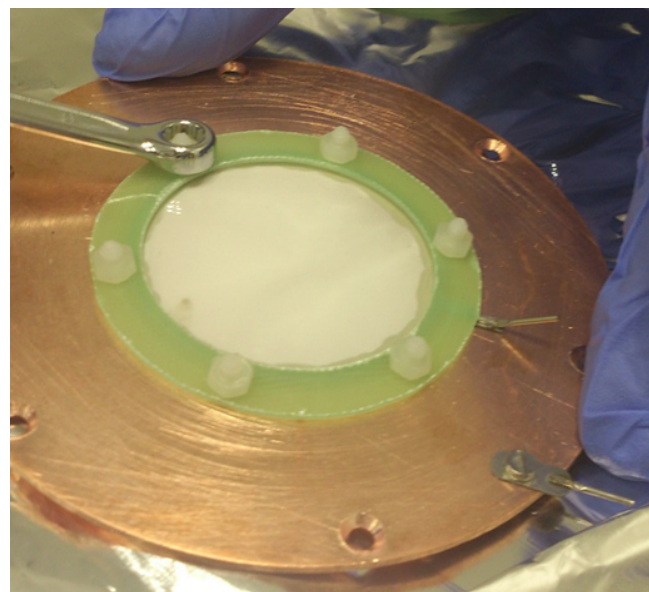
Figure 4.4: Removing the MCP from the electrostatic lens.

Figure 4.5: Beam image on the phosphor screen without MCP.
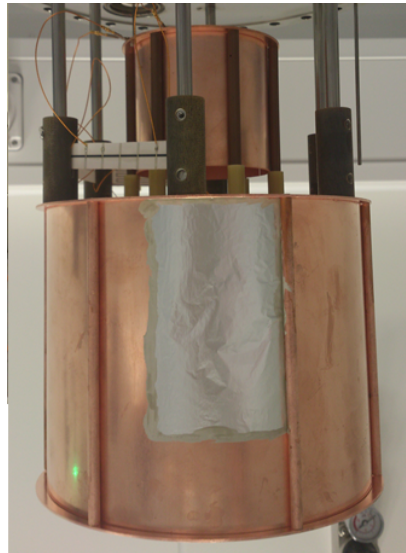
Figure 4.6: Closed beam hole with a thin 0.1 μm (1000 Å) aluminum foil using conductive glue.

4.3 Measurement of the beam intensity

To obtain a quantitative measurement of the beam intensity, data analysis was performed by means of the ImageJ program [18, 19]. Examples of beam images taken at different beam currents and measured by the Faraday cup are presented in Figure 4.7.

The maximum intensity of each image was determined by selecting twenty pixel areas around the maximum. The average was calculated for each of those areas to limit the effect of fluctuations. The uncertainty was calculated as the standard deviation. Currents and their maximum intensities together with uncertainties are reported in Table 4.1. The image intensity versus beam current is presented in Figure 4.8. There is a nonlinear behavior at low currents. To obtain a beam current-intensity relation, a fit was performed using GNUPLOT [20].

For the function, the following power-law dependence was used:

$$y = \sqrt{ax} + bx + c$$

As presented in Figure 4.8, this function reproduces the data well. From the fit, the following parameters were extracted:

- $a = 742.002 \pm 70.54$
- $b = -0.855375 \pm 0.108$
- $c = 52.9744 \pm 3.731$

The reduced chisquare value ($\tilde{\chi}^2$) was found to be 1.09.
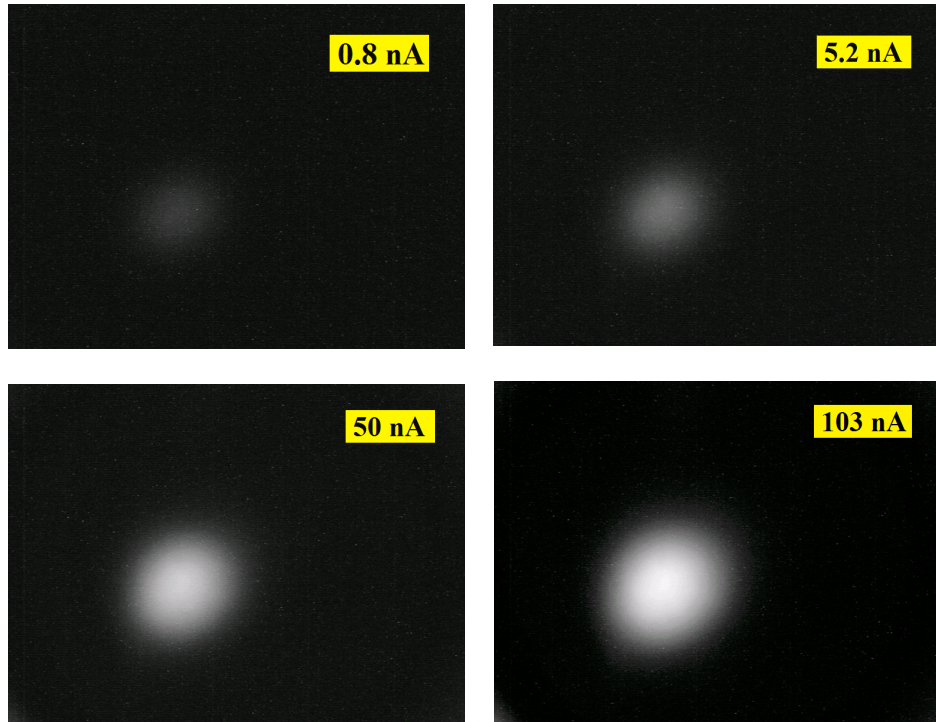
Figure 4.7: Beam images at different currents measured by the Faraday cup.

Current (nA)	Intensity (Arbitrary units)	Current (nA)	Intensity (Arbitrary units)
0.2	59.2 ± 6.0	32	175.0 ± 2.5
0.4	63.8 ± 6.9	39	191.3 ± 2.8
0.8	76.3 ± 7.5	40	194.7 ± 2.8
1.4	86.5 ± 6.7	41	194.7 ± 2.8
5.2	115.5 ± 3.3	50	200.0 ± 2.5
11	133.8 ± 4.8	79	226.0 ± 2.6
23	164.5 ± 3.1	103	242.5 ± 2.3

Table 4.1: Beam intensity and its uncertainty for different currents.
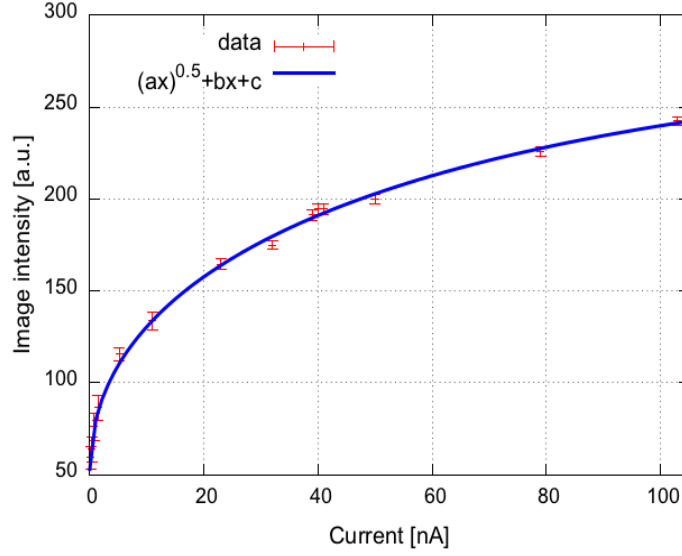
Figure 4.8: Image intensity versus beam current. A non-linear behavior is observed at low intensities. The line corresponds to the power-law fit.

4.4 Measurement of the demagnification

As explained in Subsection 2.2.2, an inverted and demagnified two-dimensional image of the ion beam can be obtained with the BISE detector. The knowledge of the demagnification factor D is crucial to quantify the dimensions of the beam. To measure it, a collimator was installed along the path of the beam. Two different multiple-hole aluminum collimators were used. The idea was to produce several secondary beams emerging from the holes of the collimator and to evaluate the distances of these beams in the image obtained with BISE.

A schematic view of the first collimator with five holes is presented in Figure 4.9. The non-symmetric position of the holes was chosen to recognize the inverted image on the phosphor screen. The collimator was placed at the beam entry of the BISE, as shown in Figure 4.10.
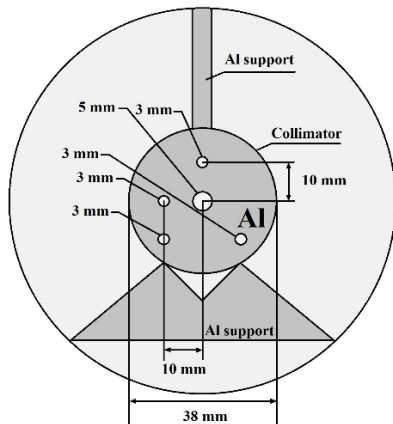
Figure 4.9: A schematic view of a 10 mm thick five-hole collimator.
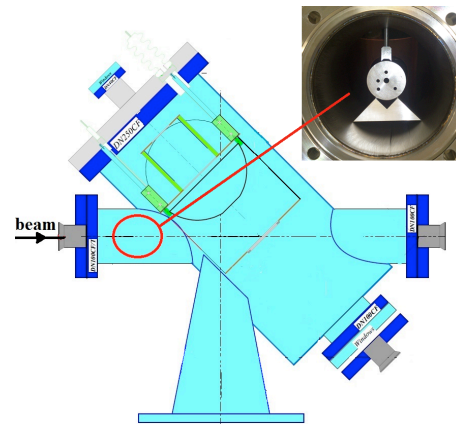
Figure 4.10: Position of the multiple-hole collimator inside the BISE.

Using millimeter paper in front of the CCD camera (Fig. 4.11), one can calculate how many pixels correspond to one millimeter. This correspondence is found to be:

1 mm = 14.4 ± 0.1 px.

The simulation provides a value the demagnification factor of the inverted image. It was found to be:

$D_{COMSOL} \simeq 0.212 \pm 0.005$.

Furthermore, the ratio of major and minor axes was determined as:

$F_{COMSOL} = 1.41 \pm 0.02$.

This result is due to the 45 degrees inclination of the foil and to the fact that distortions are negligible.

The image of the five-hole collimator is reported in Figure 4.12. The analysis of this image was performed using the ImageJ program together with a program I wrote in MATLAB [21].

The dependence of the image intensity on X and Y axes are shown in Figures 4.13 and 4.14. The projections are performed according to the lines indicated in Figure 4.12.

With this collimator, the five holes were unfortunately not distinguishable, probably due to the poor resolution. This problem is still under investigation. To obtain an estimation of the demagnification and the ratio between the major and the minor axes in these conditions, an approximate procedure was used. The main signal was supposed to be at the center of the image due to the central hole. The border of the image was supposed to occur due to the circular border of the collimator. With these assumptions, the *image* length x' (y') was taken as a distance on the X (Y) axis between the central maximum (due to the central hole) and minimum of the left and right valleys (due to the border of the collimator). Two values of x' (y') (right and left) were obtained and averaged. The *object* length x was taken simply as the radius of the collimator.
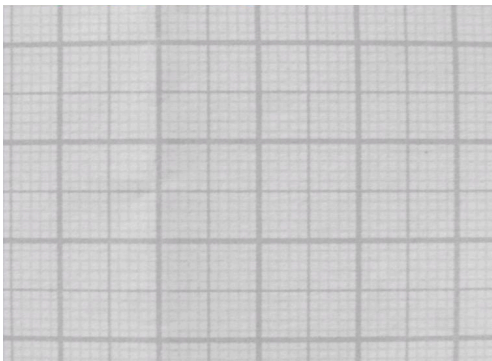
Figure 4.11: Millimeter paper in front of the CCD camera located at the same distance as the phosphor screen.
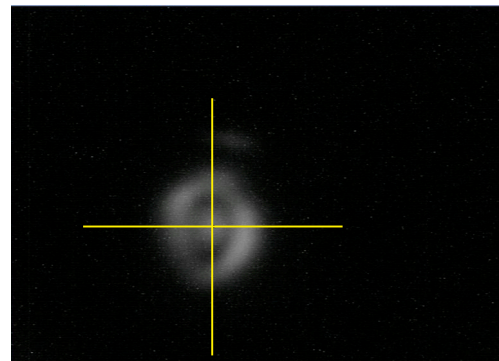
Figure 4.12: Inverted image of the beam obtained with the five-hole collimator. The lines correspond to the projections of Figures 4.13 and 4.14.
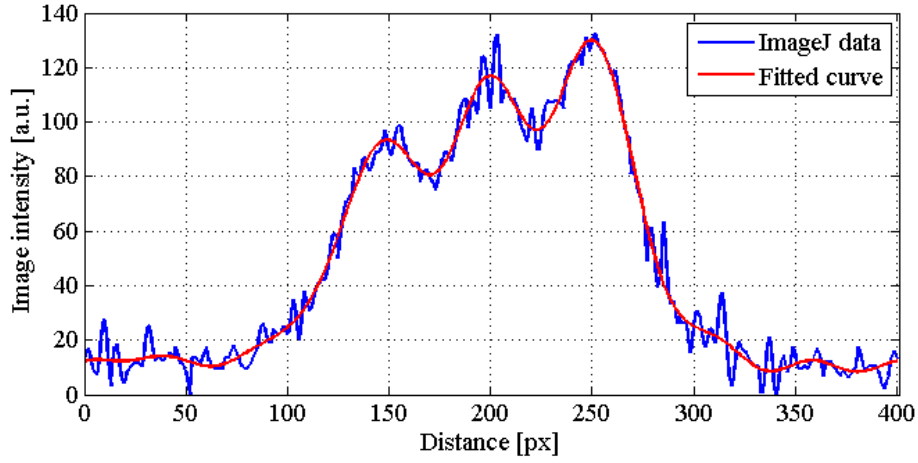
Figure 4.13: Dependence of the image intensity on the distance (X axis).
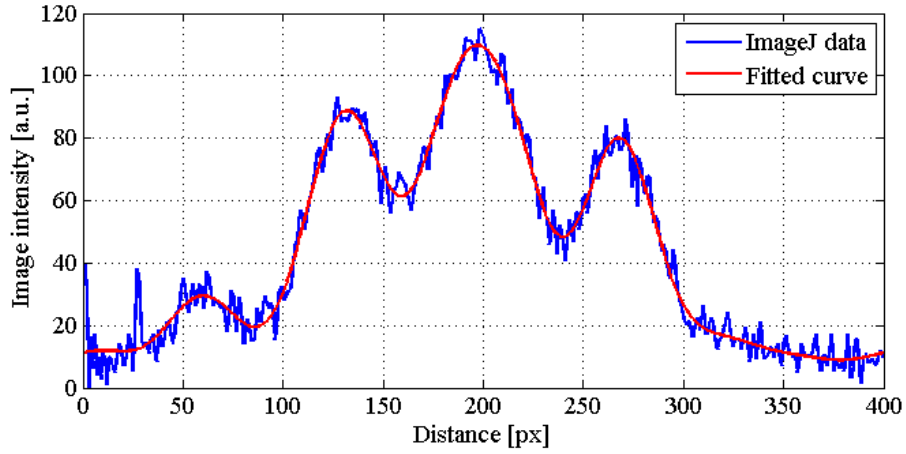
Figure 4.14: Dependence of the image intensity on the distance (Y axis).

With this analysis, the ratio between the major and the minor axes of the image was found to be:

$x' = 1.82 \pm 0.14$ mm, $y' = 2.80 \pm 0.22$ mm, $r_{coll.} = 19 \pm 0.01$ mm

$$F_{exp.1} = \frac{b}{a} = \frac{y'}{x'} = 1.54 \pm 0.17.$$

This result is compatible with the expected value of 1.41.
For the demagnification factor D, it was obtained:

$$D_{exp.1} = \frac{x'}{x} = \frac{x'}{r_{coll.}} = 0.096 \pm 0.007.$$

This value was found to be about two times smaller with respect to the expected value given by COMSOL. For further investigation of this problem, quantitative measurements were needed.

36

For this purpose a simpler three-hole collimator was constructed. This new device was supposed to simplify the determination of the collimator-hole position using the steering and focusing magnets. It was calculated that only one hole could be irradiated at the time and that the beam image should disappear in BISE when passing from one hole to the other.

A schematic view of the second collimator with three holes is presented in Figure 4.15. It was installed at the same place as the first one (Fig. 4.10). It has to be noted that this collimator was larger and no more circular in order to completely stop the beam when not passing through one of the holes.

Beam tests were performed and the beam was focused on each collimator hole. It was verified that images corresponding to single holes could be obtained in a reproducible way. No image was observable when the beam was passing form one hole to the other. The images related to the three holes are reported in Figure 4.16. The intensity of the first image is a bit larger due to the larger diameter of the central hole.
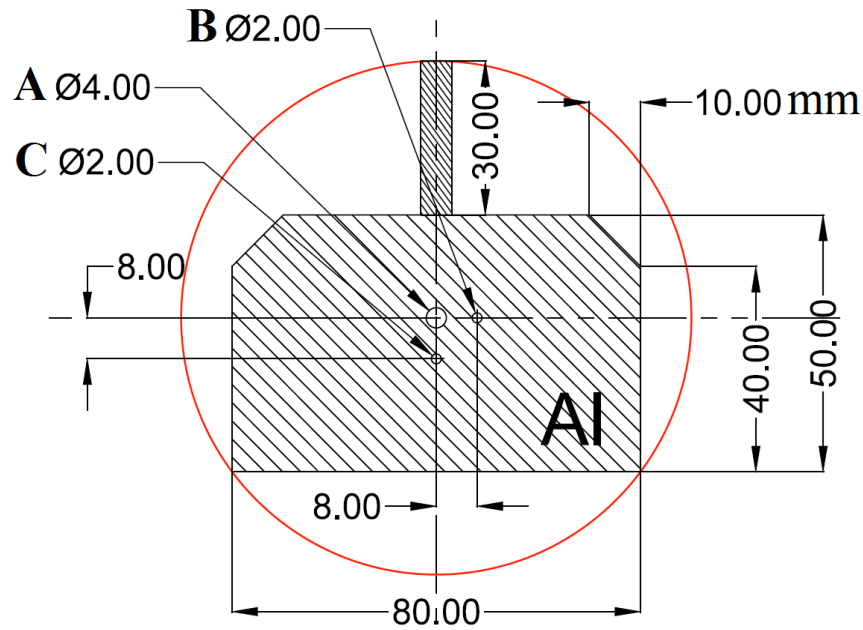
Figure 4.15: Schematic view of the 5 mm thick three-hole collimator.
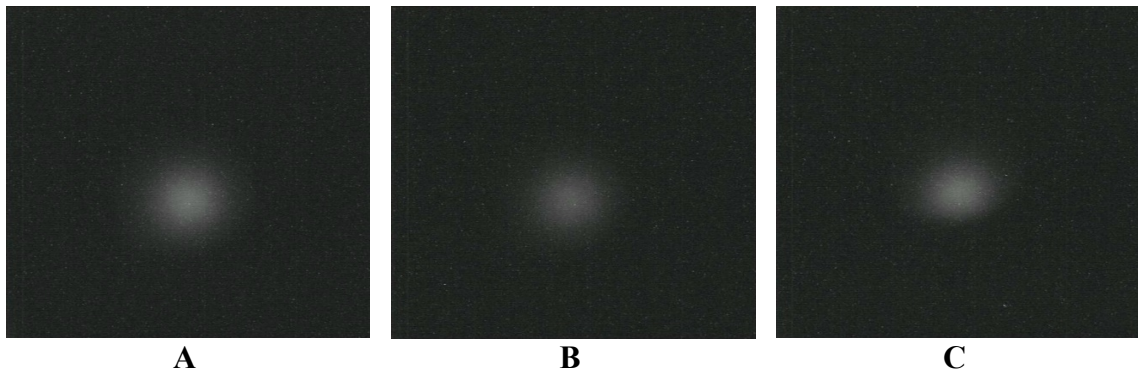
Figure 4.16: Experimental measurements of images corresponding to the three holes of the three-hole collimator.

The position in X and Y axes of the maximum of intensity was obtained for each hole using the ImageJ program. The calculated positions of the maximum intensity of each image are presented in Figure 4.17. The demagnification factor D and the ratio between the major and minor axes F were found to be:

$$D_{exp.2} = \frac{x'}{x} = \frac{A'B'}{AB} \simeq 0.08 \pm 0.02,$$

$$F_{exp.2} = \frac{A'C'}{A'B'} \simeq 1.57 \pm 0.53.$$

A counterclockwise shift of A', B' and C' could be due to the non-perfect leveling of the CCD camera or the multi-hole collimator.

There is good agreement between simulation and experimental results for the major and minor axes ratio F. For the demagnification factor D, this more precise measurements confirms the result obtained with the five-hole collimator and the discrepancy with the expected value by COMSOL. This discrepancy is not understood at present and could be due to non-uniformities of the electric field in the focusing system. This problem is presently under investigation.
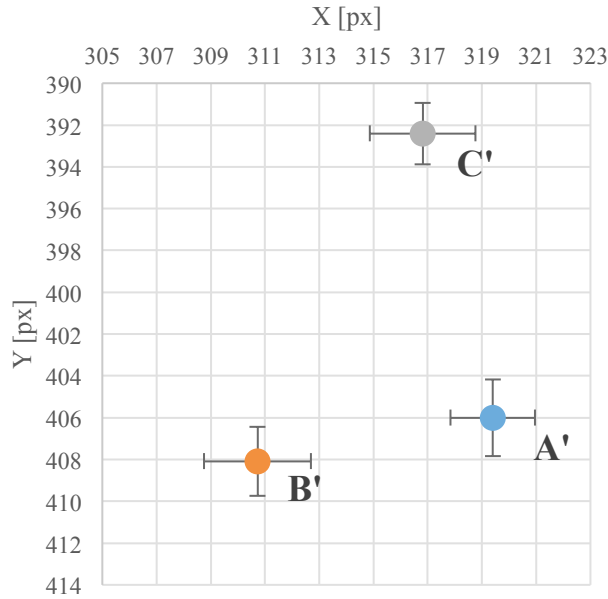
Figure 4.17: Calculated positions in BISE of three holes.

4.5 Beam profile measurement

A beam profile has usually the smooth shape (*top-hat*) of 2D-Gaussian distribution. The beam profile of the 18MeV proton beam was obtained with the BISE detector (Fig. 4.18) and was analyzed by means of ImageJ and MATLAB. Beam profile projections on the X and Y axes are shown in Figures 4.19 and 4.20. A 3D surface plot of the beam is reported in Figure 4.21.

These images can be obtained with BISE on-line. This detector can be successfully used during irradiation without destroying the beam. On-line information on beam intensity, position, and shape is important for an optimal use of the beam. This is the case of medical applications such as radioisotope production and hadrontherapy where extreme care is mandatory.
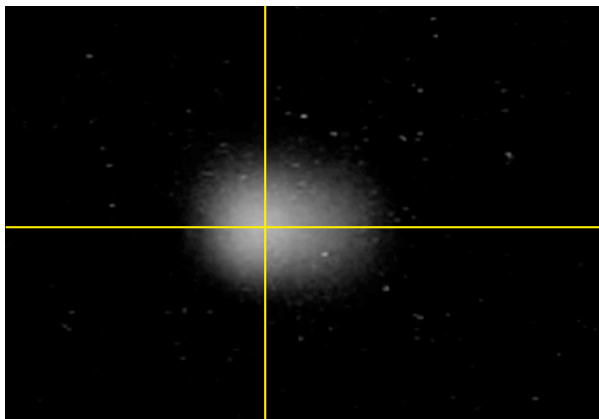
Figure 4.18: On-line beam profile measured with the BISE beam monitor and obtained with the CCD signal on a video monitor. The lines correspond to the projections of Figures 4.19 and 4.20.
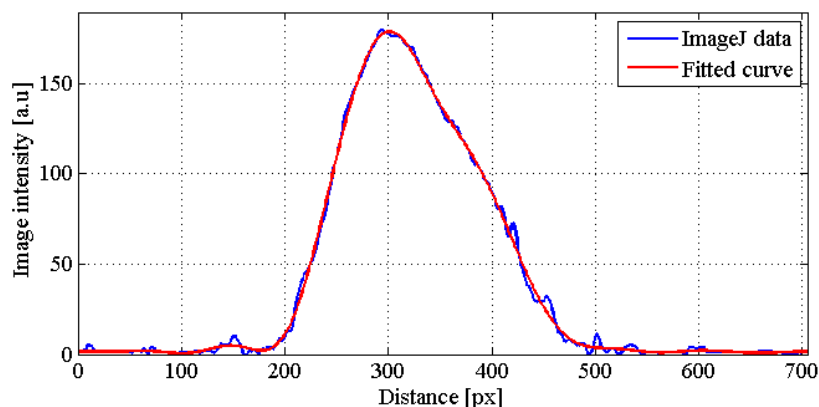
Figure 4.19: Beam profile dependence of the image intensity on the X axis.
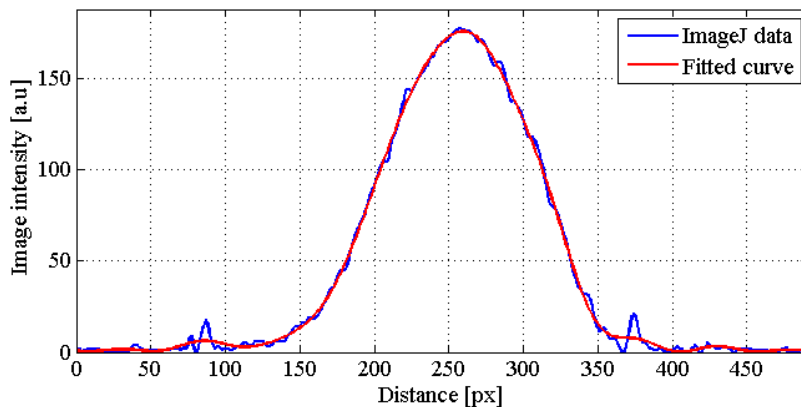
Figure 4.20: Beam profile dependence of the image intensity on the Y axis.
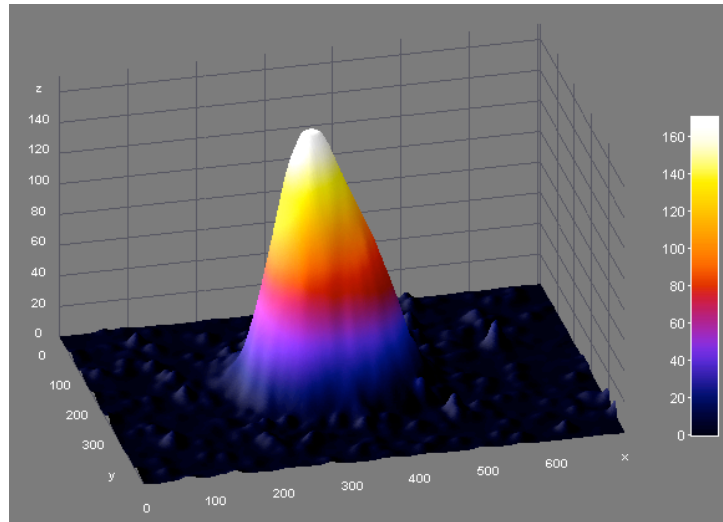
Figure 4.21: 3D surface plot of the beam profile intensity.

Conclusions

This thesis was centered on the development of a BISE detector, which was conceived by the candidate for on-line non-destructive monitoring of accelerated ion beams. This device is based on the detection of secondary electrons produced by the beam when traversing a thin metallic foil.

The BISE detector was studied, improved and tested at the Bern 18 MeV cyclotron laboratory, which provides beams for radioisotope production and research by means of a beam transfer line (BTL).

An independent vacuum system was developed by the candidate to reach high vacuum in the BISE chamber in stand-alone mode. This system is based on specific valves, primary and turbo pumps. Vacuum levels of the order of 10^{-6} mbar were reached, allowing a good functionality of the apparatus.

To simulate the electric field of the focusing system and to optimize the path of secondary electrons, 2D and 3D models using the COMSOL Multiphysics software were developed. These simulations were required for understanding the physics of the focusing system and for improving the performances of the BISE. Improvements included closing the beam entrance hole with a thin aluminum foil and using only a P47 phosphor screen to obtain the image of the beam at high beam intensities.

The BISE was installed in the BTL of the Bern cyclotron. An alignment system based on lasers was developed to assure a correct positioning of the apparatus in the BTL. The intensity of the beam image was studied as a function of the beam current. The dependence between the image intensity and the beam current was found to follow a power-law function. The parameters of this function were determined by means of a fit. This function allows measuring the beam current on-line on the basis of the non-destructive measurements performed by BISE.

The demagnification factor together with the ratio of major and minor axes of the ellipse produced by the beam were estimated with simulations. The demagnification was measured experimentally using a specifically designed multi-hole collimators. These collimators allowed forming secondary beams at known distance in the sensing foil of BISE. The measurement of the demagnification factor is found to be two times smaller with respect to the value expected in the simulations. The reason of this discrepancy is not known and will be the focus of further studies. This effect could be due distortions produced in the path of the electrons by the focusing system. Good agreement between experimental data and simulation is found for the ratio between the major and minor axes of the image produced by the beam. The beam transverse profile was measured and studied with several settings of the BTL. In particular, focusing and defocusing effects can be visualized on-line with BISE.

The BISE detector is a powerful instrument and is suitable for most beam lines. It allows non-destructive on-line monitoring of the intensity, position and shape of the beams. It can be used in medical applications to control beams in different intensity ranges, as in the case of cancer hadrontherapy or of radioisotope production. The work, performed in this Master thesis, allowed to substantially improve the prototype including in particular the realization of the vacuum system, simulations in COMSOL,

the alignment of the BISE detector in the beam line, and beam tests as well as the data analysis. Furthermore, this work may open the way to developments, future applications and, eventually, to the industrialization of the device.

Acknowledgements

References

[1]   L. Badano, *Development of a Novel Beam Monitor for Real-time Measurements of Hadrontherapy Beams*, 2005, Louis Pasteur: Strasbourg.

[2]   S. Braccini, A. Ereditato et al., *The new Bern cyclotron laboratory for radioisotopes production and research*, International Particle Accelerator Conference (IPAC), 2011: San Sebastian, Spain, p. 3618-3620.

[3]   COMSOL Multiphysics (FEA), URL *http://www.comsol.com/*, 2014.

[4]   A. Degiovanni, S. Braccini, E. V. Kirillova et al., *Emittance measurements at the Strasbourg TR24 cyclotron for the addition of 65 MeV linac booster*, 2013, Vancouver, Canada.

[5]   S. Braccini, A. Ereditato, E. Kirillova et al., *An innovative on-line beam-monitoring detector based on the emission of secondary electrons,* International Conference on Translational Research in Radiation Oncology / Physics for Health in Europe. 2014. Geneva, Switzerland: Radiotherapy & Oncology, **110**.

[6]   S. Braccini, *Particle Accelerators and Detectors for medical Diagnostic and Therapy*, 2013, LHEP: Bern.

[7]   U. Raich, *Beam diagnostics*, *CERN Accelerator School*, 2006, Zeegse, Netherlands.

[8]   S. Braccini et al., *A beam monitor detector based on doped silica and optical fibres*, Journal of Instrumentation, 2012, **44** (19).

[9]   S. Braccini et al., *An Innovative Beam Monitor Detector for the New Bern Cyclotron Laboratory.* Radiotherapy and Oncology, 2012. **102**, Supplement 1: p. S76.

[10]   M. Caccia et al., *Silicon Ultra fast Cameras for electron and γ sources In Medical Applications*, Nuclear Physics B, September 2003, **125** p. 133-138.

[11]   L. Badano et al., *Secondary Emission Monitor for Low-Interception Monitoring (SLIM): An Innovative Nondestructive Beam Monitor for the Extraction Lines of a Hadrontherapy Center*, IEEE Trans. Nucl. Sci., 2004, **51** (6): p. 2990-2998.

[12]   P. Höß, K.Fleder, *Response of very fast decay phosphors in image intensifier tubes for CCD readout devices*, 24th International Congress on High-Speed Photography and Photonics, 2001, Proc. SPIE 4183.

[13]   Simion, URL *http://simion.com/*, 2014.

[14]   H. Rothard et al., *Secondary Electron Yields from thin Foils : a possible Probe for the Electronic Stopping Power of heavy Ions*, Phys. Rev. A, 1990. **41**: p. 2521.

[15]   J. F. Ziegler, M. D. Ziegler, J. P. Biersack, *SRIM – The stopping and range of ions in matter (2010)*. Nuclear Instruments and Methods in Physics Research Section B: Beam Interactions with Materials and Atoms, 2010, **268** (11–12): p. 1818-1823.

[16]   D. A. Dahl, *Simion for the personal computer in reflection.* International Journal of Mass Spectrometry, 2000, **200** (1–3): p. 3-25.

[17]   J. L. Wiza, *Microchannel plate detectors.* Nuclear Instruments and Methods in Physics, 1979. **162**: p. 587 - 601.

[18]   W. Burger, M. Burger, *Digital Image Processing: An Algorithmic Approach Using Java.* 2013, Springer.

[19]   ImageJ, URL *http://rsb.info.nih.gov/ij/*, 2014.

[20]   T. Williams, C. Kelley, *GNUPLOT 4.6*, *An Interactive Plotting Program*, Editor: D. Crawford, 2014.

[21]   A. Gilat, V. Subramaniam, *Numerical Methods with MATLAB*, 2009.

Appendix A

Design of the BISE detector

The following drawings were provided to me by G. Molinari of the TERA Foundation at CERN.
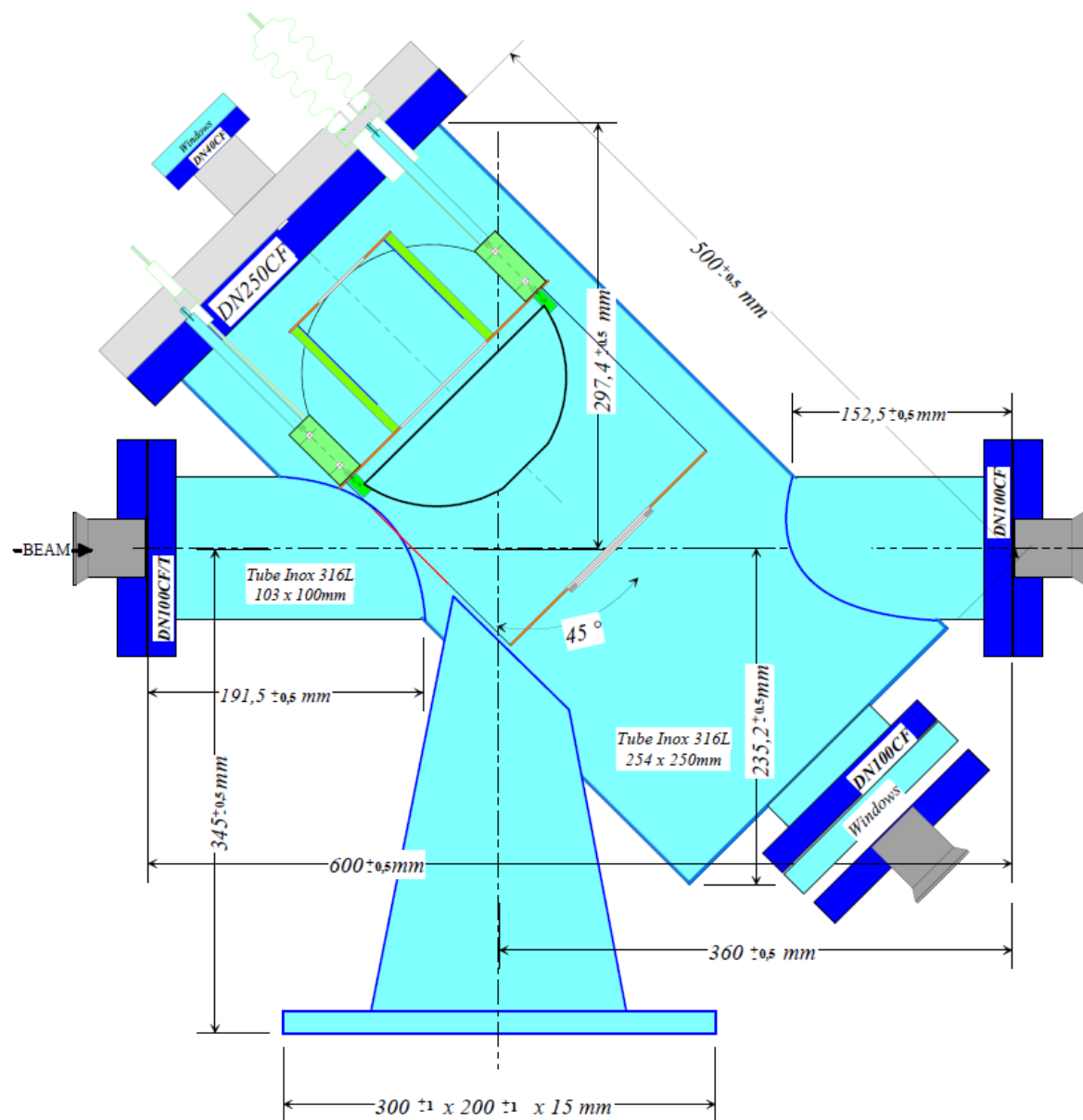
Figure A.1: Design of the vacuum chamber.

Installation tool inox 304L

Φ=6mm L= 400 mm

M2,5x L=5mm

3 x Φ 2.2 /120°

inox 304L
ep.1,5mm

Φ 80 ±0,1

Φ 74 +0,1

Φ 68 ±0,1

M2,5

Φ 96 ±0,1

3 x M2 /120°

Φ 90 ±0,1

Φ 80 ±0,1

inox 304L
ep.1,5mm

Φ 74 +0,1

Φ 68 ±0,1

6

Φ 2,7
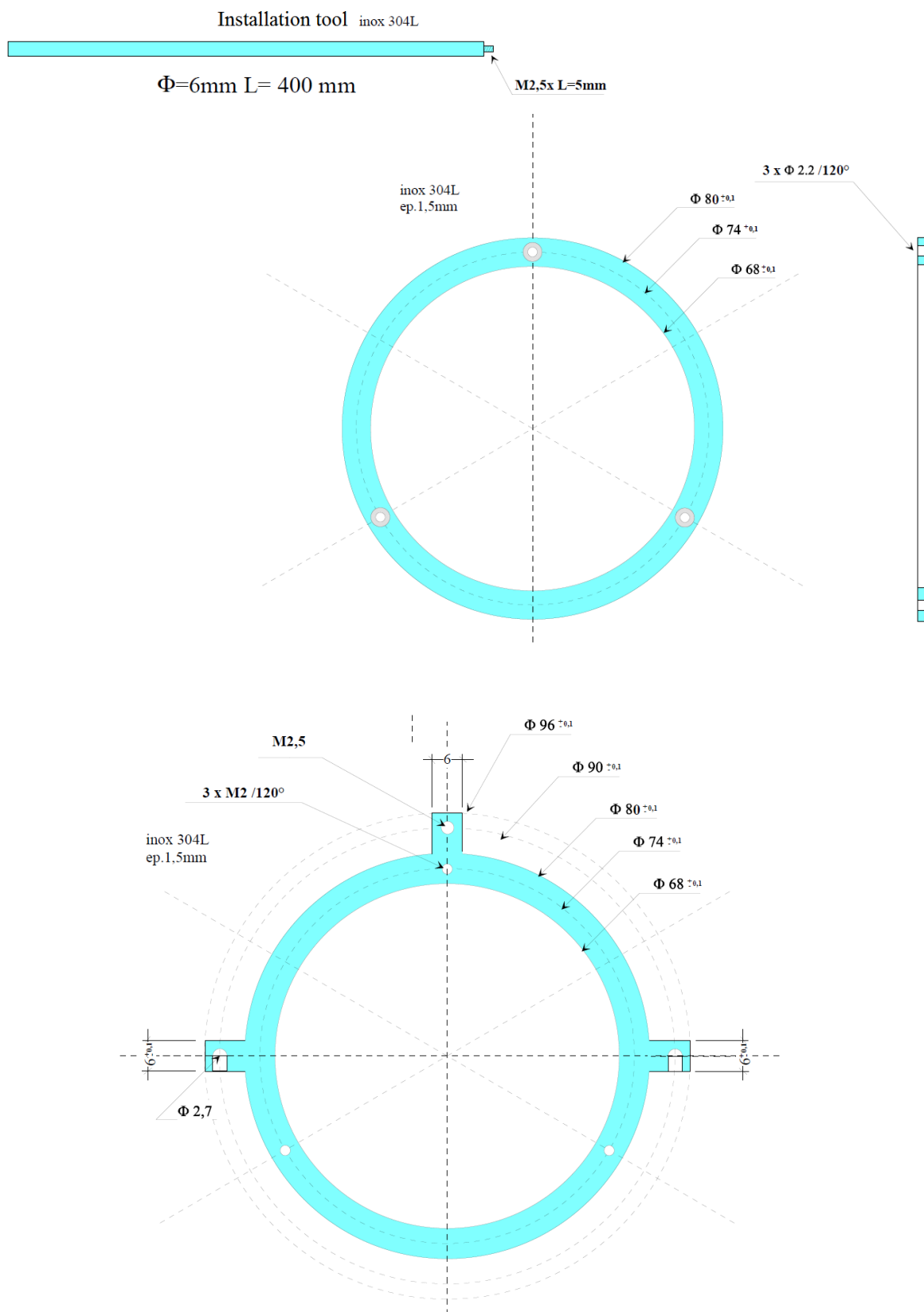
Figure A.2: Support for an Al foil with installation tool.
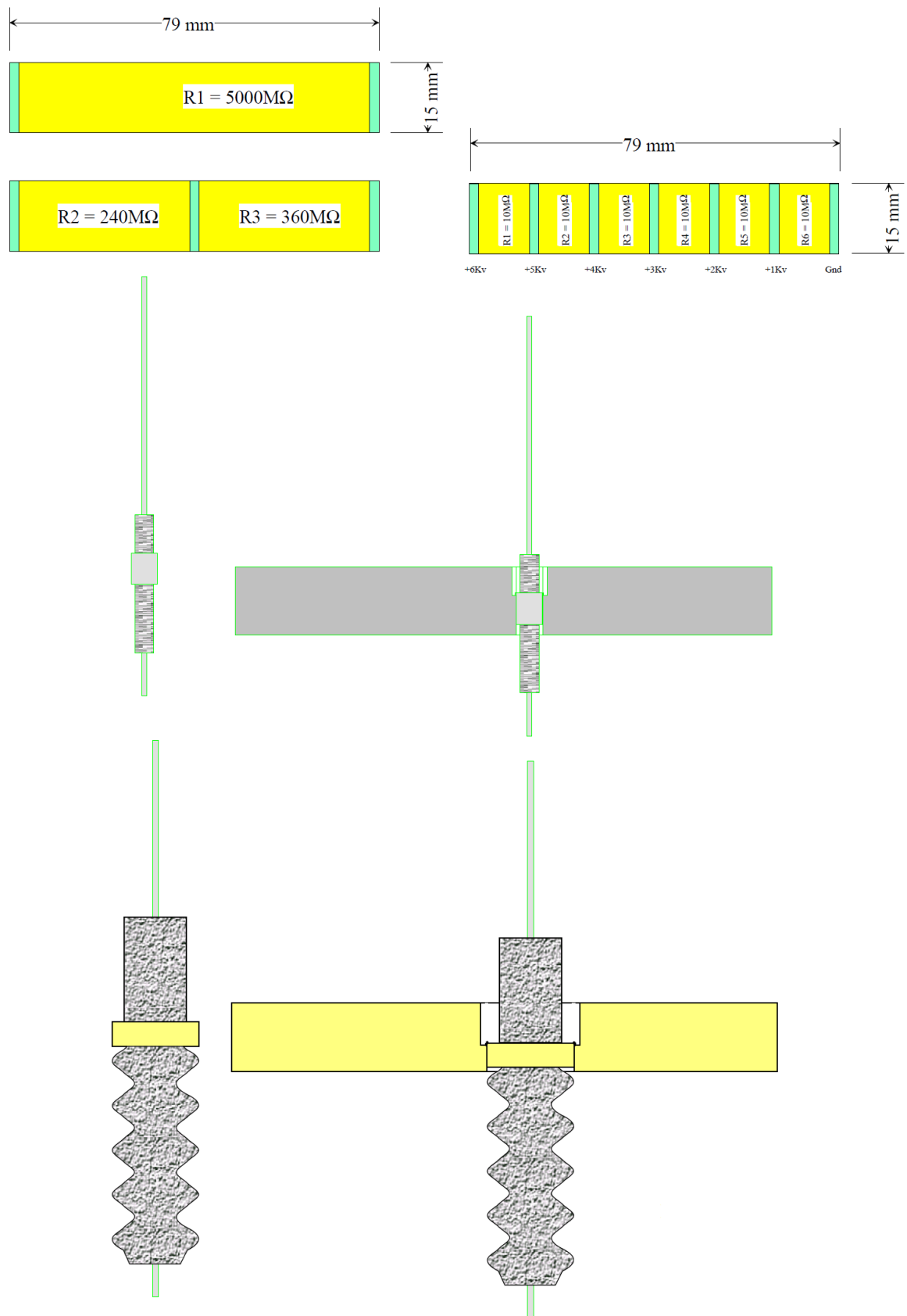
Figure A.3: Bias resistors on ceramic.

Figure A.4: Polarization electrodes and MCP.

Figure A.5: Spare parts of the electrostatic lens: Fiber Glass, copper spacers, plate cylinder.

min 20 mm

in fil

in mcp

in -Hv+fil

$\Phi\ 200\ ^{+}_{-}\ 0,1$

$\Phi\ 182\ ^{+}_{-}\ 0,1$

DN 250

6 x M 4 x 8   60°
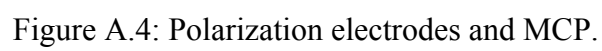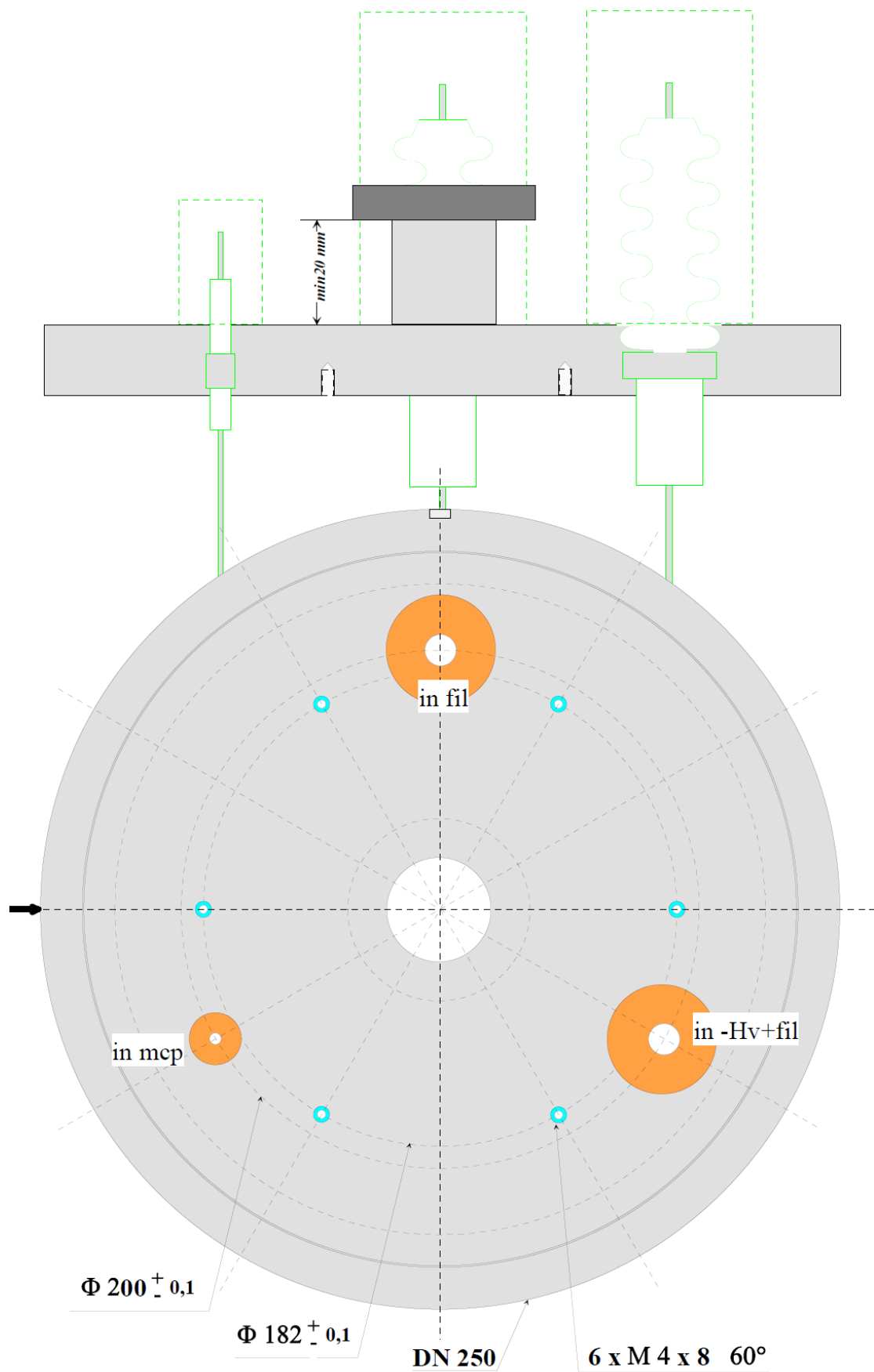
Figure A.6: Flange DN250 of the electrostatic lens.
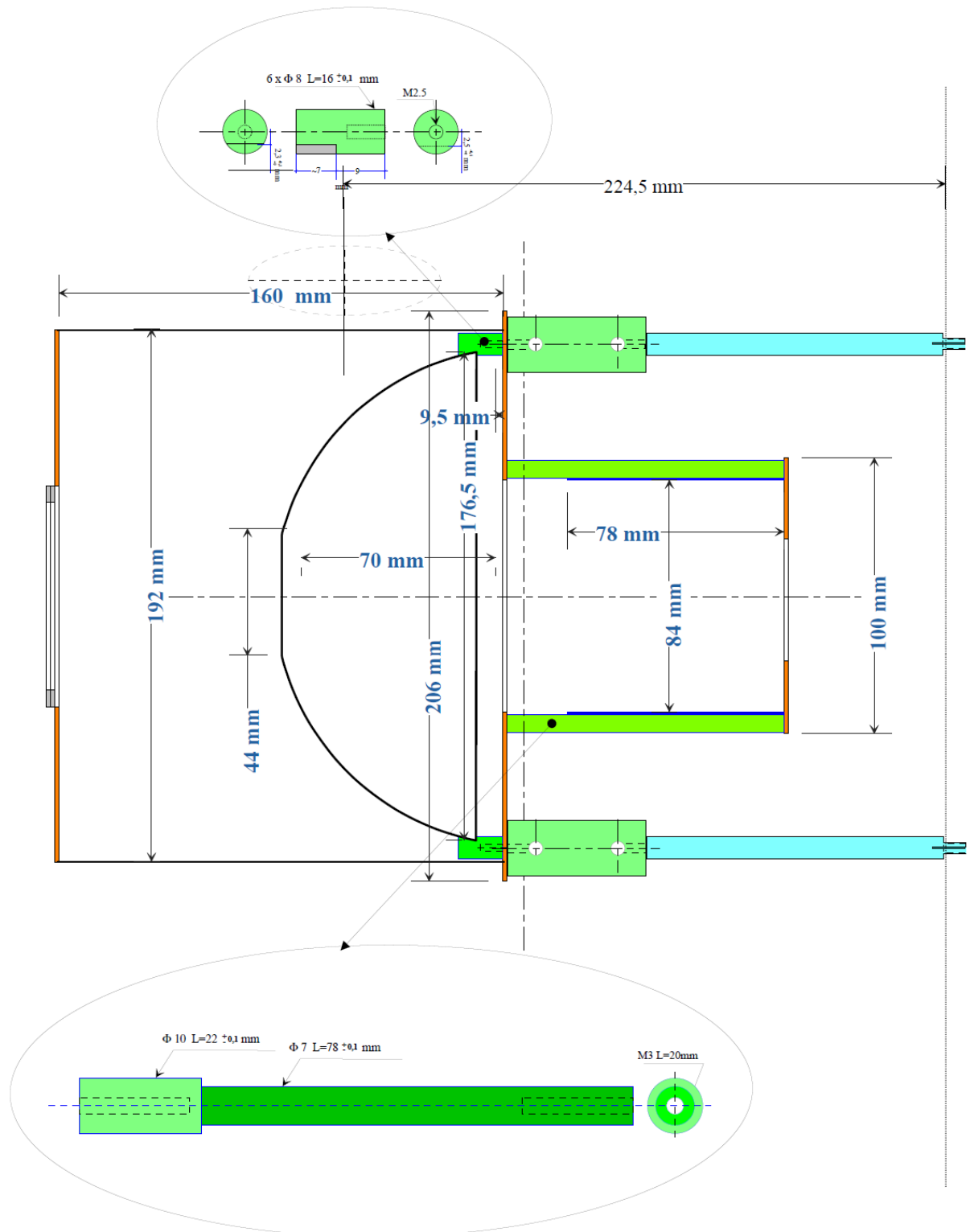
Figure A.7: Scheme of the electrostatic lens.
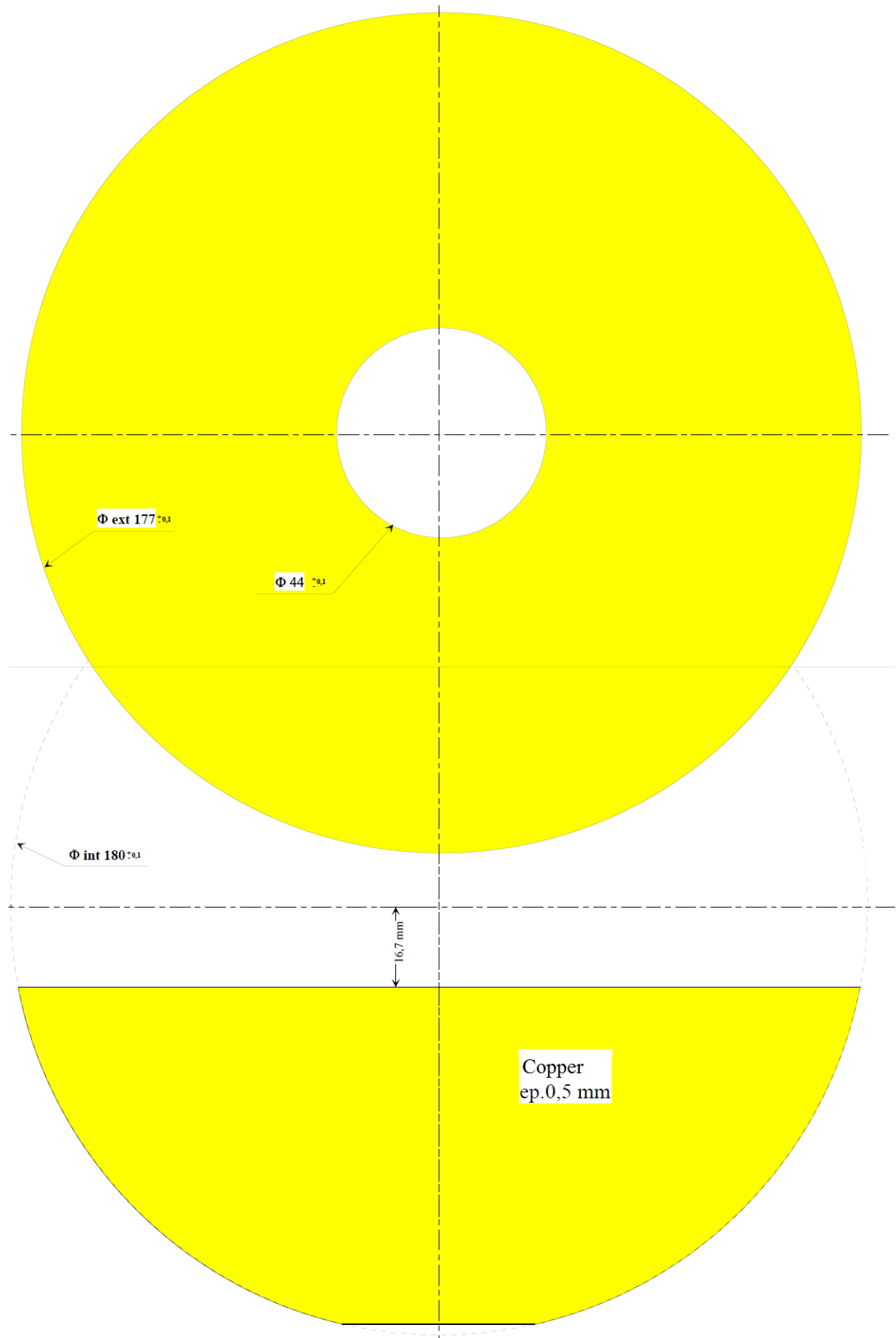
Figure A.8: The spherical segment of the electrostatic lens.
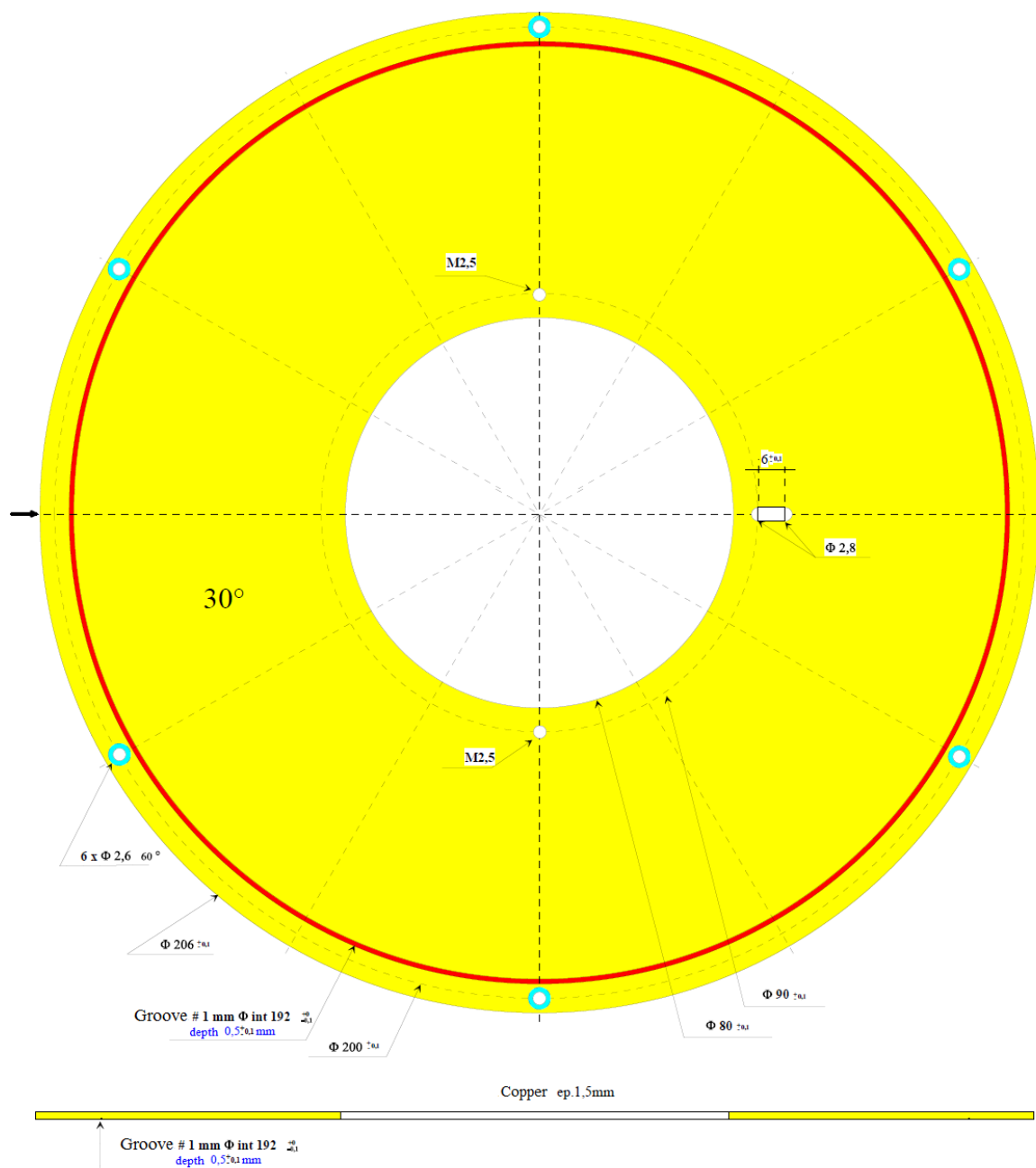
Figure A.9: Bottom of the big electrode cylinder of the electrostatic lens.
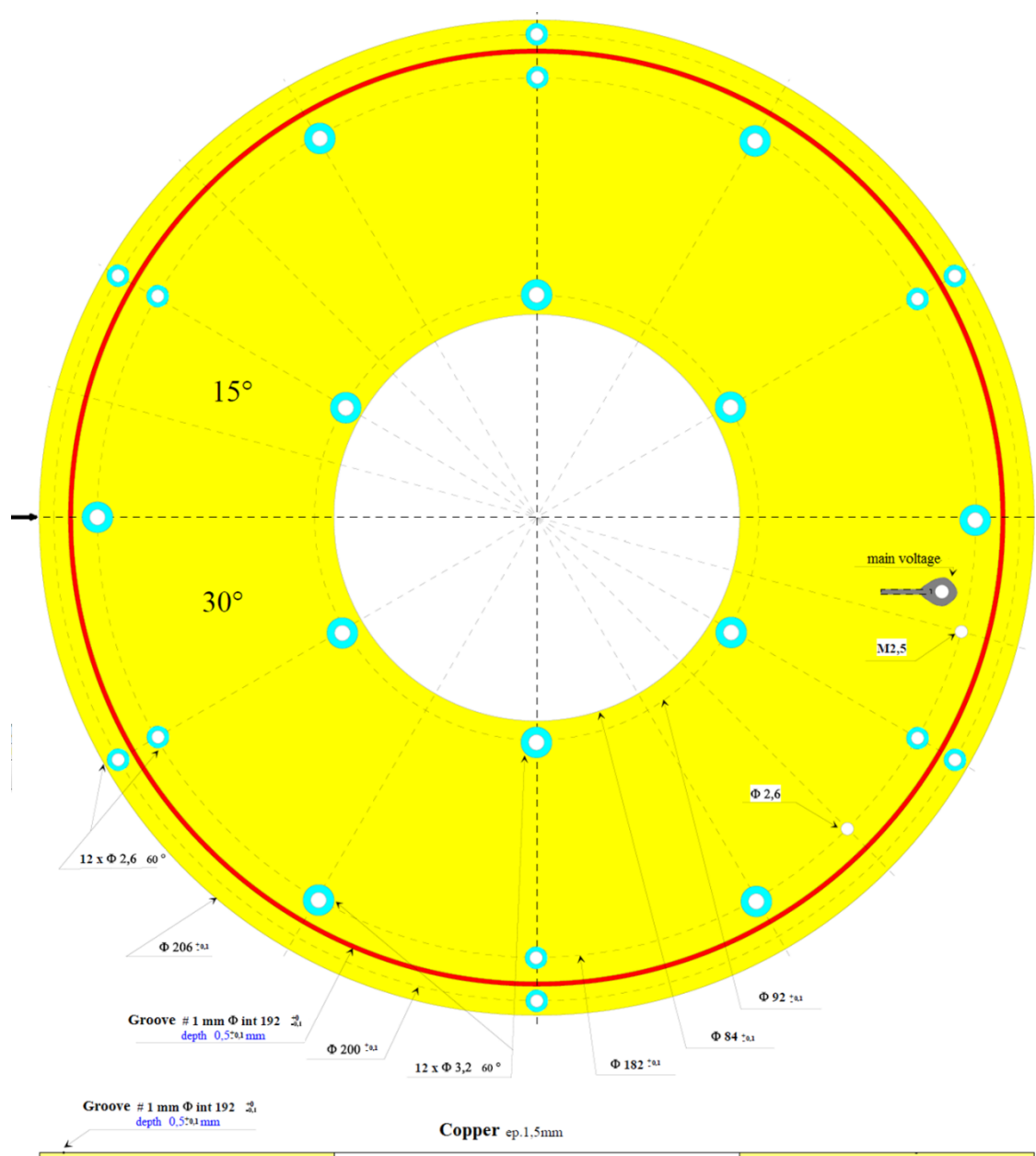
Figure A.10: Top of the big electrode cylinder of the electrostatic lens.

Groove # 1 mm Φ int 84 $^{+0}_{-0,1}$ Copper ep.1,5mm
depth $0,5^{+0,1}$ mm

Type D

30°

30°

6 x M 2,5   60 °

Φ 50 $^{+0,1}$

Φ 100 $^{+0,1}$

Φ 43 $^{+0,1}$

Φ 92 $^{+0,1}$

M2,5

main voltage connection

Groove # 1 mm Φ int 84 $^{+0}_{-0,1}$
depth $0,5^{+0,1}$ mm

6 x Φ 3,2   60 °

6 x 3,2   60 °

Φ 50 $^{+0,1}$

Φ 43 $^{+0,1}$

**Fiber glass thickness 1 mm
2 pieces**

Φ 57 $^{+0,1}$
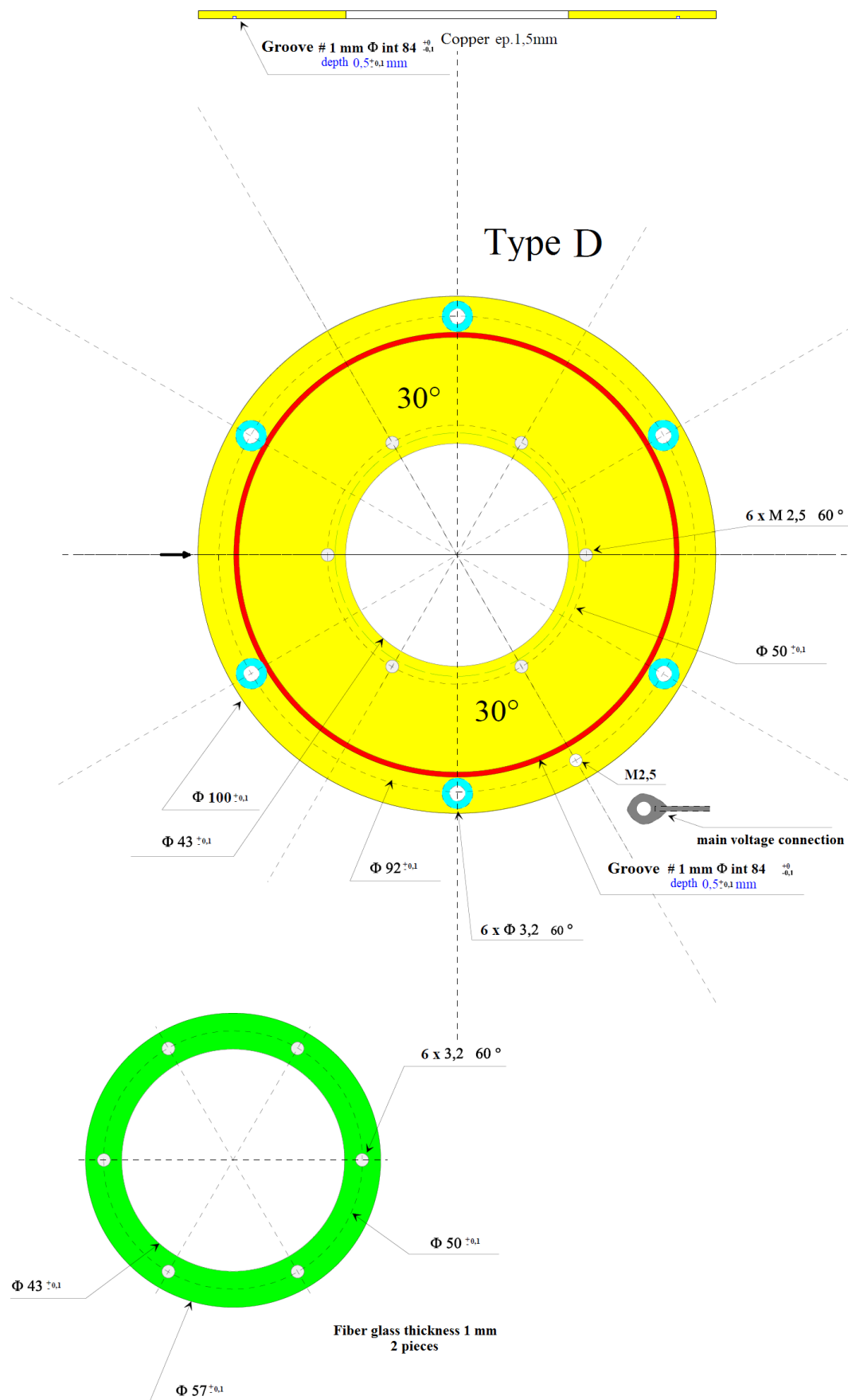
Figure A.11: Top of the small electrode cylinder and insulator for MCP and P47.
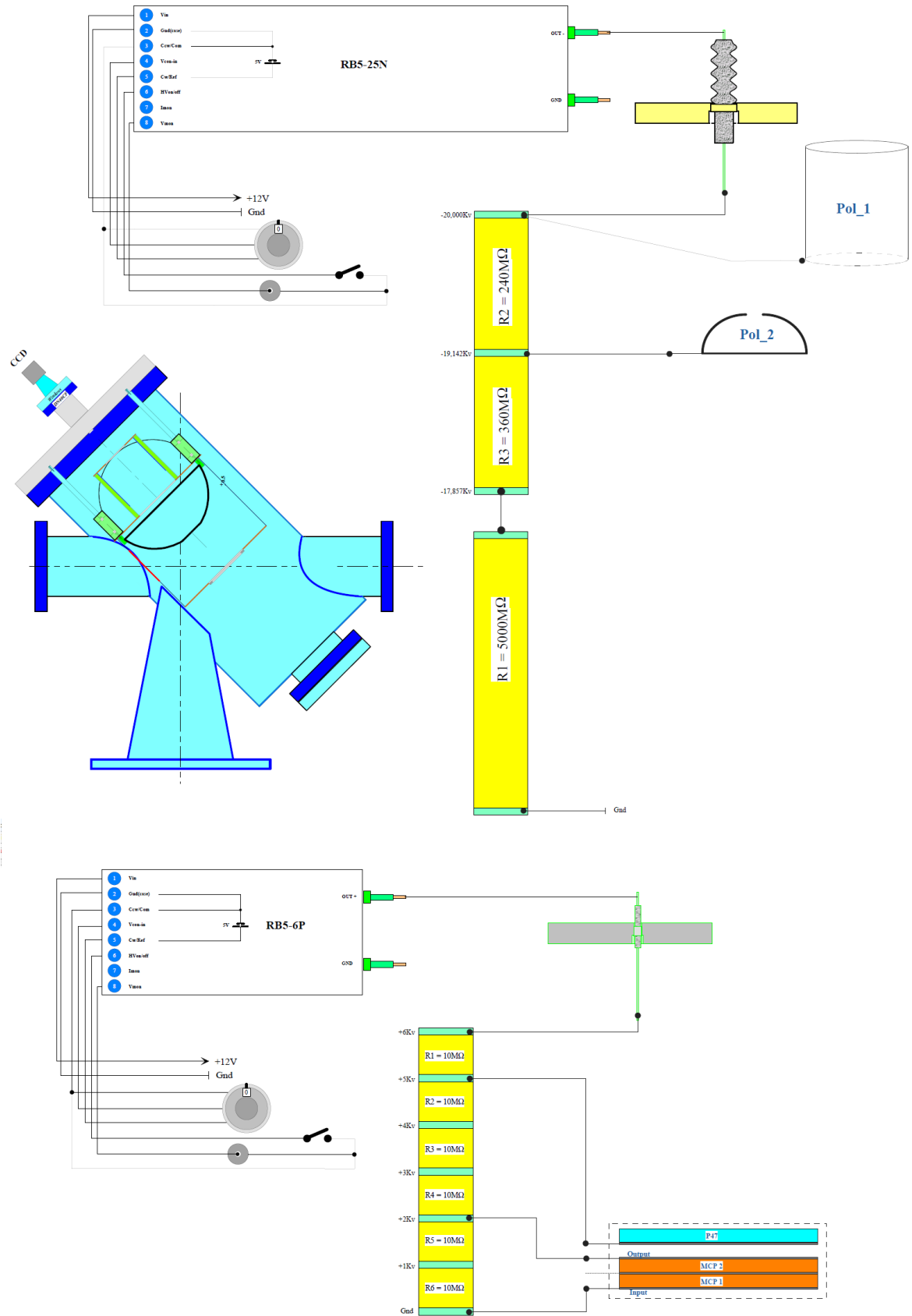
Figure A.12: Electrical scheme of the BISE detector.
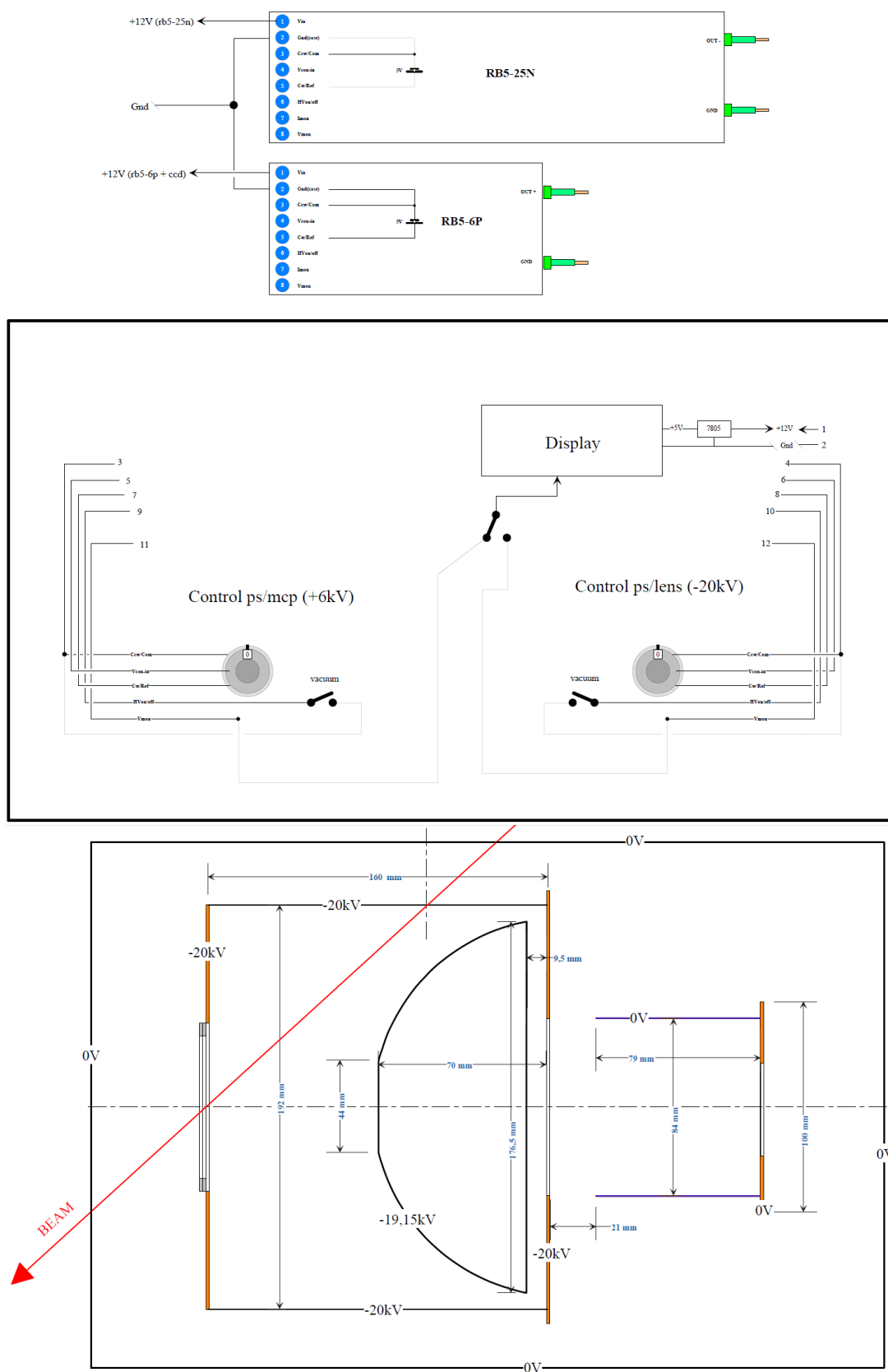
Figure A.13: Control panel of high voltage and a schematic view of the focusing system.

Appendix B

Additional simulations in COMSOL
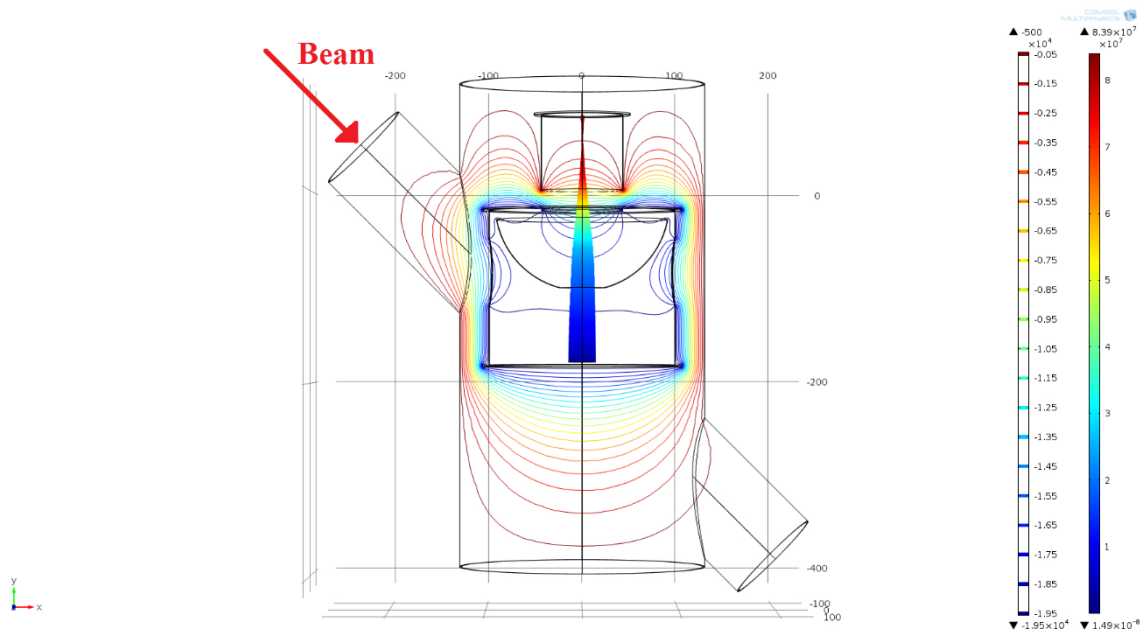
Figure B.1: COMSOL 3D full simulation of the particle trajectories and electric potential contours inside the vacuum chamber and the electrostatic lens with two holes.
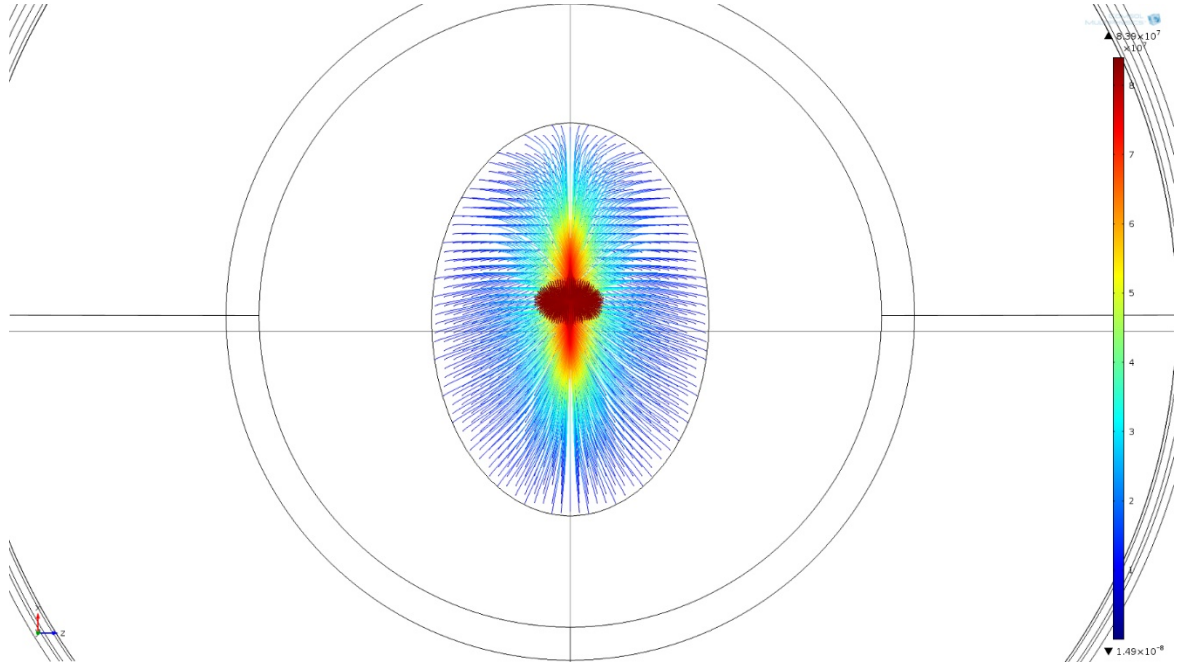
Figure B.2: COMSOL 3D full simulation of the particle trajectories in the electrostatic lens with two holes. Top view from Figure B.1. The entry of the beam is located at the bottom of the plot.
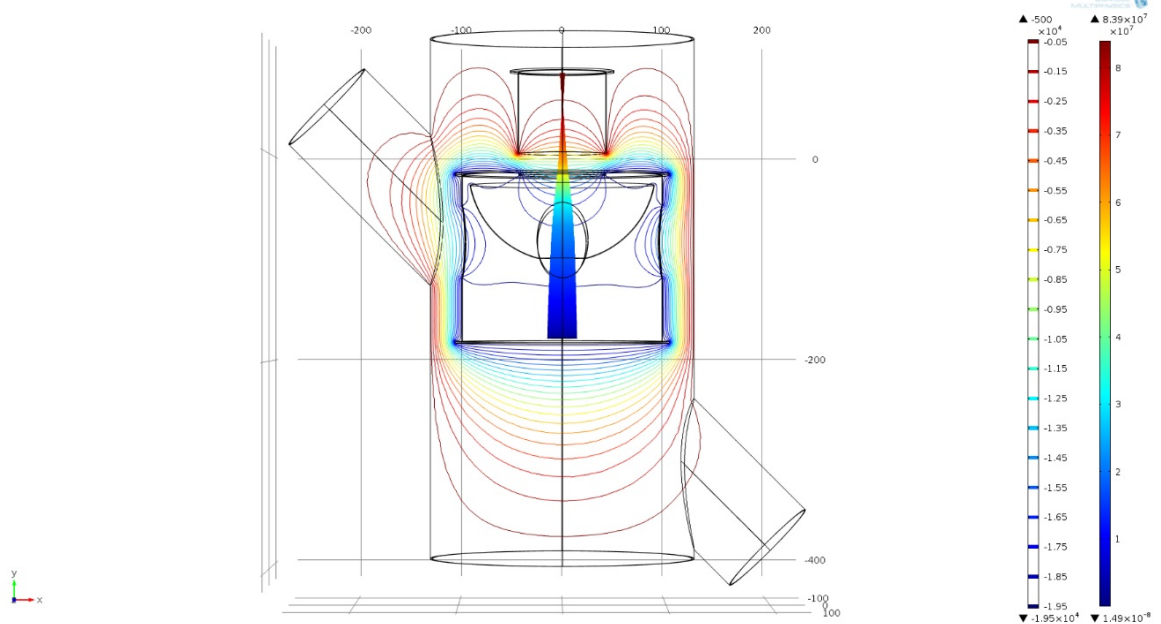
Figure B.3: COMSOL 3D full simulation of the particle trajectories and electric potential contours inside the vacuum chamber and the electrostatic lens with four holes.
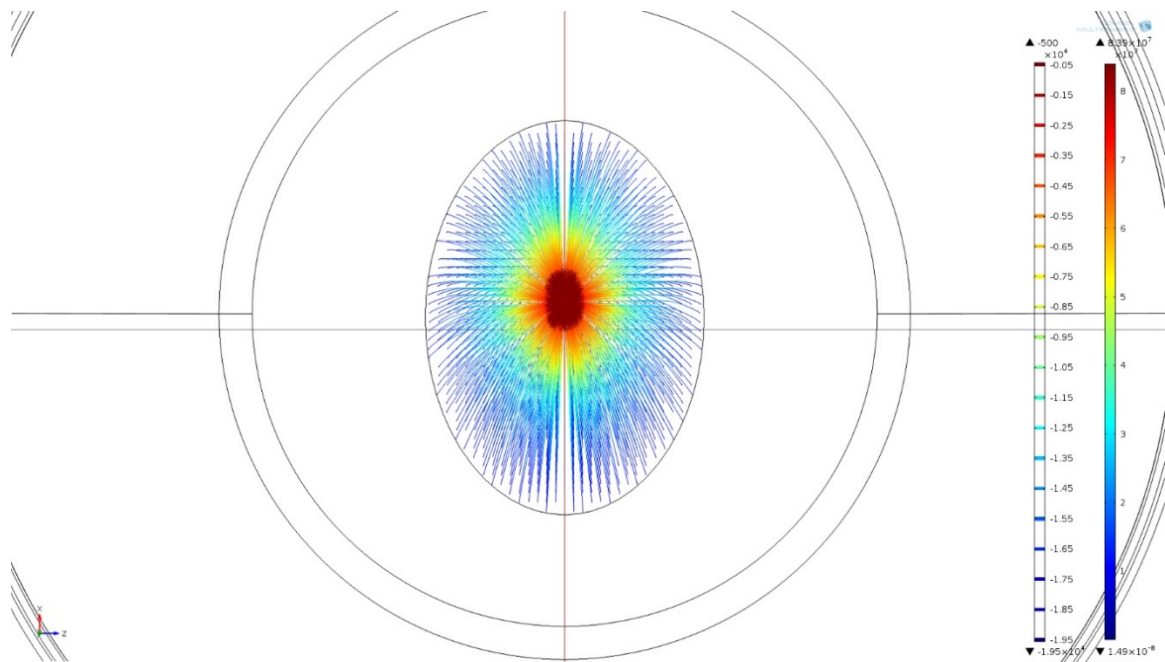
Figure B.4: COMSOL 3D full simulation of the particle trajectories in the electrostatic lens with four holes. Top view from Figure B.1. The entry of the beam is located at the bottom of the plot.
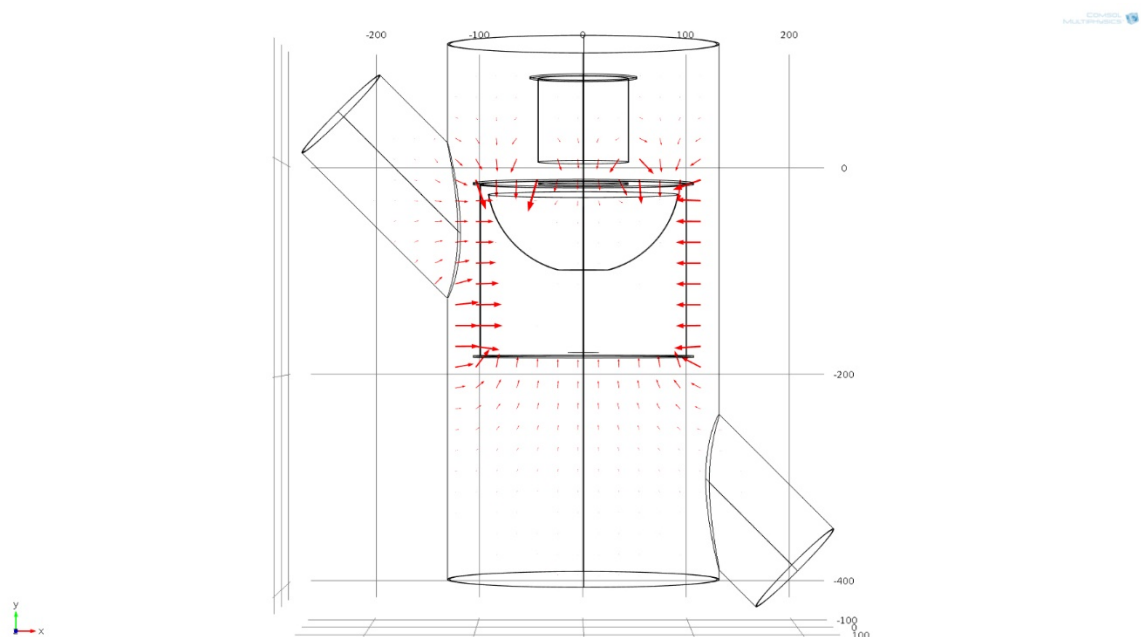
Figure B.5: COMSOL 3D full simulation of the electric field (arrows) in the vacuum chamber and the electrostatic lens without hole.
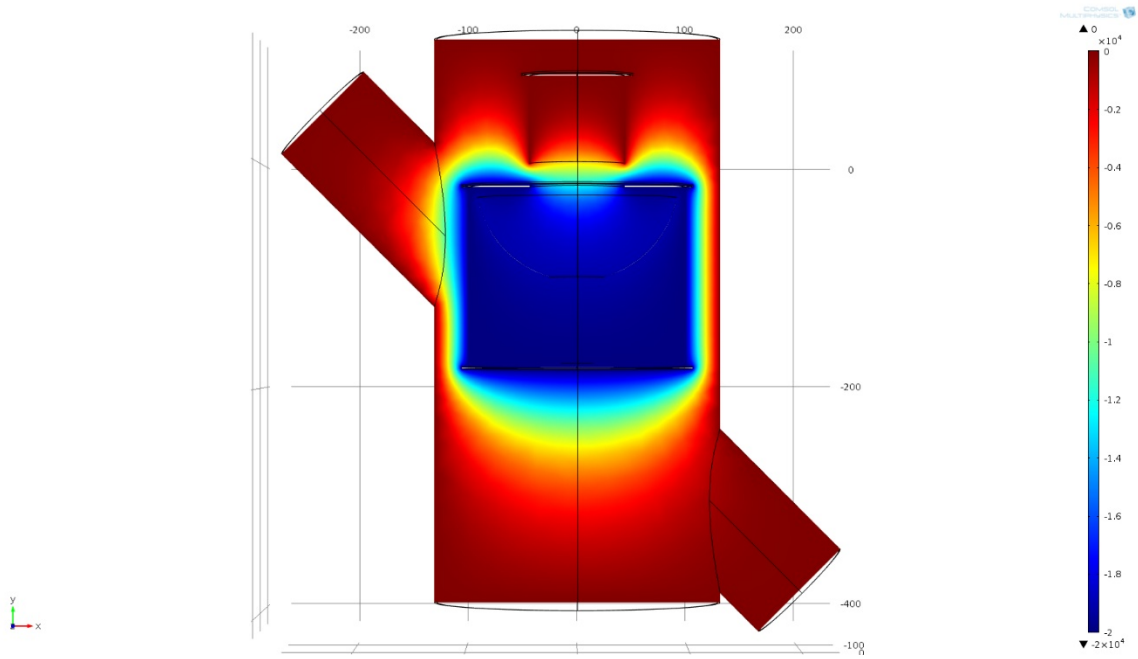
Figure B.6: COMSOL 3D full simulation of the electric potential (surface) in the vacuum chamber and the electrostatic lens with the hole closed with a thin foil.

Appendix C

Publications

The following publications are reprinted in this appendix:

1. A. Degiovanni, S. Braccini, E. V. Kirillova et al., *Emittance measurements at the Strasbourg TR24 cyclotron for the addition of 65 MeV linac booster*, 2013, Vancouver, Canada.

2. S. Braccini, A. Ereditato, E. Kirillova et al., *An innovative on-line beam-monitoring detector based on the emission of secondary electrons,* International Conference on Translational Research in Radiation Oncology / Physics for Health in Europe. 2014. Geneva, Switzerland: Radiotherapy & Oncology, **110**.

EMITTANCE MEASUREMENTS AT THE STRASBOURG TR24 CYCLOTRON FOR THE ADDITION OF A 65 MeV LINAC BOOSTER

A. Degiovanni[#], TERA, Novara, Italy and EPFL, Lausanne, Switzerland

U. Amaldi, S. Benedetti, D. Bergesio, A. Garonna, G. Molinari, TERA, Novara, Italy

E. van Lier, R.L. Watt, ACSI, Richmond, B.C., Canada

D. Brasse, M. Pellicioli, M. Rousseau, J. Schuler, IPHC, Strasbourg, France

S. Braccini, E.V. Kirillova, LHEP-AEC, University of Bern, Bern, Switzerland

Abstract

The long term plans of IPHC foresee the installation of a linac that will boost the energy of the protons of the Strasbourg TR24 cyclotron from 24 MeV to 65 MeV. A Cell Coupled Linac, designed by the TERA Foundation, could be used for this purpose. To compute the transverse acceptances of the linac, the horizontal and vertical emittances of the extracted proton beam need to be measured. The secondary emission detector BISE (Beam Imaging with Secondary Electrons) built by TERA and under development at the Bern 18 MeV IBA cyclotron will be used in Strasbourg for the final measurements. The results of the preliminary measurements of the transverse beam profiles are reported together with the development of BISE, the description of the linac structure and the calculation of the expected output current based on the dynamics of the accelerated proton beam.

INTRODUCTION

The Cyrcé cyclotron (CYclotron pour la ReCherche et l'Enseignement) has recently been installed at IPHC (Institut Pluridisciplinaire Hubert Curien) for the development of new radiolabelled molecules based on the research and production of radio-isotopes for diagnostics and medical treatments. The TR24 cyclotron produced and commercialized by ACSI (Canada) delivers a 16-25 MeV proton beam on two extraction ports with intensity from few nA up to 500 μA. The facility will start soon to produce ^{18}F (half-life period 110 min) and ^{64}Cu (half-life period 12,7h). Using standard targets, 15 possible isotopes can be produced with this accelerator.

The long term plans of IPHC foresee the installation of a linac for boosting the energy of the protons from 24 MeV to 65 MeV. The TERA Foundation has developed in the last decades high RF frequency Cell Coupled Linacs (CCL) designed to be coupled with cyclotrons to boost their energy for applications in proton therapy [1]. A 3 GHz CCL, designed by the TERA Foundation, could be used for this purpose.

To compute the transverse acceptances of the linac, the horizontal and vertical emittances of the extracted proton beam need to be measured. Preliminary measurements were conducted at IPHC, in collaboration with ACSI. Further measurements are planned with the secondary emission detector BISE (Beam Imaging with Secondary

Electrons) built by TERA and under development at the Bern 18 MeV IBA cyclotron [2].

CYCLOTRON BEAM MEASUREMENTS

The TR24 installed at IPHC in Strasbourg is shown in Fig. 1. The cyclotron has two exit ports. One is equipped with targets for cell irradiation, while the second one is not used at the moment. The second extraction beam port has been commissioned for performing the beam measurements and is shown in Fig. 1.

Figure 1: Picture of the TR24 cyclotron installed at IPHC in Strasbourg. The water cooled beam dump provided by ACSI is visible at the end of the beam pipe.

Preliminary beam profile measurements have been performed at the beginning of July 2013 using Gafchromic™ EBT3 films and adding two pieces of beam pipe in order to obtain profiles at different distances from the extraction point. Meanwhile, the BISE detector is under development and test at the Bern cyclotron.

Preliminary Measurements at IPHC

The absence of a dedicated extraction beam line limited the first measurements to an analysis of beam profiles at different positions from the extraction port (0 m, 0.4 m and 0.7 m), obtained by connecting two pieces of beam pipe (100 mm diameter) to the exit port 2 of the cyclotron. The alignment of the beam pipe was based on results of simulations of beam trajectories in the cyclotron. The pieces of beam pipes were electrically isolated by placing polymeric gaskets, so that it was possible to monitor the beam current on the wall of the beam pipe and on the beam dump, during the irradiation.

_____
#alberto.degiovanni@cern.ch

Gafchromic™ EBT3 films have been used to obtain an image of the beam profile. Two methods of irradiation have been used: (i) indirect irradiation and (ii) direct irradiation. In the first case the image was obtained by exposing the dosimetric film to the radiation induced onto a water cooled beam dump made of aluminium and provided by ACSI (see Fig. 1). The time of exposure was calculated from the measured activity at the start of the exposure in order to obtain the same integrated dose. In the case of direct irradiation, the dosimetric film was placed into the beam line between a thin aluminium plate of 2.5 mm and the beam dump.

The images collected with indirect method, with the corresponding reconstructed images (obtained from the scan of the dosimetric films with MATLAB), are presented in Fig. 2. The FWHM have been evaluated from the reconstructed images, after noise subtraction and normalization, and are plotted with respect to the distance from the extraction port in Fig. 3.
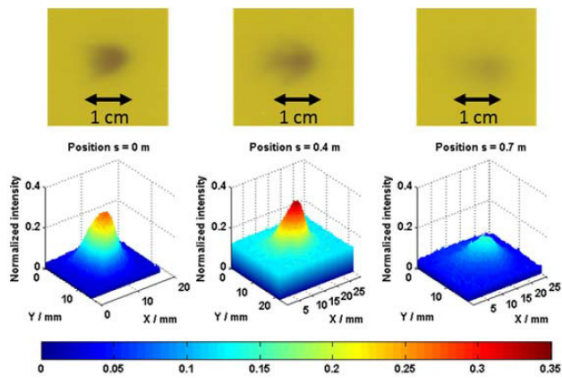
Figure 2: Summary of indirect measurements.
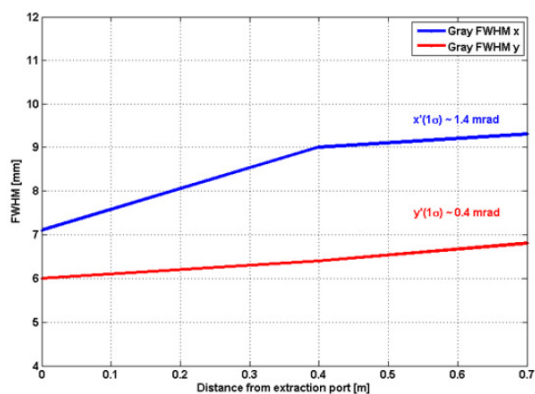
Figure 3: Measured FWHMs of the two transverse beam profiles with respect to the distance from the extraction port.

The preliminary measurements show an increase in the transverse beam profile which corresponds to a divergence of about 1.4 mrad in the horizontal plane and of 0.4 mrad in the vertical plane (1 rms). While the further data is required to calculate emittances, the preliminary results indicate an upper limit of 17 and 5 π mm mrad for

the geometrical emittance (4rms). A second measurement campaign will be performed with the use of the BISE detector to obtain a more precise estimate.

Development and Beam Tests of the BISE Detector at the Bern Cyclotron

The BISE detector was designed and built by TERA for the on-line control of the intensity and shape of ion beams along the beam lines. A similar apparatus was previously developed [3]. BISE is based on the detection of low energy (< 50 eV) secondary electrons emitted by a thin aluminium foil (of about 0.8 μm) traversed by the ions, allowing for a minimal perturbation of the beam. The detector operates under vacuum and consists of an electrostatic lens used to focus and accelerate the secondary electrons at the energy of 20 keV. The electric field produced by the lens is such that the electrons reach a plane where a de-magnified image of the primary ion beam is formed with minimal distortion. Here, a sensor is located to detect the 20 keV electrons that form the image. The choice of the sensor was driven by simplicity, reliability and cost-effectiveness criteria. Furthermore, in case of currents of the order of a few μA, the produced neutron fluxes do not allow the use of radiation-sensitive devices. The sensor of BISE is composed by a phosphor screen (P47) read out by a CCD camera. To amplify the signal, in case of beam currents in the nA range or less, a micro channel plate can be used in front of the phosphor. BISE is now under development and test in collaboration with LHEP at the new Bern 18 MeV cyclotron laboratory, where a specific beam transfer line ending in a separate bunker has been constructed to perform research activities [2]. The experimental set-up is shown in Fig. 4.

Figure 4: The BISE detector installed in the beam transfer line of the Bern cyclotron. The foil and the electrostatic lens are contained in the cylinder located at 45 degrees with respect to the beam direction.

These developments aim at the optimization of the electrostatic lens and, in particular, at the use of BISE for currents in the μA range, typical of radioisotopes production. Simulations have been performed using SIMION and COMSOL to study the optimal configuration of the electrostatic lens, the magnification

Beam Dynamics

Beam Transport

and the resolution of the images. A beam test campaign is presently on-going and the first preliminary results are reported in Fig. 5.
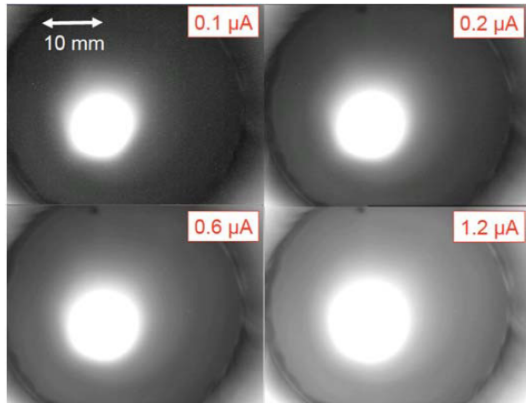
Figure 5: Images of an 18 MeV proton beam at several intensities obtained with the BISE detector. The intensity is measured by means of a Faraday cup located at the end of the beam line.

These first results show that the detector equipped only with a phosphor screen is able to operate in wide range of beam intensities. The measurement of the magnification will be performed by interposing a multi-hole collimator in front of the thin foil. This method will also allow assessing possible distortions. For the measurement of the beam intensity through the analysis of the detected images, the detector will be calibrated by means of a specific high-sensitivity Faraday cup.

CYCLINAC DESIGN

A cyclinac is an accelerator complex formed by a cyclotron and a linac used as a booster [1]. The main parameters of the design for the linac boosting the proton beam from 24 to 65 MeV are summarized in Table 1.

Table 1: Main Parameters of the Linac

Parameter	Value
Frequency [MHz]	2998.5
Number of RF units	2
Number of tanks per RF unit	4
Number of cells per tank	14-15
Bore hole diameter [mm]	7
Units length [m]	2.19-2.84
Effective shunt impedance ZT^2 [MΩ/m]	22.3-51.8
Average electric field on axis E_0 [MV/m]	14.6
Maximum surface electric field [MV/m]	75.0
Peak power per RF unit [MW]	10
RF pulse length [μs]	4
Repetition rate [Hz]	100
Duty cycle [%]	0.04

The 5 meter long linac is made of two independent RF units. With the addition of other RF units, higher energies could also be reached. Moreover, the accelerating performance increases at higher energies due to higher

Beam Dynamics

Beam Transport

shunt impedance values [4]. ACSI will modify the cyclotron source, so that the extracted beam will be chopped in 4 μs long pulses at the same repetition rate of the linac.

Beam Current at the End of the Linac

In Fig. 6, the linac transmission has been computed considering different values of the transverse emittances of the input beam. A continuous beam with 0.24 MeV energy spread has been considered for the simulations. The plotted results represent the transmitted particles with energy within ± 3% of the peak value (65 MeV).
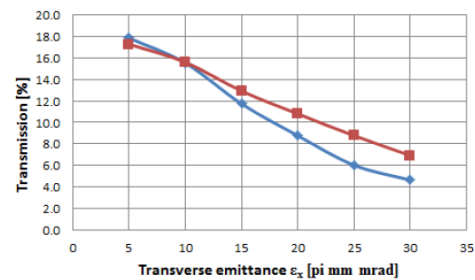
Figure 6: Linac transmission considering a ratio between ε_x and ε_y of 0.5 (blue curve) and 0.25 (red curve).

For a current of 300 μA from the cyclotron, the expected current is in the range of 14 to 57 μA, considering emittances of 30-15 or 5-2.5 π mm mrad.

SUMMARY

Preliminary beam profile measurements have been performed by ACSI, TERA and IPHC at the TR24 cyclotron installed at IPHC in Strasbourg. The measurements will be completed by using the non-destructive beam detector BISE, which is now under test and development at the Bern cyclotron. A linac design to boost the beam energy from 24 to 65 MeV is proposed and will be optimized based on the information obtained during the final beam measurements.

ACKNOWLEDGMENT

REFERENCES

[1] U. Amaldi, et al., Accelerators for hadrontherapy: From Lawrence cyclotrons to linacs, NIM A 620(2010)563-577

[2] S. Braccini, et al., The new Bern cyclotron laboratory for radioisotope production and research, in Proc. of IPAC2011, p. 3618-20

[3] L. Badano, et al., Secondary Emission Monitor for Low-Interception Monitoring (SLIM): An Innovative Nondestructive Beam Monitor for the Extraction Lines of a Hadrontherapy Center, IEEE Trans. Nucl. Sci., vol. 51, no. 6, pp.2990 -2998, 2004

[4] U. Amaldi, S. Braccini and P. Puggioni, High Frequency Linacs for Hadrontherapy, RAST, Vol. 2 (2009), 111-131.

331

Conclusions: PlanIt is an open platform for research institutions that can help, contribute and share their knowledge for one common objective: clinical endpoint.

It is a platform giving an impartial and objective tool for optimizing the planning for typical cases of cancer pathologies and verifying which is the best convenient radiation therapy. This avoids an inopportune use of sophisticated advanced radiation techniques when it is not giving clinically any real advantage.

VPatient module provides a powerfull tool for testing and comparing plans on fully realistic phantom with the potentiality of creating virtual different pathologies.

Keywords: Treatment Planning, radiation therapy, Ion Beam Therapy, Virtual patient.

27

Augmented Reality tools for particle therapy facilities

F. Bourhaleb[1,2], G. Petrone[3]
[1]I-See, Torino, Italy
[2]INFN, Italy
[3]Department of computer science, University of Turin, Italy

Purpose: Particle therapy facilities represent excellence centers that are results of advanced multidisciplinary research and high-technology equipments. A need of a Augmented Reality (AR) dedicated tools to integrate the important and sophisticated amount of information is an evident advantage in the optimization of the facility workflow.

Such tool set provides better management of information that usually are collected but not used due to difficulties in manipulating and accessing information.

According to the operator task the AR software infrastructure activate different level and kind of data and information.

A look at augmented reality features emphasizes a strong and better use of the potentialities of all the applications contributing for a better treatment.

Materials/methods: Our AR application has a software infrastructure that is managing different level of access.

All information related to the patient and the medical environment are hosted in a private cloud platform and the only needed acess is a wi-fi connectivity.

Information are stored and ordered according different levels and relevance to the purpose considered.

According to the role of the user, the access is redirected to a predetermined kind of relevant information and use.

The only hardware needed for the final user is a simple tablet.

Results: The AR application we present is a prototype for particle therapy center since they are   typical case of facilities where an optimized virtual medical environment makes the communication easier and so the facility work-flow managed better.

In this work we present an example with three levels of use of the same AR application: medical doctor, medical physicists and technical engineer.

Conclusions: AR is nowadays a powerful tool for integrating information and giving in real time all knowledge needed to get the best management of resources dedicated to the patient.

Particle therapy centers are perfect candidates for taking full advantage for the potentiality of AR as an application and a service in the e-heathcare field.
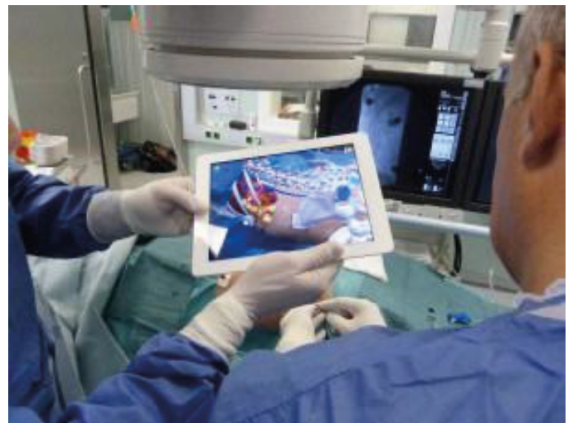
Keywords: Augmented Reality, radiation therapy, Ion Beam Therapy.
References:
Photo courtesy of Medical Augmented Reality

28

An innovative on-line beam-monitoring detector based on the emission of secondary electrons

S. Braccini[1], D. Bergesio[2], A. Ereditato[1], E. Kirilova[1], G. Molinari[2], K.P. Nesteruk[1], P. Scampoli[1,3], U. Amaldi[2]
[1]AEC-LHEP University of Bern, Switzerland
[2]TERA Foundation, Novara, Italy
[3]Department of Physics University of Naples Federico II, Italy

Purpose: The BISE (Beam Imaging with Secondary Electrons) detector was designed and built by TERA for the on-line control of the intensity and shape of ion beams along transfer lines. It is aimed at operating in a large range of beam currents, form fractions of nA typical of particle therapy to several µA used in radioisotope production.

Materials and methods: BISE is based on the detection of low energy (< 50 eV) secondary electrons emitted by a thin aluminum foil (of about 0.8 µm) traversed by the ions. It represents the evolution of an apparatus previously developed by TERA [1]. The foil is placed at 45 degrees with respect to the beam direction and simulations show that the particles are subject only to a negligible perturbation. In this way, the detector can be continuously kept in the beam. The detector operates under vacuum and consists of an electrostatic lens used to focalize and accelerate the secondary electrons at the energy of 20 keV. The electric field produced by the lens is such that the electrons reach a plane where an inverted de-magnified image of the primary ion beam is formed. Here a sensor is located to detect the image. Simulations were performed using SIMION and COMSOL to study the optimal configuration of the electrostatic lens, the magnification and the resolution of the images. The sensor was chosen on the basis of its simplicity, reliability and cost-effectiveness. A phosphor screen (P47) read out by a CCD camera is used. In case of beam currents below the nA range, a micro channel plate can be added in front of the phosphor to amplify the signal. BISE is now under development and test in collaboration with LHEP at the new Bern cyclotron laboratory, where a specific beam transfer line ending in a separate bunker has been constructed to perform research activities [2]. The experimental set-up is shown in Fig. 1 (left).

Results: The first images of an 18 MeV proton beam are reported in Fig. 1 (right). They demonstrate that the detector equipped only with a phosphor screen is able to operate in wide range of beam intensities. The measurement of the magnification is ongoing and is performed by interposing a multi-hole collimator in front of the thin foil. The possibility of using a laser beam for the precise

assessment of possible distortions is also considered. For the calibration and measurement of the beam intensity through the analysis of the detected images, a specific high-sensitivity Faraday cup has been constructed and will be installed at the end of the beam line.

Conclusions: An on-line beam-monitoring detector based on the emission of secondary electrons was designed, constructed and tested. On the basis of the first beam tests, further developments are ongoing.
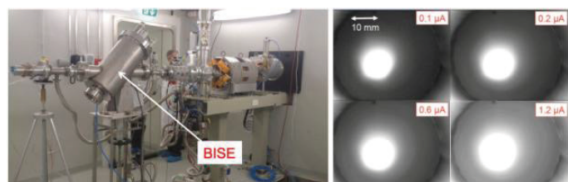

Figure 1. The BISE detector installed in the beam transfer line of the Bern cyclotron (left). Images of an 18 MeV proton beam at different intensities (right).

Keywords: Beam monitoring; Radioisotope production; Particle therapy

References:
[1] L. Badano et al., IEEE Trans. Nucl. Sci. 51 (2004) 2990
[2] S. Braccini et al., Proc. of IPAC2011, 3618.

29
Dose distribution characterization in the halo of proton pencil beams with emulsion film detectors
S. Braccini[1], A. Ariga[1], T. Ariga[1], A. Ereditato[1], F. Giacoppo[1], C. Pistillo[1], P. Scampoli[1,2]
[1]AEC-LHEP University of Bern, Switzerland
[2]Department of Physics University of Naples Federico II, Italy

Purpose: This work is aimed at the experimental characterization of the dose distribution in the beam halo region of a clinical proton pencil beam using a novel method based on nuclear emulsion detectors.

Materials and methods: Nuclear emulsion films allow for high-precision tracking of charged particles. Specific detectors can be built by interposing double-sided emulsion films with a tissue equivalent material to measure proton tracks in the proton therapy energy range. This technique has been recently used for proton radiography [1]. A 15 cm long detector composed by 60 emulsion films and PMMA plastic sheets was constructed and exposed to a 138 MeV proton pencil beam directed towards its center using the Gantry 1 at PSI. While the track density is too high to be measured in correspondence of the pencil beam, this method allows counting single proton tracks in the halo along the depth of the detector. This region is particularly interesting since the corresponding dose can be located outside the target volume and could potentially lead to undesired secondary effects. A Monte Carlo simulation was performed using Geant4 to optimize the design of the detector and to assess the average dose delivered by each proton in the halo. Following the chemical development and the automatic microscopic scanning of the emulsion films, three areas in the halo region were selected at about 2 cm distance from the beam axis (Fig. 1 - left). Here, proton tracks were identified and efficiently separated from the background by means of their high ionization loss.

Results: Data were analyzed at several depths and the corresponding angular distributions showed that the protons in the halo region could be subdivided into two components (Fig. 1 - right). The former is dominating at small depths and is almost parallel with respect to the beam axis. It is generated up-stream with respect to the detector, in the gantry and in the nozzle. The latter is characterized by large

angles and is due to the multiple scattering of the protons inside the tissue equivalent material of the detector. This second component dominates at larger depths. The identification of the proton tracks, together with the corresponding dose estimated by Monte Carlo, allows assessing an upper limit of the dose in the beam halo region. It was found to be less than 3×10^{-4} Gy for a delivery of 2 Gy in the spot region.

Conclusions: A new method to measure the dose in the beam halo region of a clinical proton pencil beam based on nuclear emulsion detectors is proposed and successfully tested.
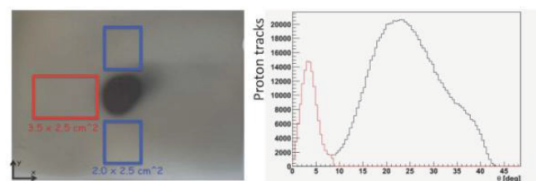

Figure 1. A nuclear emulsion film exposed to a 138 MeV proton pencil beam where the selected regions for the analysis are indicated (left). Angular distribution of the proton tracks at 7.3 cm depth. The first almost parallel component is indicated in red while the one due to multiple scattering in black (right).

Keywords: Radiation dose; Nuclear emulsion detectors; Proton therapy

References:
[1] S. Braccini et al., First results on proton radiography with nuclear emulsion detectors, Journal of Instrumentation 2010 JINST 54 P09001.

30
Studying inter- and intrafraction motion mitigation with sequential 4DCTs of lung tumor patients
R. Brevet[1], C. Bert[1,2], M. Durante[1], C. Graeff[1], D. Richter[1,2]
[1]GSI, Darmstadt, Germany
[2]UK Erlangen, Germany

Compared to conventional radiotherapy, physical and biological properties of scanned carbon ion beam therapy can allow a more accurate irradiation. Treatment of moving tumors can be problematic due to range sensitivity and interplay effects. Purpose of this study is to investigate if dedicated optimization of treatment planning parameters and ITV-PTV margins provide a solution.

For 5 NSCLC lung tumor patients from MDACC (The University of Texas MD Anderson Cancer Center), a total of 38 weekly 4DCT datasets were available. Reference phases of each subsequent CT were registered rigidly to mimic patient setup. Motion phases of each 4DCT were registered non-rigidly. Single field gating plans were simulated using the GSI treatment planning system TRiP4D, including 4D-dose reconstructions. Plans were initially optimized to the ITV without additional margins but considering motion related range changes. First, the impact of variations in focus size and length of the gating window (GW) on dose coverage (V95) and conformity number (CN) was analyzed. Three beam foci (6, 10 and 15 mm full width at half maximum) and three GW (11.9, 30 and 50% of the amplitude) were studied. Then, the influence of range (3mm water-equivalent + 3%) and isotropic (3mm) ITV-PTV margins on V95 and CN were investigated. Combination of both margins was also analyzed.

The initial treatment plans resulted in V95 of 98.8% (96.6% to 100%) and CN of 0.6 (0.53 to 0.7). Anatomic variations such as patient misalignment or tissue drifts caused the largest effects on dose coverage. For all patients, such variations

Appendix D

Measurements with a nine millimeter hole in the aluminum foil

An aluminum foil which covered the beam entry hole was removed in these measurements to avoid undesired secondary electrons from its surface. Without this foil the cylindrical symmetry of the electric field in the focusing system broke down. The aluminum foil at the bottom of the cylinder was replaced by a foil with a hole of nine millimeter in diameter located at its center. It was expected to see no signal on the CCD camera with a proton beam aimed at the hole. The foil in its support ring is presented in Figure D.1. The foil was installed in the same way as it is shown in Figure 2.12.

For the proper measurements of the ratio F of major and minor axes and the demagnification factor D, additional simulations were needed. Due to the broken electrostatic symmetry in the focusing system, the demagnification factor D and the ratio F were calculated in YX plane using COMSOL. The results of the simulations are presented in Figures D.2, D.3 and D.4.

The demagnification factors $D_{X,COMSOL}$ and $D_{Y,COMSOL}$ were found to be:

$D_{X,COMSOL} = 0.2185 \pm 0.0017,$
$D_{Y,COMSOL} = 0.1803 \pm 0.0018.$

The ratio F of major and minor axes was found to be:
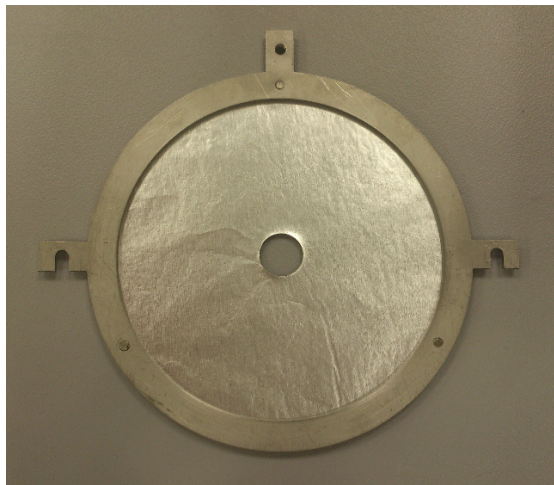
$F_{YX,COMSOL} = 1.2115 \pm 0.0155.$

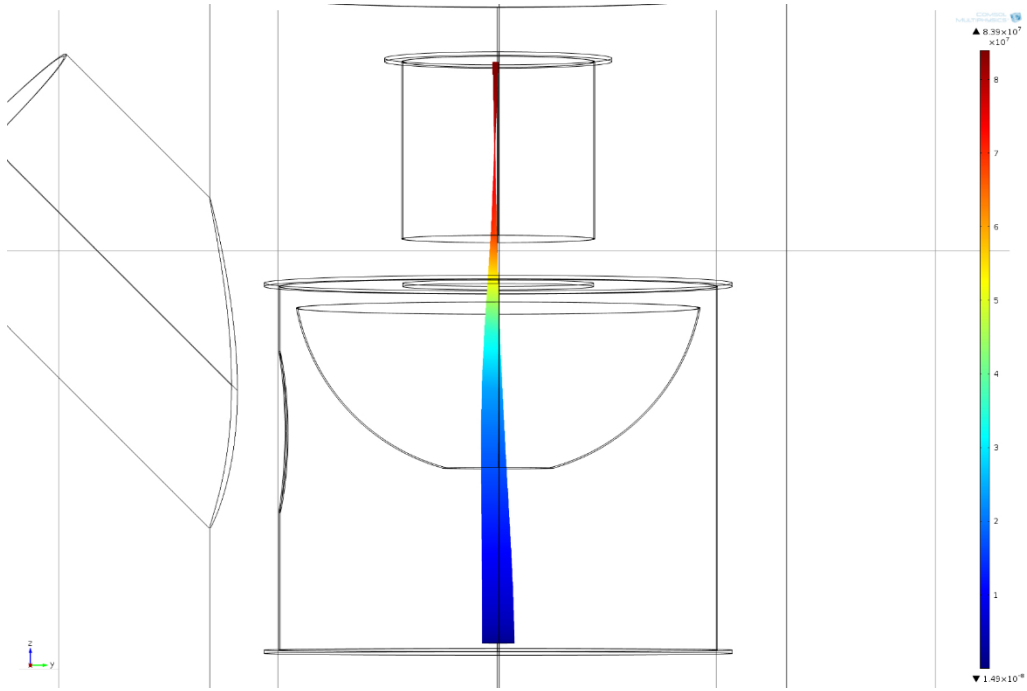Figure D.1: Aluminum foil with a 9 mm-diameter hole.

Figure D.2: COMSOL 3D full simulation (ZY plane) of the particle trajectories from the aluminium foil with a nine millimetre hole at the center. The beam entry hole is opened. The particle trajectories are curved due to the asymmetry inside the focusing system.
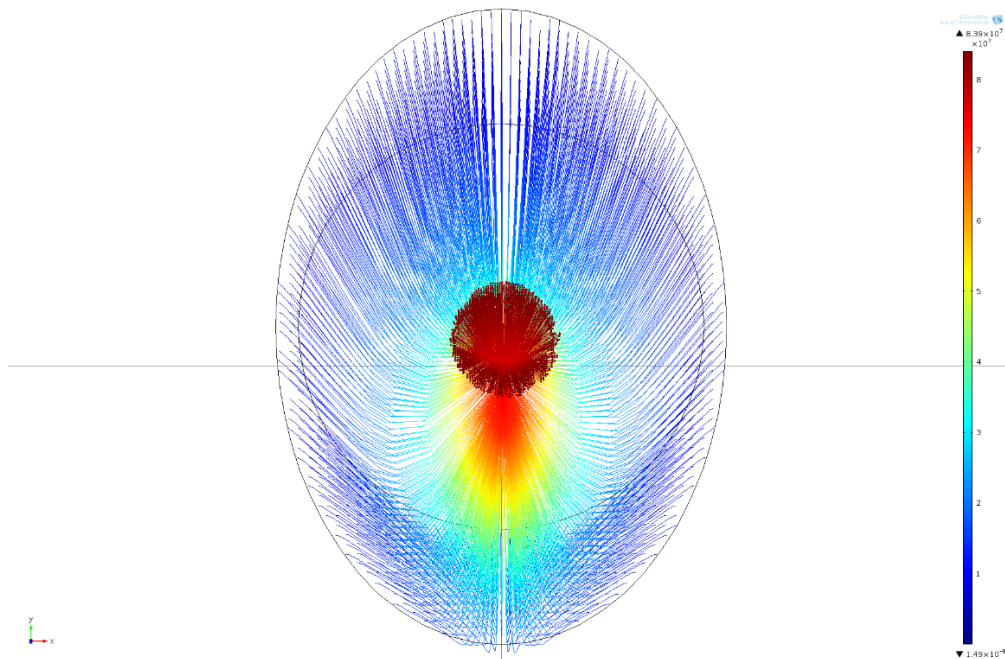

Figure D.3: COMSOL 3D full simulation (YX plane) of the particle trajectories in the focusing system from the aluminium foil with a nine millimetre hole at the center. Particles start accelerating from the oval layer (dark blue) and stop on the phosphor screen (dark red).Top view from Figure D.2. The entry of the beam is located at the bottom of the plot.
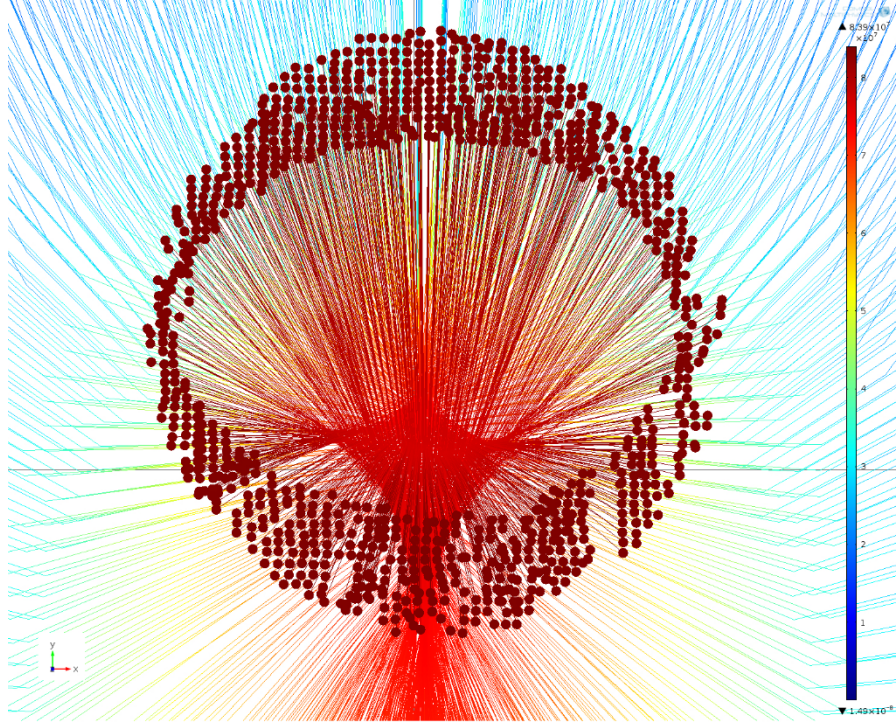
Figure D.4: Zoomed Figure D.3. Dark red points correspond to particles stopped on the phosphor screen. An inner oval corresponds to a compressed image in Y axis of the nine millimetre hole.

To experimentally determine the ratio F and the demagnification factor D a beam focused vertically and horizontally was used. We expected the image of the hole as it is shown in Figure D.4. The corresponding images were recorded and are presented in Figures D.5 and D.6. The dependence of the image intensity on X and Y axes are shown in Figures D.7 and D.8. The projections are performed according to the lines indicated in Figures D.5 and D.6. The analysis of the images was conducted with ImageJ and MATLAB programs.

To perform a quantitative measurements of the major and minor axes ratio F and demagnification factor D, approximate procedures were used. The minimal signal (Figures D.7 and D.8, point C) was supposed to be at the center of the image due to the hole in the foil. Areas near the minimum (Figures D.7 and D.8, points B and D) were supposed to occur due to secondary electrons extracted from the foil around the hole. With these assumptions, an *image* length of the hole x' (y') was taken as a distance on the X (Y) axis between the central minimum (Figures D.7 and D.8, point C) and a half maximum of the left and right peaks (Figures D.7 and D.8, DC/2 and CD/2). Two values of x' (y') (right and left) were obtained and averaged. An *object* length was taken as the radius of the hole.

$x'_{hole} = (B_xC_x + C_xD_x)/2 = 1.838 \pm 0.046$ mm,
$y'_{hole} = (B_yC_y + C_yD_y)/2 = 1.418 \pm 0.055$ mm,
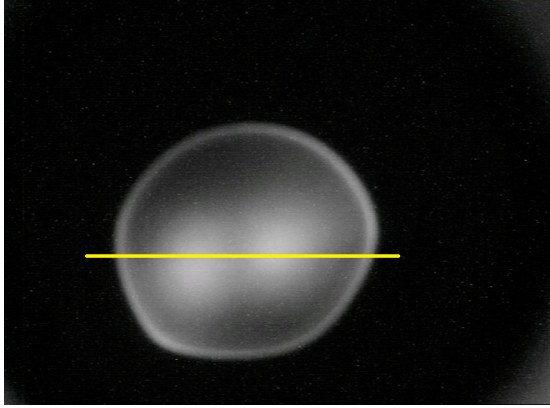$r_{hole} = 4.5 \pm 0.005$ mm.

Figure D.5: Image of the hole with a beam focused vertically. The line corresponds to the projection of Figure D.7.
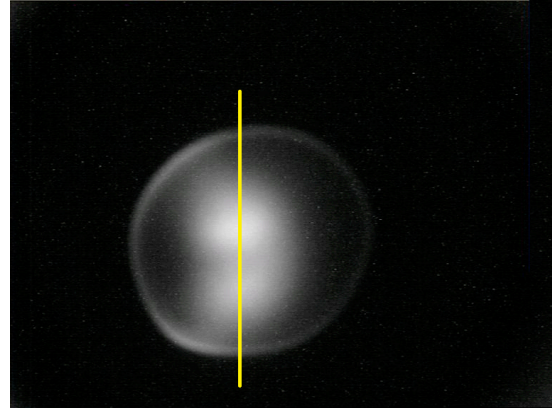
Figure D.6: Image of the hole with a beam focused horizontally. The line corresponds to the projection of Figure D.8.
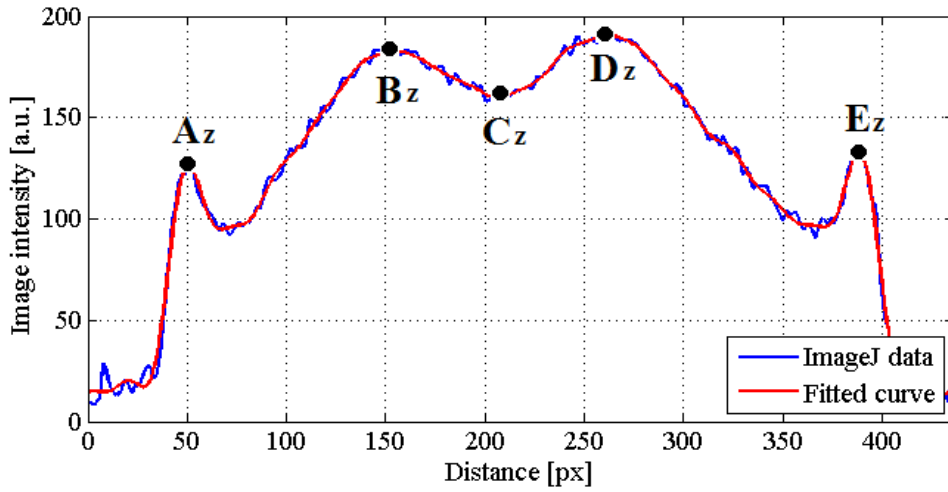

Figure D.7: Dependence of the image intensity on the distance with a beam focused vertically (X axis).
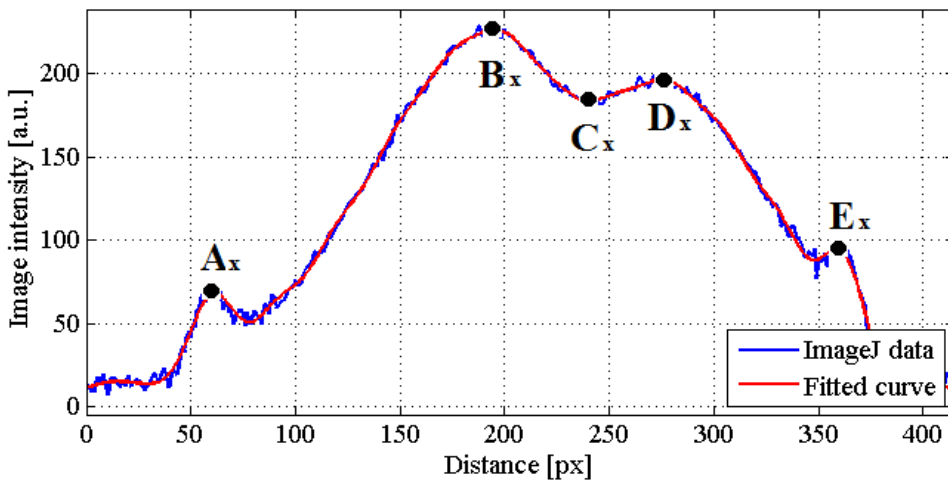

Figure D.8: Dependence of the image intensity on the distance with a beam focused horizontally (Y axis).

With this analysis, the demagnification factors and the ratio F were found to be:

$D_{x,hole} = x'_{hole} / r_{hole} = 0.408 \pm 0.010$,
$D_{y,hole} = y'_{hole} / r_{hole} = 0.315 \pm 0.012$,
$F_{hole} = x'_{hole} / y'_{hole} = 1.296 \pm 0.036$.

The measurement of the demagnification in our approximation was found to be two times larger with respect to the value expected from simulations. The reason of this discrepancy is unknown and need to be further studied. This effect could be due to the choice of the approximation. It is difficult to estimate where is the hole border between points B and D (Figures D.7 and D.8). Nevertheless, there is a good agreement between experimental data and simulations for the ratio of major and minor axes.

During the experiment, the disappearing of the beam image was obtained focusing the beam at the position of the hole.

To observe the border of the phosphor screen P47 an additional measurement was performed. For this purpose, with no voltage in the electrostatic lens, a light was pointed through the glass window (Figures 2.4 and 4.1) on the 9 mm hole and it partially covered the phosphor screen. Light was directed left and right, therefore two images were recorded. These images were superimposed to perform the analysis of the diameter of the phosphor screen d'_{P47} and of the hole d'_{hole}, which were observer in the image (Fig. D.9).
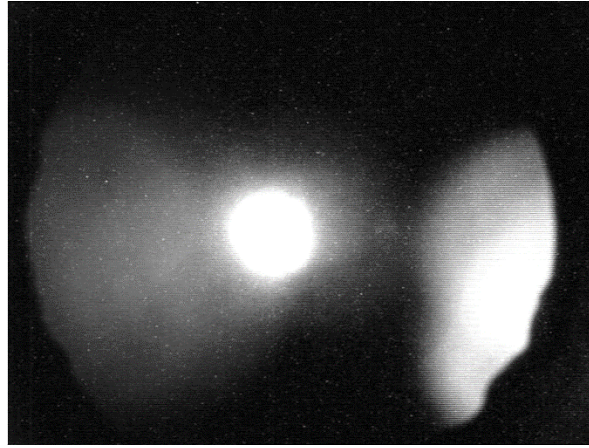

Figure D.9: Superimposed image on the CCD camera of the light pointed left and right through the 9 mm hole with no voltage on the electrostatic lens.

A real value d_{P47} was taken from the drawings of BISE (Fig. A.11).

$d'_{P47} = 48.16 \pm 0.19$ mm,
$d_{P47} = 43 \pm 0.1$ mm,
$d'_{hole} = 7.14 \pm 0.1$ mm.

The difference between the two values of the diameter of the phosphor screen could be due to distortions in the optics of the CCD camera or to uneven edges of the phosphor

screen. The area of the hole was saturated and had a circular form. From Figure D.9 one can assume that the halo border seen in Figures D.5 and D.6 could be due to the border of the spherical segment in the focusing system.

E r k l ä r u n g

gemäss Art. 28 Abs. 2 RSL 05

Name/Vorname: *Elena Kirillova*

Matrikelnummer: *12-128-245*

Studiengang: *Master in Experimental Physics*

Bachelor ☐   Master ☒   Dissertation ☐

Titel der Arbeit: *Study and Test of a Beam Monitor Detector at the Bern Medical Cyclotron*

LeiterIn der Arbeit: *Prof. Dr. Antonio Ereditato*

PD Dr. Saverio Braccini

Ich erkläre hiermit, dass ich diese Arbeit selbständig verfasst und keine anderen als die angegebenen Quellen benutzt habe. Alle Stellen, die wörtlich oder sinngemäss aus Quellen entnommen wurden, habe ich als solche gekennzeichnet. Mir ist bekannt, dass andernfalls der Senat gemäss Artikel 36 Absatz 1 Buchstabe o des Gesetztes vom 5. September 1996 über die Universität zum Entzug des auf Grund dieser Arbeit verliehenen Titels berechtigt ist.

Bern, 15.07.2014

Ort/Datum

Elena Kirillova